

**STUDY ON STRUCTURE-PROPERTY RELATIONSHIP OF  
GRAFT-TYPE FLUORINATED POLYMER ELECTROLYTE  
MEMBRANES USING QUANTUM BEAMS**

(量子ビームを利用したグラフト型フッ素系高分子  
電解質膜の構造 / 機能相関に関する研究)

トラン ユイ タップ

# Contents

<b>Chapter 1. General Introduction.....</b>	<b>1</b>
1.1. Polymer electrolyte fuel cell.....	1
1.2. Pre-irradiation grafting method for preparation of graft-type PEM.....	4
1.3. Hierarchical structure-property relationship of graft-type PEM .....	5
1.4. Current challenges of PEM fuel cell and objective of this study .....	6
<b>Chapter 2. Experimental.....</b>	<b>13</b>
2.1. Introduction .....	13
2.2. Materials .....	14
2.3. Preparation of graft-type ETFE-PEMs .....	15
2.4. Electrolyte properties.....	18
2.4.1. Water uptake.....	18
2.4.2. Ion exchange capacity .....	18
2.4.3. Proton conductivity .....	19
2.4.4. Mechanical properties .....	21
2.5. Characterization.....	24
2.5.1. Thermo gravimetric analysis .....	24
2.5.2. Differential scanning calorimetry.....	24
2.5.3. Field emission scanning electron microscope observation .....	25
2.5.4. Small and ultra angle X-ray scattering (SAXS/USAXS) measurement.....	25
2.5.4.1. Measurement .....	25
2.5.4.2. Analysis of SAXS profiles .....	29
<b>Chapter 3. Properties of graft-type PEM .....</b>	<b>37</b>
3.1. Introduction .....	37
3.2. Preparation and electrochemical properties of ETFE-PEM .....	38
3.3. Grafting degree dependence of thermal stability, mechanical properties, and crystallinity.....	40
3.4. Proton conductivity of ETFE-PEMs under various RH .....	49
3.5. Mechanical properties at dry and humidified conditions .....	51

3.6. Conclusions .....	53
<b>Chapter 4. Structure analysis of graft-type PEM.....</b>	<b>55</b>
4.1. Introduction.....	55
4.2. The variation of hierarchical structure by preparation procedures.....	56
4.3. The variation of hierarchical structure with grafting degree .....	59
4.4. The variation of hierarchical structure at dry and hydrated states.....	68
4.5. The variation of hierarchical structure by direct observation.....	75
4.6. Conclusion .....	77
<b>Chapter 5. Background correction of SAXS profiles in high q-range.....</b>	<b>79</b>
5.1. Introduction.....	79
5.2. Hierarchical structures in high $q$ range.....	80
5.3. Background corrections .....	82
5.4. Hierarchical structure analysis with background corrections.....	86
5.5. Conclusions.....	92
<b>Chapter 6. Structure-property relationship of graft-type PEM.....</b>	<b>94</b>
6.1. Introduction.....	94
6.2. Structure–property relationship of ETFE-PEM.....	94
6.3. Conclusions.....	99
<b>Chapter 7. General Conclusion .....</b>	<b>101</b>
<b>Publications .....</b>	<b>105</b>
<b>Presentations .....</b>	<b>105</b>
<b>Scientific reports .....</b>	<b>108</b>
<b>Awards .....</b>	<b>108</b>
<b>Acknowledgements .....</b>	<b>109</b>

# Chapter 1. General Introduction

## 1.1. Polymer electrolyte fuel cell

Fuel cell is an electrochemical device generating electric power via chemical reaction of fuels such as H<sub>2</sub>, methanol, ethanol, etc. and turned to electrical energy. In a fuel cell system, the chemical energy related to electrochemical reaction of the fuel with oxidant directly change into the water, electronic, and heat [1]. The central core of the fuel cell is the membrane electrode assembly (MEA) which consists of electrocatalyst and membrane. Fuel cells are commonly classified by the nature of the used electrolyte. Based on this classification, fuel cell includes: (1) Polymer electrolyte fuel cell (PEFCs), (2) phosphoric acid fuel cell (PAFCs), (3) molten carbonate fuel cell (MCFC), (4) solid oxide fuel cell (SOFC), and (5) alkaline fuel cell (AFC). Among such type of fuel cells, polymer electrolyte fuel cells (PEFCs) have attracted much interest for solving environmental problems because its efficient high-power generation is expected to reduce fossil fuel consumption. Hydrogen-type fuel cells, such as residential cogeneration systems and fuel cell vehicles, are expected to reduce CO<sub>2</sub> emissions, which is a main source of greenhouse effects [2-4]. Polymer electrolyte membranes (PEMs), which serve as both a separator to gas permeation from the anode to cathode as well as a solid electrolyte, have been considered as one of the key components of a PEM fuel cell because their properties required for high fuel cell performance, such as ionic conductance, mechanical strength, chemical and thermal stability, are directly related to their power generation efficiency and durability under severe operating conditions [5].

Operating principle of a H<sub>2</sub>/O<sub>2</sub> PEM fuel cell with acidic electrolyte membrane is showed in **Fig. 1-1**. In summary, the reactions occurred in a fuel cell using hydrogen as a fuel can be briefly described as following. Hydrogen in anode electrode is released electrons and changed into a hydrogen ion. The released electrons move through foreign circuit towards the cathode and produce the electrical current using for cell phone, laptop computer, automobile, etc. Anodic and cathodic reactions are done in the PEM fuel cell in following:

Anodic reaction:  $\text{H}_2 \rightarrow 2\text{H}^+ + 2\text{e}^-$ ,

Cathodic reaction:  $\frac{1}{2} \text{O}_2 + 2\text{e}^- + 2\text{H}^+ \rightarrow \text{H}_2\text{O}$ ,

Overall reaction:  $2\text{H}_2 + \text{O}_2 \rightarrow 2\text{H}_2\text{O}$ .

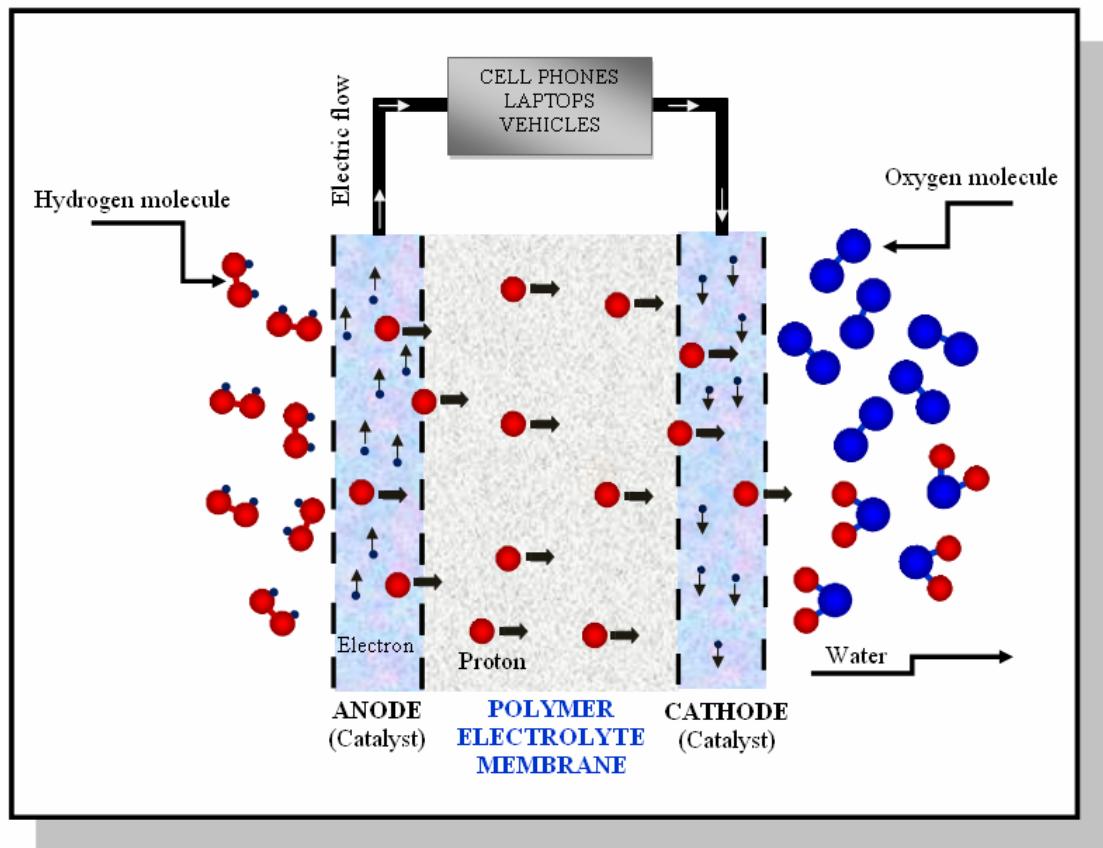


**Fig. 1-1.** Operating principle of a  $\text{H}_2/\text{O}_2$  fuel cell.

Protons are generated at anode and transported from anode to cathode, where water is formed.

Most of the PEFCs operate at temperatures up to  $100\text{ }^\circ\text{C}$ , while some PEFCs utilize so-called high temperature polymer electrolyte membranes, which operate beyond  $100\text{ }^\circ\text{C}$ .

To be applied in PEM fuel cell, the PEM materials should meet the following requirements: (i) high proton conductivity even at low relative humidity (RH) and high temperature, (ii) low fuel permeability, (iii) high chemical and thermal stability, (iv) good

mechanical properties in both the dry and hydrates states, (v) sufficient water uptake but moderate swelling, (vi) substantial morphological and dimensional stability, (vii) easy fabrication to form the membrane electrode assembly, (viii) a competitive cost-effective, and (ix) sufficient long-term durability [6].

Perfluorosulfonic acid (PFSA) membranes, such as Nafion, are the current state-of-the-art PEM materials because of their excellent chemical and physical stability along with high proton conductivity under a wide range of relative humidity at moderate operation temperatures (< 80 °C). The chemical structures of perfluorosulfonic acid (PFSA) membranes are showed in **Fig. 1-2**. However, the PFSA membranes suffer critical drawbacks, such as high fuel crossover, limited operation temperature in fuel cell, and high production cost. Under the more severe operating conditions requested by industry (> 80 °C, < 50% RH), proton conductivity of PFSA membranes drops significantly, leading to the decrease in fuel cell performance [7,8]. Thus, this is crucial to develop new PEM materials which exhibit high levels of proton conductivity at high temperature and low relative humidity (RH) but satisfying other PEM properties such as mechanical integrity for high fuel cell performance.

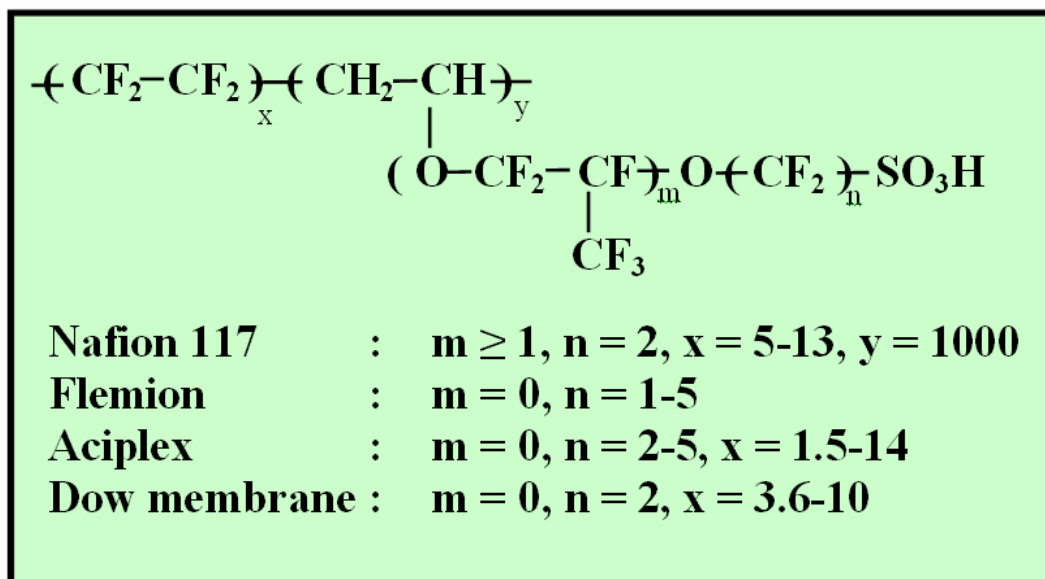


**Fig. 1-2.** Chemical structure of perfluorosulfonic acid (PFSA) membranes.

## 1.2. Pre-irradiation grafting method for preparation of graft-type PEM

A pre-irradiation grafting method, in which polymer substrates are first irradiated using quantum beams, and then immersed in a monomer solution for graft polymerization, is a widely recognized technique for the introduction of a new functional graft polymer phase directly into polymer substrates while maintaining the substrate's inherent characteristics such as thermal stability, mechanical strength, and crystallinity. Therefore, this radiation technique has been applied to the preparation of PEM materials for fuel cells by the sulfonation of grafted films [9,10]. The schematic diagram of radiation-induced grafting method to prepare graft-type PEM materials is showed in **Fig. 1-3**.

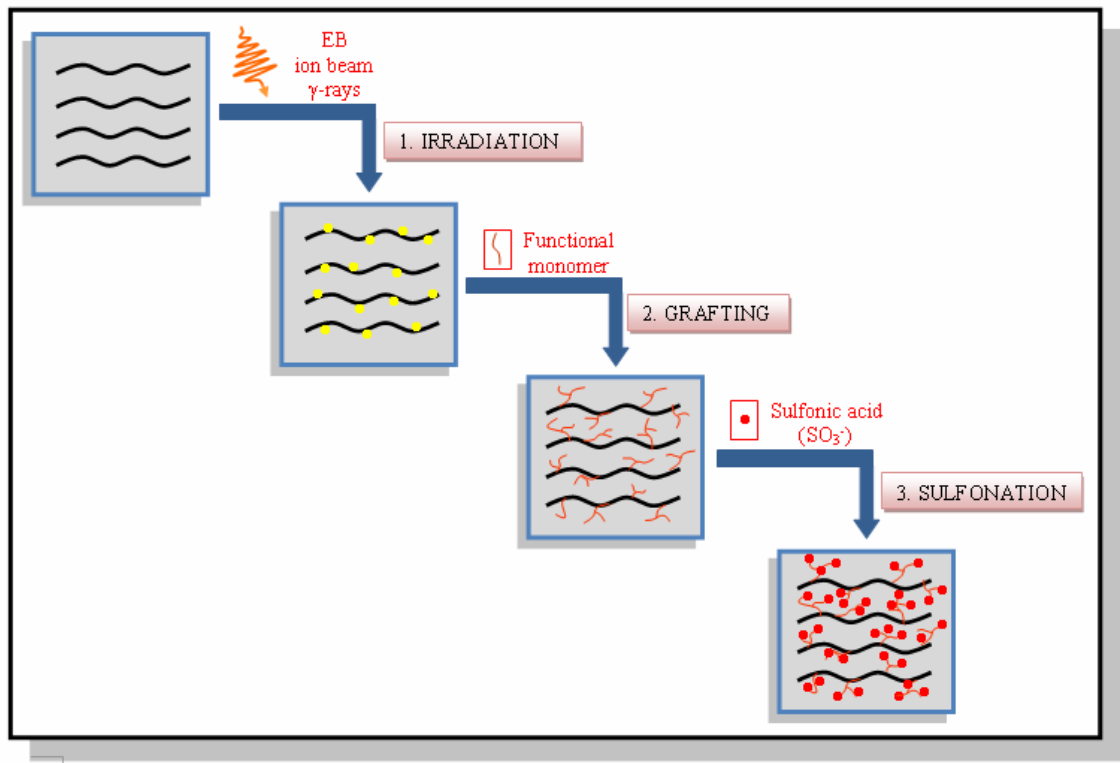


**Fig. 1-3.** Schematic diagram of radiation-induced grafting method to prepare graft-type PEM.

The radiation grafting process onto base polymer substrate is briefly described as following. The polymer substrates are first irradiated by ionizing radiation such as gamma ray, electron beam, and ion beam to produce free radicals. These radicals in the amorphous domains are considered to quickly vanish because of the recombination and disproportionation reactions between two radicals. However, the radicals in crystalline domains are expected to survive because the polymer chain motion in these phases is strongly restricted. When the radicals in the crystalline phases move to the interface between crystalline and amorphous domains, they encounter monomers that can diffuse only in the amorphous phases, resulting in the initiation of graft polymerization. The graft chains are then diffused mainly into the amorphous phases because the monomers cannot easily permeate into the crystalline phases [11,12].

There are many parameters, which strongly affect radiation-induced graft polymerization process and subsequently the grafting and sulfonation degree in the obtained membranes. These parameters include (i) the nature of base polymer (film thickness, crystallinity, chemical structure and components) and monomer, (ii) the nature of radiation, irradiation dose and dose rate, and (iii) grafting conditions (solvent, temperature, concentration of monomer, addition of crosslinking agent) [10,11,13]. Variation of these parameters causes significant changes in the grafting degree (*GD*) and therefore, a real chance to closely control the compositions and the properties of the membranes can be achieved. A combination of these parameters has to be adapted to obtain successful grafting reactions and achieve desired membrane structure.

### **1.3. Hierarchical structure-property relationship of graft-type PEM**

Fundamental understanding of the structure-property relationship of PEM is crucial not only with respect to fundamental research but also for the improvement of cost, performance, and durability of PEM fuel cell [9,10,14,15]. The different regions of interest of the graft-type PEM include crystalline, amorphous, and graft domains as showed in **Fig. 1-4**. The graft materials mainly exist in the amorphous domains where the graft monomers easily diffuse onto from a film surface. The hierarchical structures related to such three domains include the crystalline structures (lamellar structures, connectivity of crystallites), conducting layers

consisting of graft polymers (size, shape, and connectivity), the internal structures of the conducting layers (aggregations and distributions of the ionic groups and water), and the phase separation between the hydrophobic polymer substrates and hydrophilic graft domains. Regarding the lamellar structures, the interfacial thickness, which is the size of the boundary between the crystallite and amorphous layers, must be considered for quantitative determination of the lengths of the crystalline and amorphous layers in the lamellar stacks.

The crystalline domains have been considered to govern thermal stability, mechanical properties (tensile strength, elongation) and proton conductivity (the decrease of crystallinity leads to increase of conductivity). The amorphous domains consist of graft materials and ionic groups which swell with water. Thus, such domains are expected to govern the proton conductivity, water uptake, and chemical stability. However, in the real complex PEM system, each structure can relate to several electrochemical as well as mechanical properties. For instance, decrease of crystallinity due to the distortion of crystallites leads to increase the proton conductivity but decrease tensile strength of membrane [15].

Recently, the main concern of structure-property relationships of PEM is to design the PEM materials which exhibit higher levels of proton conductivity via higher ionic content and/or improved proton transport pathway, without excessive swelling with water [15,16]. The increase of ionic content leads to the increase order of the hydrophilic domains which are favorable for higher levels of proton conductivity. However, higher ionic content makes membranes possible to absorb higher water molecules resulting in the loss of mechanical integrity. Thus, controlling the orientation and alignment of ionic domains to improve proton transport pathway is higher desirable and an area requiring greater study.

#### **1.4. Current challenges of PEM fuel cell and objective of this study**

Recently, the main concern for PEM fuel cells have become higher proton conductivity at low relative humidity (RH) (<50% RH) and high temperatures (>80 °C) and superior mechanical properties under humid conditions (100% RH), because these properties control the power generation efficiency and durability under extreme operating conditions in fuel cell systems [17]. One solution to this problem is to increase the ion exchange capacity (*IEC*),

which is related to conductivity of the PEM consisting of a small number of water molecules. However, PEMs with higher *IEC* exhibit severe damage in a hydrated state under flooding conditions. One promising strategy for improving the conductivity even with fewer water molecules in PEMs is to use block-type aromatic hydrocarbon polymers that consist of hydrophilic and hydrophobic units. For example, block-type poly(arylene ether sulfone)s [18,19], and polyimides [20,21] show compatible or even higher conductivity than Nafion and moderate water uptake in a fully hydrated state. However, block-type aromatic hydrocarbon polymers have critical issues that include insufficient durability and significant conductivity dependence on the relative humidity.

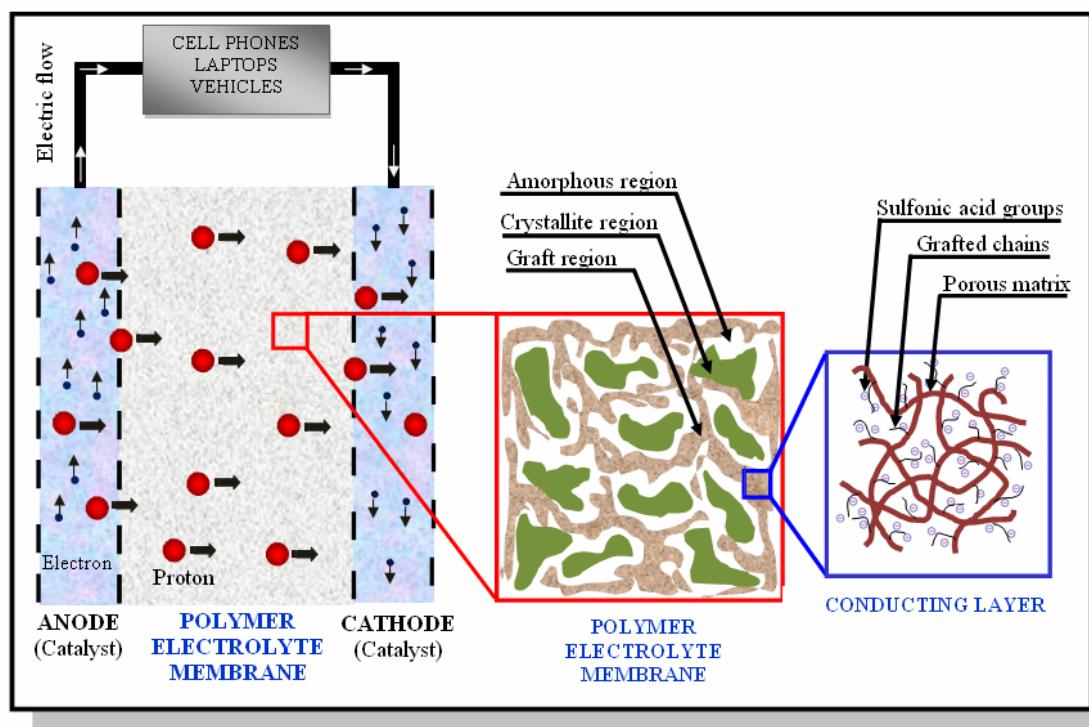


**Fig. 1-4.** Systematical illustration of hierarchical structures of graft-type PEM.

Another approach to overcome this problem is to use aromatic hydrocarbon-based PEMs that have condensed sulfonic acid groups [22-25]. Although these PEM materials show pronounced hydrophilic/hydrophobic phase-separated morphology with well-interconnected proton transport pathways leading to high conductivity at high temperatures and low relative humidity, oxidative degradation occurs in the hydrophilic blocks.

Graft-type PEM, as one of the promising material candidates, may be able to overcome the above problems because the graft-type PEM comprises of substrate films that have a mechanically tough crystalline phase and various functional grafted polymer phases directly bonded to the polymer main chain [13]. In addition, introducing sulfonated graft side chains into the polymer main chain is an excellent approach to prepare PEM materials because the *IEC* values can be easily controlled using grafting degrees and well-defined hydrophilic/hydrophobic phase-separated structures are produced by sulfonation [26,27].

The partially fluorinated poly(ethylene-co-tetrafluoroethylene) (ETFE) film made of hydrocarbon and fluorocarbon segments has strong radiation resistance for high doses of irradiation and robust mechanical strength for long time durability of fuel cell operation [28]. Thus, poly(styrene sulfonic acid)-grafted ETFE polymer electrolyte membrane (ETFE-PEM) have been intensively investigated by our group [28-34] and others [16, 35-38] as promising graft-type PEM candidates because of their moderate PEM properties such as conductance, mechanical strength, and thermal stability, particularly for direct methanol type fuel cell (DMFC) applications. The ETFE-PEM conductance at ambient conditions of 0.011–0.089 S/cm was reported to increase with the grafting degree (*GD*) by 14.3%–34%. This corresponds to an *IEC* of 1.01–1.86 mmol/g and a moderate water uptake of 19.9%–44.4% [30,37]. In addition, the *GD* effects and crosslinking level on thermal stability, crystallinity, and mechanical properties were investigated in detail [39,40]. However, to date the ETFE-PEM grafting degrees reported are limited to 55% (*IEC* = 2.4 mmol/g); furthermore, there has been no report on the RH dependence of the proton conductivity and mechanical properties. Moreover, there have been several reports concerning the structures of lamellae and their internal structures relating to the ion-conducting layers in ETFE-PEMs using small angle X-ray/neutron scattering (SAXS/SANS) measurements [16,41-43]. However, the structural analysis of ETFE-PEM has not been conducted in detail for elucidating the origin of the superior properties of ETFE-PEM. In addition, the effects of background scattering and the

diffuse phase boundary on the structures have not been considered, although the background is very crucial in these structural scale ranges (particularly in the high- $q$  ranges).

Therefore, herein, the effects of RH on the conductance and mechanical properties (tensile strength, elongation at break) of ETFE-PEMs as a function of  $IEC$  (0–3.3 mmol/g) are discussed in comparison to Nafion-212. Thermal stability and crystallinity were also evaluated using thermo gravimetric analysis (TGA), and differential scanning calorimetry (DSC). We focused on proton conductivity at low RH (30% RH) and mechanical properties at high RH (100% RH), which are the main concerns for PEMs because they govern the power efficiency and durability under severe operating conditions in fuel cell systems.

For structure analysis, the higher-order structures of ETFE-PEM under dry and hydrated states were investigated using a wide  $q$ -range observation ( $4 \times 10^{-3} \text{ nm}^{-1} \leq q \leq 10 \text{ nm}^{-1}$ ) in SAXS/USAXS by comparison with the profiles of precursor original ETFE and polystyrene-grafted ETFE films (grafted-ETFE) because the grafted PEMs are well known to keep somewhat crystalline structures and graft polymer phases of precursor original and grafted films. In addition, the structure changes with a wide range of  $GD$  ( $0 \leq GD \leq 117\%$ ) were observed to optimize the membrane's structures for high fuel cell performance. The background scattering intensity ( $I_B(q)$ ) due to thermal scattering (also known as liquid scattering) and amorphous phase scattering in the high- $q$  range is also evaluated for ETFE-PEMs and their precursor films because the background is very crucial in this region where ionomer peak, one of the most important structures of membrane, is located. The hierarchical structures of ETFE-PEM characterized by SAXS measurement was compared with the direct images obtained from field emission scanning electron microscope (FE-SEM).

On the basic of the results obtained from SAXS measurements, the relationship between the hierarchical structures and electrolyte properties of ETFE-PEMs such as proton conductivity, mechanical strength, crystallinity, and water uptake is discussed and compared with those of Nafion-212.

## References

- 1) M. Winter, R.J. Brodd, Chem. Rev. 104 (2004) 4245-4269.
- 2) B. Smitha, S. Sridhar, A.A. Khan, J. Memb. Sci. 259 (2005) 10-26.
- 3) A. Veziroglu, R. Macario, International Journal of Hydrogen Energy 33 (2008) 4444-4455.
- 4) M.A. Hickner, H. Ghassemi, Y.S. Kim, B.R. Einsla, J.E. McGrath, Chem. Rev. 104 (2004) 4587-4612.
- 5) S.J. Peighambardoust, S. Rowshanzamir, M. Amjadi, Int. Journal Hydrogen Energy 35 (2010) 9349-9384.
- 6) H. Zhang, P.K. Shen, Chem. Rev., 112 (2012) 2780-2832.
- 7) R. Borup, J. Meyers, B. Pivovar, Y.S. Kim, R. Mukundan, N. Garland, D. Myyers, M. Wilson, F. Garzon, D. Wood, P. Zelenay, P. Zelenay, K. More, K. Stroh, T. Zawodzinski, J. Boncella, J.E. McGrath, M. Inaba, K. Miyatake, M. Hori, K. Ota, Z. Ogumi, S. Miyata, A. Nishikata, Z. Siroma, Y. Uchimoto, K. Yasuda, K. Kimjima, N. Iwashita, Chem. Rev. 107 (2007) 3904-3951.
- 8) Q. Li, R. He, J.O. Jensen, N.J. Bjerrum, Chem. Mater. 15 (2003), 4896-4915.
- 9) M. Tamada, Y. Maekawa, "Radiation Processing of Polymers and Its Applications." In *Charged Particles and Photon Interactions with Matter*, Hatano, Y., Katsumura, Y., Mozumder A. (Eds.), CRC Press, Boca Raton (Chapter 27), CRC Press, Boca Raton, 2011, 737-759.
- 10) M.M. Nasef, E.A. Hegazy, Prog. Polym. Sci. 29 (2004) 499-561.
- 11) S. Sawada, D. Yamaguchi, A. Putra, S. Koizumi, Y. Maekawa, Polymer Journal (2012) 1-5.
- 12) H. Iwase, S. Sawada, T. Yamaki, Y. Maekawa, S. Koizumi, International Journal of Polymer Science 2011 (2011) 1-7.
- 13) M.M. Nasef, O. Güven, Progress in polymer science 37 (2012) 1597-1656.
- 14) H. Iwase, S. Sawada, T. Yamaki, S. Koizumi, M. Ohnuma, Y. Maekawa, Macromolecules 45 (2012) 9121-9127.
- 15) T.J. Peckham, S. Holdcroft, Adv. Mater., 22 (2010) 4667-4690.
- 16) K. Jokela, R., Serimaa, M. Torkkeli, F. Sundholm, T. Kallio, G. Sundholm, J. Polym. Sci. Polym. Phys. Ed. 40 (2002) 1539-1555.

- 17) K. Miyatake, B. Bae, M. Watanabe, *Polym. Chem.* 2 (2011) 1919-1929.
- 18) B. Bae, K. Miyatake, M. Watanabe, *Macromolecules* 42 (2009) 1873-1880.
- 19) K. Miyatake, Y. Chikashige, E. Higuchi, M. Watanabe, *J. Am. Chem. Soc.* 129 (2007) 3879-3887.
- 20) N. Asano, M. Aoki, S. Suzuki, K. Miyatake, H. Uchida, M. Watanabe, *J. Am. Chem. Soc.* 128 (2006) 1762-1769.
- 21) M.L. Einsla, Y.S. Kim, M. Hawley, H. Lee, J.E. McGrath, B. Liu, M.D. Guiver, B.S. Pivovar, *Chem. Mater.* 20, (2008) 5636-5642.
- 22) B. Bae, T. Yoda, K. Miyatake, H. Uchida, M. Watanabe, *Angew. Chem., Int. Ed.* 49 (2010) 317-320.
- 23) B. Bae, K. Miyatake, M. Uchida, H. Uchida, Y. Sakiyama, T. Okanishi, M. Watanabe, *ACS Appl. Mater. Interfaces* 3 (2011) 2786-2793.
- 24) K. Matsumoto, T. Higashihara, M. Ueda, *Macromolecules* 42 (2009) 1161-1166.
- 25) T. Suda, K. Yamazaki, H. Kawakami, *J. Power Sour.* 195 (2010) 4641-4646.
- 26) L. Gubler, S.A. Gürsel, G.G. Scherer, *Fuel Cell* 5 (2005) 317-335.
- 27) S. Alkan Gürsel, M. Eikerling, L. Gubler, B. Gupta, S. Holdcroft, D.J. Jones, A.A. Kornyshev, T.J. Peckham, J. Rozière, G.G. Scherer, A. Siu, E. Sohr, A. Watakabe, Y. Yang, M. Yoshitake, *Advance in Polymer Science* 215, Springer, 2008.
- 28) J. Chen, M. Asano, M. Yoshida, Y. Maekawa, *J. Membr. Sci.* 277 (2006) 249-257.
- 29) J. Chen, M. Asano, M. Yoshida, Y. Maekawa, *J. Appl. Polym. Sci.* 101 (2006) 2661-2667.
- 30) J. Chen, U. Septiani, M. Asano, Y. Maekawa, H. Kubota, M. Yoshida, *J. Appl. Polym. Sci.* 103 (2006) 1966-1972.
- 31) J. Chen, M. Asano, Y. Maekawa, M. Yoshida, *J. Membr. Sci.* 296 (2007) 77-82.
- 32) U. Septiani, J. Chen, M. Asano, Y. Maekawa, M. Yoshida, H. Kubota, *J. Mater. Sci.* 42 (2007) 1330-1335.
- 33) Y. Kimura, J. Chen, M. Asano, Y. Maekawa, R. Katakai, M. Yoshida, *Nucl. Instru. And Meth. B* 263 (2007) 463-467.
- 34) Y. Kimura, M. Asano, J. Chen, Y. Maekawa, R. Katakai, M. Yoshida, *Radiat. Phys. Chem.* 77 (2008) 864-870.
- 35) A.N. Geraldes, H.A. Zen, G. Ribeiro, H.P. Ferreira, C.P. Souza, D.F. Parra, E.I. Santiago, A.B. Lugaõ, *Radia. Phys. Chem.* 79 (2010) 246-249.

- 36) S.A. Gürsel, H.B. youcef, A. Wokaun, G.G. Shherer, Nucl. Instru. And Meth. B 265 (2007) 198-203.
- 37) M. Shen, S. Roy, J.M. Kuhlmann, K. Scott, K. Lovell, J.A. Horsfall, J. Membr. Sci. 251 (2005) 121-130.
- 38) U. Lappan, U. Geißler, U. Gohs, S. Uhlmann, Radia. Phys. Chem. 79 (2010) 1067-1072.
- 39) H.B. youcef, S.A. Gürsel, A. Buisson, L. Gubler, A. Wokaun, G.G. Scherer, Fuel Cell 10 (2010) 401-410.
- 40) S.A. Gürsel, J. Schneider, H.B. youcef, A. Wokaun, G.G. Scherer, J. Appl. Polym. Sci. 108 (2008) 3577-3585.
- 41) S. Balog, U. Gasser, K. Mortensen, L. Gubler, G.G. Scherer, H.B. youcef, Macromol. Chem. Phys., 211 (2010) 635-643.
- 42) S. Balog, U. Gasser, K. Mortensen, H.B. youcef, L. Gubler, G.G. Scherer, J. Membr. Sci., 383 (2011) 50-59.
- 43) S. Balog, U. Gasser, K. Mortensen, H.B. youcef, L. Gubler, G.G. Scherer, Polymer 53 (2012) 175-182.

## Chapter 2. Experimental

### 2.1. Introduction

As presented in Chapter 1, radiation-induced graft polymerization has been a novel method to prepare PEM materials because the bulk modification of polymer films can be achieved. This is unlike other methods such as uv- or plasma- induced graft polymerization in which only surface modification of polymers can be produced [1]. Radiation-induced graft polymerization method has the flexibility of using various types of radiations (gamma-ray, electron beam, and ion beam), which are produced by already commercial courses. Other advantages of this method are the lack of addition chemical initiators or catalysts and rapid rate of polymerization because of a rapid formation of active sites on appreciate polymer matrix. The grafted yield and then *IEC* of graft-type PEM can be easily controlled by properly irradiated conditions and reaction parameters. In addition, membrane prepared by this method comprises a new functional grafted polymer phase while maintaining the substrate's inherent characteristics such as thermal stability, mechanical strength, electronic properties, and crystallinity. Thus, the functionalization of polymers by irradiation grafting of appropriate monomers has provided a unique tool to combine the characteristics of base polymer, monomer, and both of them to develop the specially designed membranes.

A combined small-angle scattering method using small- and ultra-small angle X-ray scattering (SAXS/USAXS) measurement has displayed a powerful tool to observe a wide length scale of higher-order structures of PEM from nano- to micrometers [2]. In SAXS instruments, electrons generated from a hot tungsten filament are accelerated towards a target material such as Cu, Cr, Mo, etc. in an evacuated tube, and X-rays are produced by the collision of electrons on the target. In USAXS instruments, X-ray are generated in a synchrotron where a beam of electron are accelerated to nearly the speed of light and then are bended to circulate on a closed orbit under high vacuum in a storage ring. The flux of X-ray generated in a synchrotron is many orders of magnitude greater than that of in conventional X-ray tubes. Thus, USAXS instruments allow a measurement with very short time.

Unlike SAXS measurement (reciprocal-space analysis) in which the bulk structures of specimens are analyzed, direct microscopic imagings (real-space analysis) such as SEM provide the information of morphology and structures of specimens' surface. Thus, in order to investigate fully the structure of a complex system like PEM, both imaging and scattering are necessary. Each technique acts as a check on the other. For instance, models which are consistent with SAXS profiles can be ruled out from imaging information.

In the two-phase system such as the crystalline and amorphous phases in a semicrystalline polymer (a common type of polymer to prepare graft-type PEM materials), the analysis of the scattering data from such a system allow the determination of the most general parameters such as (i) the correlation length characterizing the mean domain size, (ii) the specific interfacial boundary area, (iii) the thickness of the phase boundaries, (iv) the volume fraction of each phase, and (v) the inner surface [2,3].

Therefore, herein in this chapter, the detail procedure preparations of ETFE-PEM using pre-irradiation-induced graft polymerization are described. Then, the standard procedures of water uptake, *IEC*, thermal stability, and crystallinity measurements are also addressed. For property measurements, we focus on the effects of RH on the conductance and mechanical properties (tensile strength, elongation at break) of ETFE-PEMs. The procedure measurements of SAXS/USAXS and SEM for structural measurements are presented. In SAXS measurement, the theory of analysis of SAXS profiles is also addressed in detail.

## **2.2. Materials**

A 50- $\mu\text{m}$ -thick ETFE film was purchased from Asahi Glass Co. Ltd, Japan. Styrene, 1,2-dichloroethane, sodium chloride, and sodium hydroxide were provided from Wako Pure Chemical Industries, Ltd. Japan. Nafion-212 obtained from DuPont was pretreated by boiling for 1 h in a 3%  $\text{H}_2\text{O}_2$  solution, washing in hot pure water for 1 h, boiling for 1 h in 1 M  $\text{H}_2\text{SO}_4$ , and final rinsing in hot water again for 1 h. Acetone, toluene, sulphonic acid, and hydrogen peroxide were obtained from Wako Pure Chemical Industries, Ltd. All the organic chemicals were used without further purification. Water was purified by a Millipore Milli-Q UV system producing a resistance of 18.2  $\text{M}\Omega$  cm and a total organic carbon content of < 10 ppb.

### 2.3. Preparation of graft-type ETFE-PEMs

ETFE films were wiped up by acetone to remove impurities on the film surface. The ETFE (size  $6 \times 8 \text{ cm}^2$ ) films in a glass ampoule (90 ml) were preirradiated with  $\text{Co}^{60}$   $\gamma$ -rays (Cell No. 6, Japan Atomic Energy Agency at Takasaki, Japan) at a dose rate of 15 kGy/h under an argon atmosphere at room temperature and then immersed in a styrene solution (90 ml) in toluene at  $60 \text{ }^\circ\text{C}$ . The styrene monomer was bubbled with Argon gas for 40 min prior to grafting. The grafting reactions were carried out under inert gas ambient-controlled to avoid scavengers such as oxygen, which inhibits graft polymerization. The obtained polystyrene-grafted ETFE (grafted-ETFE) was soaked in toluene solution (60 ml) at  $50 \text{ }^\circ\text{C}$  for 24 h and wiped off the surfaces to remove the homo-polymer and the residual monomers prior to immersing in 0.2 M chlorosulfonic acid in 1,2-dichloroethane at  $50 \text{ }^\circ\text{C}$  for 6 h. The membrane was then washed with pure water (200 ml) at  $50 \text{ }^\circ\text{C}$  for 24 h to obtain poly(styrene sulfonic acid)-grafted ETFE membranes (ETFE-PEMs) (**Fig. 2-1**). The chemical structures of pristine ETFE, grafted-ETFE and ETFE-PEM are showed in **Fig. 2-2**.

The grafting degree ( $GD$ ) of the membrane was determined as follows:

$$GD(\%) = \frac{W_g - W_o}{W_o} \times 100 \quad (2-1)$$

where  $W_o$  and  $W_g$  are the weights of the films before and after graft polymerization, respectively.

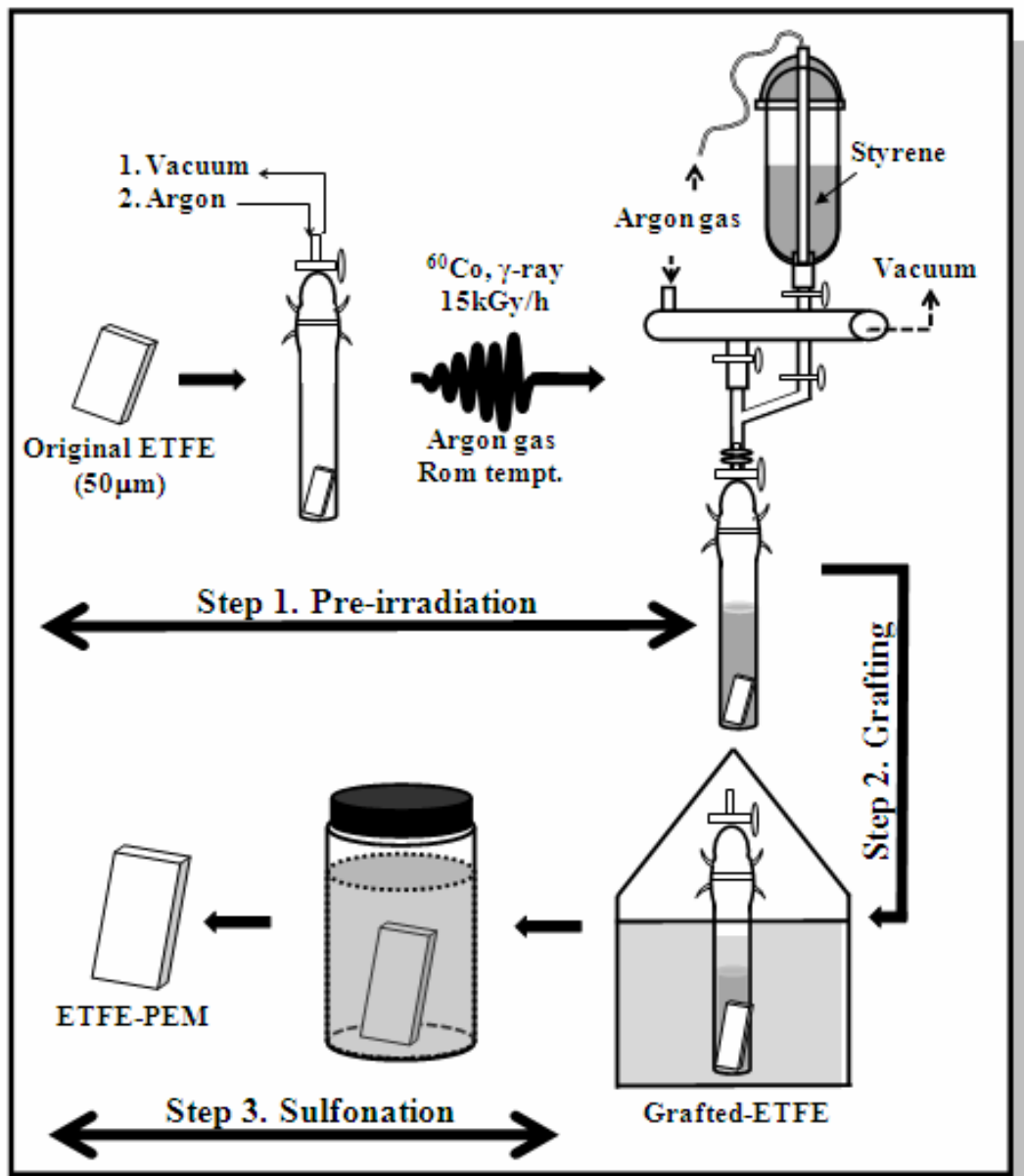
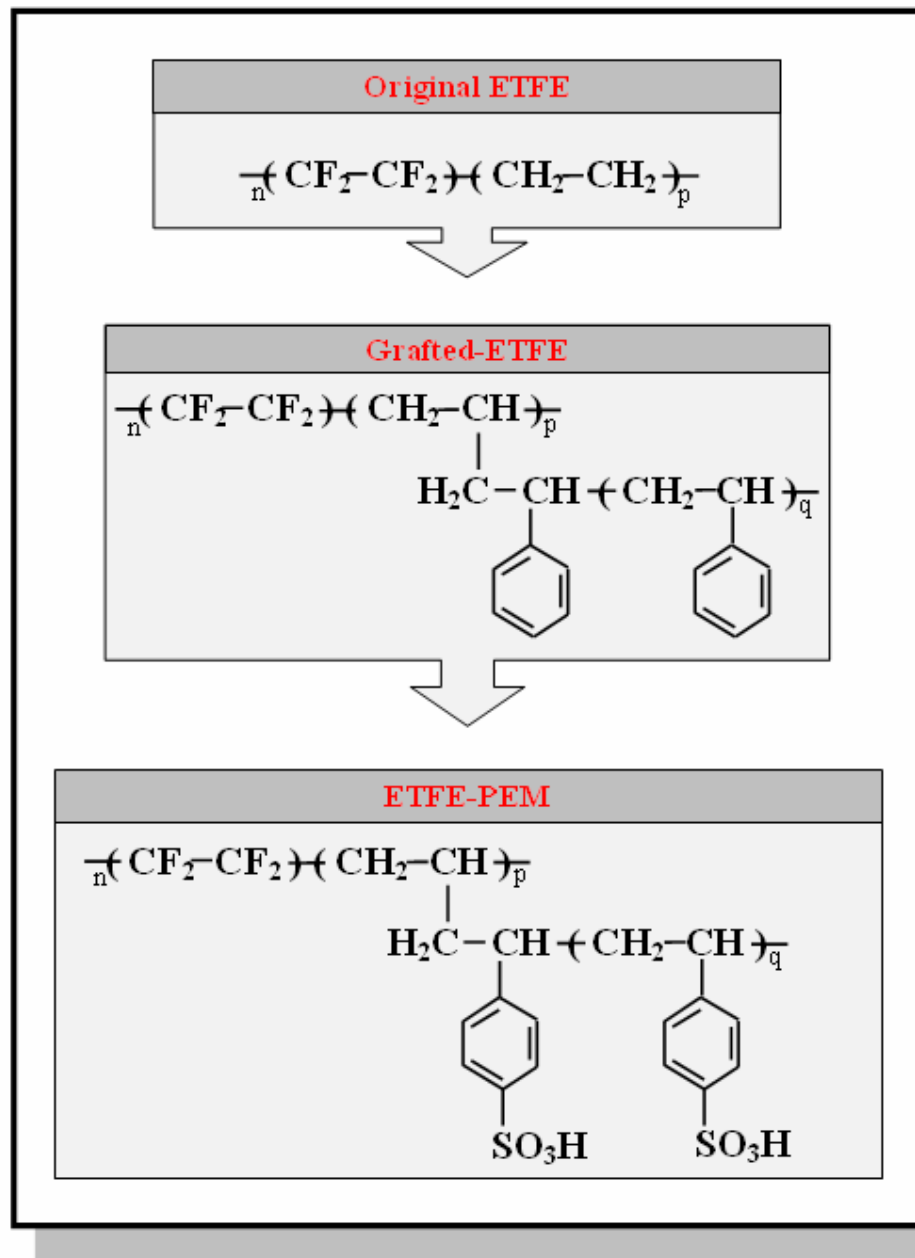


Fig. 2-1. Preparation procedures of ETFE-PEM by pre-irradiation grafting method.



**Fig. 2-2.** Chemical structures of pristine ETFE film, grafted-ETFE film, and ETFE-PEM.

## 2.4. Electrolyte properties

### 2.4.1. Water uptake

The water uptake ( $WU$ ) of membranes was determined as:

$$WU(\%) = \frac{W_{wet} - W_{dry}}{W_{dry}} \times 100 \quad (2-2)$$

where  $W_{wet}$  and  $W_{dry}$  are a weight of a hydrated and dry membrane, respectively. The membrane was dried in a vacuum oven at 40 °C until a constant weight was recorded. The weight of hydrated membrane was obtained by soaking membrane in purified water for one day and then wiped carefully with a filter paper to remove excess water on membrane's surface and immediately weighted.

### 2.4.2. Ion exchange capacity

The ion exchange capacity ( $IEC$ ) of the membranes is defined as a molar of the sulfonic acid group per dry membrane weight (mmol/g) and was determined herewith by titration analysis at room temperature. Membranes with the sulfo group ( $H^+$ ) were first converted into those with a sulfonate ( $Na^+$ ) by immersing in an aqueous 3 M NaCl solution at 50 °C for 7 h. The amount of HCl liberated from the membrane was then determined by titration with a 0.01 M NaOH solution using an automatic titrator (HIRANUMA COM-555). Thus, the  $IEC$  values can be determined using the titration results and the following equation:

$$IEC(\text{mmol} / \text{g}) = \frac{0.01 \times V_{NaOH}}{\text{Dry weight of membrane}} \quad (2-3)$$

where  $V_{NaOH}$  is the consumed volume (ml) of the 0.01 M NaOH solution.

The sulfonation degree (*SD*), which is defined as the molar ratio of sulfonic acid to monomer units of the grafted polymer chain, can be determined using the results of titration analysis and calculated by the following equation:

$$SD(\%) = \frac{0.01 \times V_{NaOH}}{W_{dry} \times \frac{GD}{(100 + GD)} / M} \times 100 \quad (2-4)$$

### 2.4.3. Proton conductivity

An in-plane proton conductivity of membranes was measured by ac impedance method with two platinum wires as electrodes using the LCR HiTESTER 3522-50 over frequency range of  $10^{-1}$  -  $10^2$  kHz at ac amplitude of 0.1 V. The ac impedance measurement was carried out in an ESPEC PR-2K temperature/humidity-controlled chamber with a working humidity range between 30 and 98% of relative humidity (RH) and temperature range of 30 – 80 °C. Membranes were equilibrated in the climate chamber at the specified RH and temperature to a constant resistance before recording the data. The proton conductivity  $\sigma$  was, then, calculated by

$$\sigma(S/cm) = \frac{h}{R \times A} \quad (2-5)$$

where  $h$  (cm) is the distance between the two electrodes,  $R$  ( $\Omega$ ) is the membrane resistance, and  $A$  ( $cm^2$ ) is the area of membranes. Schematic diagram of the conductivity measurement cell for proton conducting membranes is illustrated in **Fig. 2-3**.

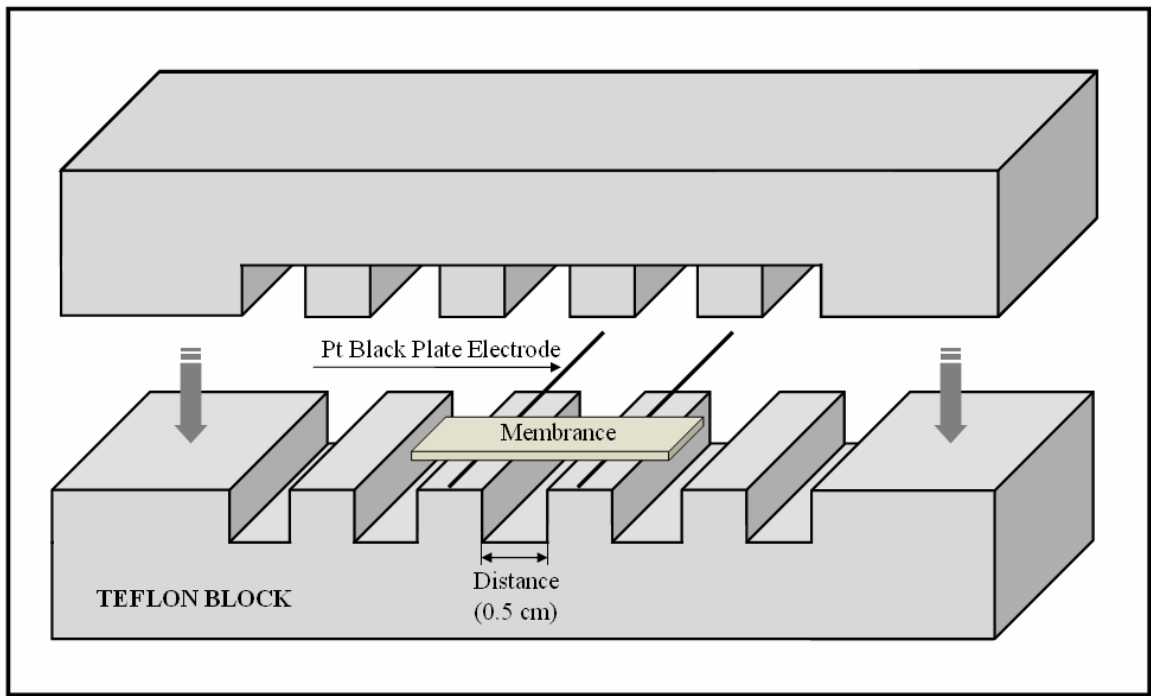


**Fig. 2-3.** Schematic diagram of the conductivity measurement cell for proton conducting membranes.

#### 2.4.4. Mechanical properties

Typical parameters of interest relating to mechanical properties include stress at maximum, stress at break, elongation at maximum, elongation at break, and Young's modulus or modulus of elasticity. For fuel cell application, stress at maximum (tensile strength) and elongation at break are important to be considered [4,5]. The term stress is used to express the loading in terms of force applied to a certain cross-sectional area of an object and calculated using:

$$\text{Stress} = \frac{\text{Force}}{\text{Cross-section area}} \quad (2-6)$$

Strain is the response of a system to an applied stress and calculated using:

$$\text{Strain} = \frac{l - l_o}{l_o} = \frac{\Delta l}{l_o} \quad (2-7)$$

where  $l_o$  is the original gauge length,  $l$  is the gauge length of extension, and  $\Delta l$  is the gauge length of specimen.

Tensile test was performed using an STA-1150 (A&D Co., Ltd, Japan) and Instron-4302 universal testing instrument at a constant crosshead speed of 10 mm/min. The mechanical properties of grafted-ETFE and ETFE-PEMs under dry state at 25 °C and under 100% RH at 80 °C were measured by the STA-1150 instrument and under dry condition (0% RH) at 80 °C were measured by Instron-4302 machine. Experimental equipments of tensile test of STA-1150 (A&D Co., Ltd, Japan) and Instron-4302 universal testing instrument are showed in **Fig. 2-4**.

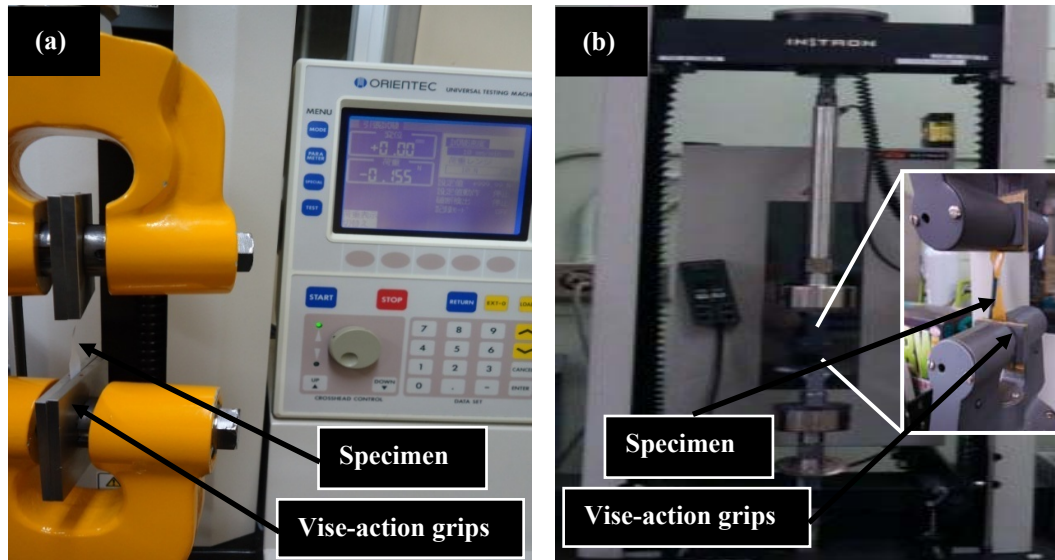


**Fig. 2-4.** Experimental equipments of tensile test: (a) STA-1150 (A&D Co., Ltd, Japan) and (b) Instron-4302 universal testing instrument.

For tensile test under 100% RH at 80 °C, a temperature-controlled water tank was used to set the desired temperature and relative humidity for testing (**Fig. 2-5**). From five to ten specimens with a dumbbell shape ( $1 \times 6.3 \text{ cm}^2$  in total and  $0.3 \times 2.6 \text{ cm}^2$  in test area) were prepared by ASTM D 1882-L instrument and each specimen subjected to a tensile test in the machining direction (**Fig. 2-6**).

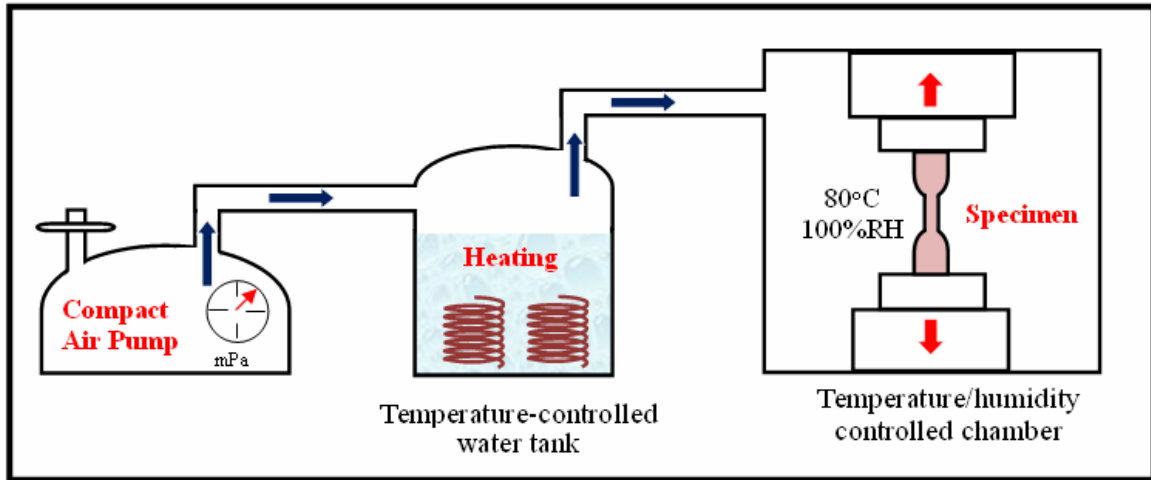


Fig. 2-5. Schematic diagram of mechanical measurement under 100% RH at 80 °C.

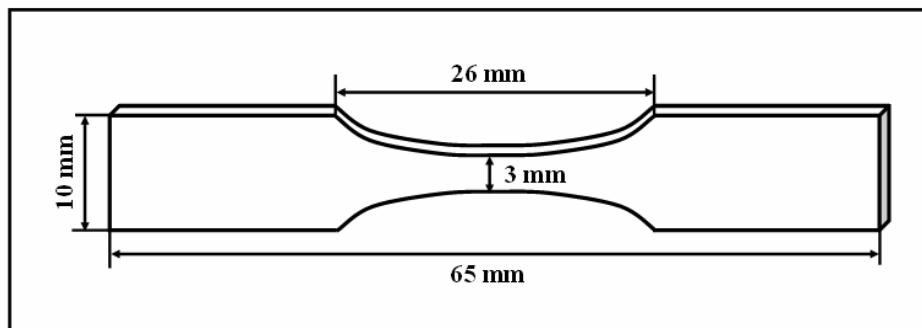


Fig. 2-6. A dumbbell-like shape of specimen for mechanical measurement.

## 2.5. Characterization

### 2.5.1. Thermo gravimetric analysis

Thermo gravimetric analysis (TGA) was performed in the temperature range from 25 °C to 600 °C at a heating rate of 10 °C/min using a Thermal Plus2/TG-DTA8120 (Rigaku, Japan). For ETFE-PEMs, the data was recorded after the membrane was kept at 150 °C for 30 min to remove excess water and solvents. The TGA curves were differentiated and then selected the minima of the derivative to determine the decomposition temperature. The thermal degradation onset temperature of the samples measured by TGA was used as a reference for DSC measurement.

### 2.5.2. Differential scanning calorimetry

Differential scanning calorimetry (DSC) was carried out using Thermo Plus2/DSC8230 (Rigaku, Japan) at a heating rate of 10 °C/min in a temperature range of 30 - 330 °C. Indium ( $T_m = 156.6$  °C), lead ( $T_m = 327.5$  °C), and tin ( $T_m = 231.9$  °C) standards were used for the temperature and energy calibration. A nitrogen gas pure through the specimens was kept a constant rate of 100 ml/min and the samples were cut to yield weight of 4 – 5 mg for both DSC and TGA measurements. The degree of crystallinity of samples was determined as:

$$DC(\%) = \frac{\Delta H_m}{\Delta H_{m100}} \times (1 + GD\%) \times 100 \quad (2-8)$$

where  $\Delta H_m$  is the heat of fusion of films, determined by the area of the melting peak and  $\Delta H_{m100}$  is the heat of fusion of 100% crystalline ETFE (113.4 J/g) [6,7].

### 2.5.3. Field emission scanning electron microscope observation

The surface morphologies of samples were observed by a Jeol JSM-6700F FE-SEM. The membranes were pre-treated by immersing the membranes into AgNO<sub>3</sub> 0.5 M solution for 14 hours at RT and then, were washed with pure water for one day at RT. Samples were then, equilibrated for several days in the ambient conditions under which it was observed. By SEM observation, all membranes were sputtered with a 2 nm gold layer. Images were obtained using a SEI mode of FE-SEM with an accelerating voltage of 5 kV and working distance of ~ 10 mm.

### 2.5.4. Small and ultra angle X-ray scattering (SAXS/USAXS) measurement

#### 2.5.4.1. Measurement

The principle of SAXS measurement is showed in **Fig. 2-7**. SAXS measurements were performed at the National Institute of Material Science (NIMS) and at Super Photon ring-8 GeV (SPring-8), Japan. At NIMS, two fine-focus SAXS instruments with Mo-K<sub>α</sub> ( $\lambda_{\alpha} = 0.07$  nm; Rigaku NANO-Viewer, Tokyo, Japan) and Cr-K<sub>α</sub> ( $\lambda_{\alpha} = 0.23$  nm; Bruker NanoSTAR, Germany) X-rays were utilized. The characteristic K<sub>α</sub>-radiation was selected and focused by two-dimensional confocal mirrors and Göbel mirrors for the Mo- and Cr-SAXS, respectively. The 2D scattering X-rays were then recorded using a multi-wire gas-filled 2D detector (Bruker, HiStar, Germany). The sample–detector distance was 35 cm for the Mo-SAXS and 105.6 cm for the Cr-SAXS (**Fig. 2-8** and **Fig. 2-9**).

At SPring-8, SAXS measurement was performed by USAXS at beam line BL19B2 using the incident X-ray energy of 18 keV ( $\lambda = 0.0688$  nm). The scattering X-rays were detected by the two-dimensional hybrid pixel array detectors, PILATUS (pixel apparatus) (**Fig. 2-10**). A sample- detector distance is 42 m converting to  $q$ -range of  $0.0038 \text{ nm}^{-1} \leq q \leq 0.242 \text{ nm}^{-1}$  where  $q$  is referred to as the modulus of the scattering vector given by

$$q = \frac{4\pi}{\lambda} \times \sin(\theta) \quad (2-9)$$

where  $2\theta$  is the scattering angle and  $\lambda$  is the wavelength of the incident radiation. Thus, both pinhole SAXS measurement at NIMS and SPring-8 were carried out to cover a wide  $q$ -range observation ( $0.0038 \text{ nm}^{-1} \leq q \leq 10.5 \text{ nm}^{-1}$ ) corresponding to a large Bragg spacing ( $d$ -spacing) scale ( $0.6 \text{ nm} \leq d \leq 1650 \text{ nm}$ ) with

$$d = \frac{2\pi}{q} \quad (2-10)$$

All the SAXS profiles after subtracting noise and background were converted to the absolute intensity by using the secondary standard of glassy carbon [8]. Because both SAXS instruments consist of a pinhole collimation system with a beam diameter of less than 1 mm, SAXS profiles can be obtained with high resolution, low background, and no considerable smearing data.

Hydrated samples had twice measured continuously at SPring-8 to obtain SAXS profiles to ensure that there were no artifacts due to water evaporation. **Fig. 2-11** shows SAXS profiles of ETFE-PEM with  $GD$  of 117% which possessed highest water uptake (145%). The SAXS profiles of two measurements were identical indicates that there were no variation in SAXS data were detected.

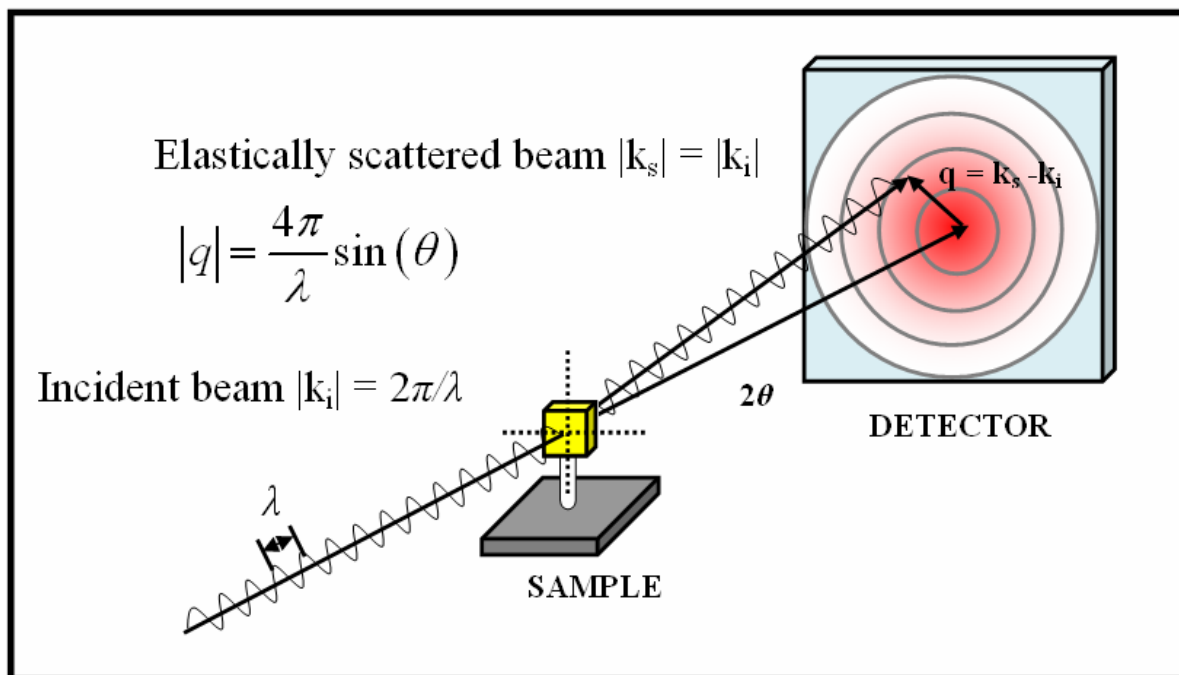


**Fig. 2-7.** Principle of SAXS measurement.



Fig. 2-8. SAXS at NIMS (Cr X-ray source).

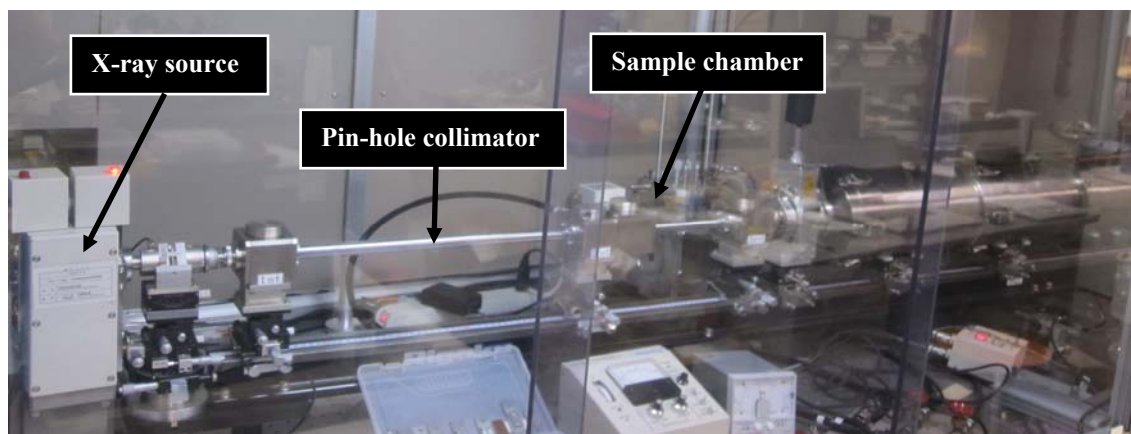


Fig. 2-9. SAXS at NIMS (Mo X-ray source).

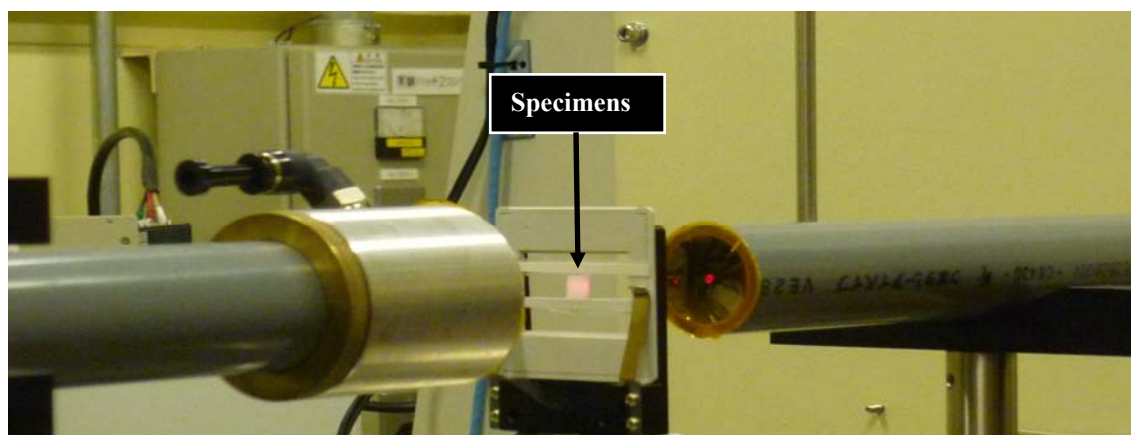
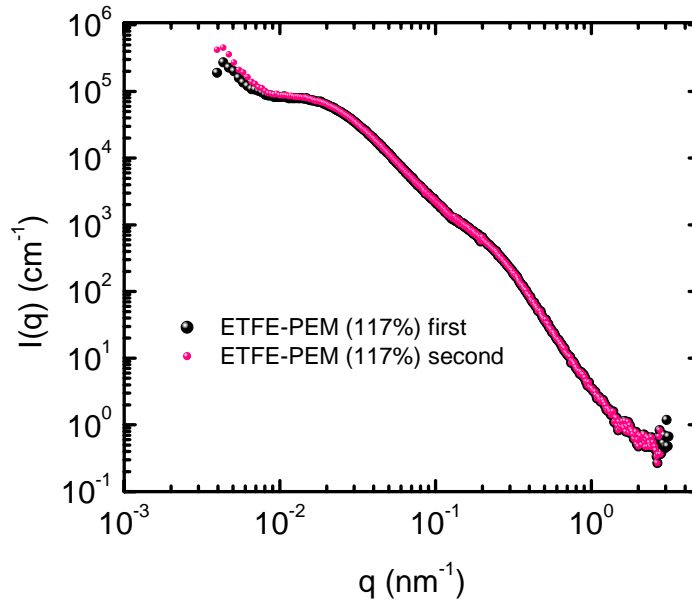


Fig. 2-10. SAXS at Spring-8 (Synchrotron X-ray source).



**Fig. 2-11.** SAXS profiles of ETFE-PEM with *GD* of 117% and water uptake is of 145%. SAXS data were recorded in three minutes to obtain the first profile and then recorded in another three minutes to obtain the second profile.

#### 2.5.4.2. Analysis of SAXS profiles

##### Porod's law

In the analysis of SAXS profiles, Porod's law is often used to investigate the interfacial behavior of two-phase system. The theory of small-angle scattering by isotropic two-phase systems predicts a decrease of the intensity proportional  $s^{-4}$  at large values of  $s$  (where  $s = q/2\pi$ ), known as Porod's law. In other words,

$$\lim_{s \rightarrow \infty} [I_p(s)] = \frac{K_p}{s^4} \quad (2-11)$$

where  $K_p$  is the so-called Porod-law constant [9]. The calculation of  $K_p$  is crucial because it is related to several certain structural parameters of the system, that is

$$K_p = \frac{S}{V} \cdot \frac{Q}{8\pi^3 \varphi_1 \varphi_2} = \frac{Q}{2\pi^3 l_p} \quad (2-12)$$

where

$$Q = 4\pi \int_0^\infty s^2 I(s) ds = V \varphi_1 \varphi_2 (\rho_1 - \rho_2)^2 \quad (2-13)$$

and  $(S/V)$  is the area of interface per unit volume,  $\varphi_1$  and  $\varphi_2$  are the volume fractions of the phases and  $\rho_1$  and  $\rho_2$  are the respective electron densities. The Porod invariant ( $Q$ ) and the Porod inhomogeneity length ( $l_p$ ) serves as a measure of the average sizes of the phases [10-12].

SAXS profiles of clear two-phase system obey  $q^{-4}$  scaling in Porod's region. On the other hand, systems with continuous symmetry do not have sharp interface and result in the deviations from Porod's law.

### **Lorentz correction**

In semicrystalline polymers, Lorentz correction has been utilized in numerous analyses of SAXS profiles in order to determine the precise  $q$ -position of the scattering maximum of the lamellar periods [13,14]. The general approach for the Lorentz correction for semicrystalline polymers is given as follows:

$$I(q) = k \theta^n I_{obs}(2\theta), \quad (2-14)$$

where  $k$  is a constant and  $n = 0$  and  $2$  for well-oriented and partially (or non) oriented samples, respectively.

## Diffuse phase boundary structure

In semicrystalline polymer, a diffuse phase boundary between crystalline and amorphous phase often occur. The existence of the diffuse phase boundary results in a depletion of high-angle scattering which causes the negative deviations from Porod's law. Determining of diffuse-boundary width is of highly interest because it may affect the mechanical properties of polymer material. Theory of determining of diffuse-boundary width from the deviations of Porod's law can be described as follow.

It is well know that the observed scattering intensity  $I_{obs}(s)$  is the Fourier transform of the autocorrelation  $\Gamma_{\rho}(r)$  of the scattering length density  $\rho(r)$  given by [2,10-12]

$$I_{obs}(s) = \int_{-\infty}^{\infty} \Gamma_{\rho}(r) e^{-iqr} dr \quad (2-15)$$

in which

$$\Gamma_{\rho}(r) = \rho^{*2}(r) = \int_{-\infty}^{\infty} \rho(u)\rho(u+r) du. \quad (2-16)$$

In a system exiting the diffuse boundary between two phases,  $\rho(r)$  can be described as the convolution product of the ideal scattering length density with sharp boundary  $\rho_{id}(r)$  and a smoothing function  $h(r)$  such that

$$\rho(r) = \rho_{id}(r) * h(r). \quad (2-17)$$

Thus,

$$I_{obs}(r) = F\{\rho^{*2}(r)\} = F\{\rho_{id}^{*2}(r)\} F\{h^{*2}(r)\} \quad (2-18)$$

where  $F\{\}$  represents a one-dimensional Fourier integral. According to Porod, the scattered intensity of ideal two-phase systems with sharp boundaries should decrease as  $s^{-4}$  at large values of  $s$ . In order words,

$$F\{\rho_{id}^{*2}(r)\} = \lim_{s \rightarrow \infty} [I_p(s)] = \frac{K_p}{s^4} \quad (2-19)$$

where  $I_p(s)$  is the Porod intensity. Thus,

$$\lim_{s \rightarrow \infty} [I_{obs}(s)] = \frac{K_p}{s^4} H^2(s) \quad (2-20)$$

where  $H(s)$  is the Fourier transform of the smoothing function  $h(r)$ , a function describing the electron density profile across the interface due to diffuse phase boundary (**Fig. 2-12**). The effect of the diffuse boundary between two phases has been found to induce the negative deviation from the Porod's law.

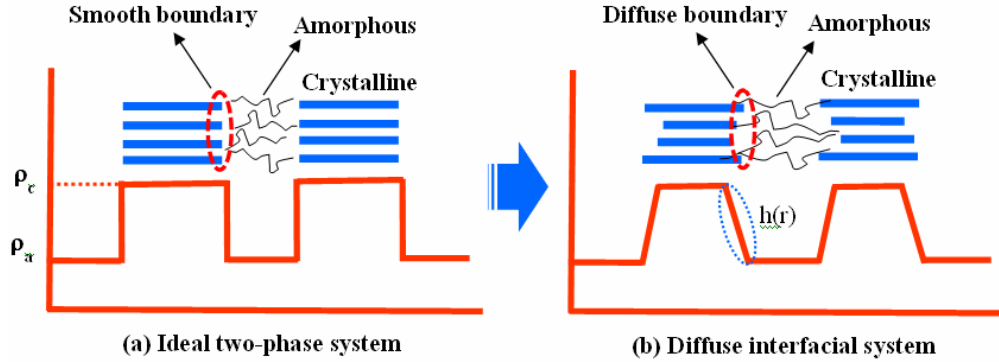


**Fig. 2-12.** Illustrations of (a) ideal two-phase system and (b) diffuse interfacial system.  $h(r)$  is the smoothing function, a function describing the electron density profile across the interface due to diffuse phase boundary.

The thermal density fluctuation in the real polymer system, on the other hand, results in the positive deviations from the Porod's law. Therefore, the scattered intensity at high  $s$  range describing in (2-20) should remove contributions of background intensity  $I_B(s)$  by determination of diffuse phase boundary. In other words, we can rewrite (2-20) at high  $q$  range as

$$I_{obs}(s) - I_B(s) = \frac{K_p}{s^4} H^2(s). \quad (2-21)$$

If the smoothing function  $h(r)$  is a Gaussian function,

$$h(r) = \frac{1}{\sqrt{2\pi}\sigma} e^{-\frac{r^2}{2\sigma^2}} \quad (2-22)$$

its Fourier transform  $H(s)$  is given by

$$H(q) = e^{-2\pi^2\sigma^2s^2} \quad (2-23)$$

where  $r$  is a space variable and  $\sigma$  is the standard deviation of the Gaussian smoothing function and is a measure of the diffuse phase boundary thickness. Combining equations of (2-21) and (2-23) leads to

$$\ln\{q^4 [I_{obs}(q) - I_B(q)]\} = \ln(K) - \sigma^2 q^2 \quad (2-24)$$

with  $K = (2\pi)^4 K_p$ .

For  $\sigma s \ll 1$ , the equation (2-23) can be rewritten as

$$H(q) \approx 1 - 2\pi^2\sigma^2s^2 \quad (2-25)$$

Substitution of (2-25) into (2-21) we can write

$$q^4 [I_{obs}(q) - I_B(q)] = (2\pi)^4 K_p - (2\pi)^4 K_p \sigma^2 q^2 \quad (2-26)$$

If the smoothing function  $h(r)$  is a rectangular function (or box function),

$$h(x) = \begin{cases} = \frac{1}{E} & \text{for } |x| < \frac{E}{2} \\ = 0 & \text{for } |x| > \frac{E}{2} \end{cases} \quad (2-27)$$

its Fourier transform  $H(s)$  is given by

$$H(s) = \frac{\sin(\pi Es)}{\pi Es} \quad (2-28)$$

For  $sE \ll 1$ , the equation (2-23) can be rewritten as

$$H(q) \approx \frac{1}{\pi Es} \left[ \pi Es - \frac{1}{3!} \cdot (\pi Es)^3 + \frac{1}{5!} \cdot (\pi Es)^5 - \dots \right] \quad (2-29)$$

Truncating the series (2-29) after second term and then substitution it into (2-21) gives

$$q^4 [I_{obs}(q) - I_B(q)] = (2\pi)^4 K_p - (2\pi)^4 K_p \cdot \frac{q^2 E^2}{12} \quad (2-30)$$

Combining equation (2-30) and (2-26) leads to

$$E = \sqrt{12}\sigma. \quad (2-31)$$

## Background correction in high $q$ -range

In the high- $q$  range of SAXS profiles of polymer materials, the background scattering due to thermal scattering (also known as liquid scattering) and amorphous phase scattering are crucial [15,16]. The background scattering intensity  $I_B(q)$  over the entire  $q$  range must contribute as an additional intensity component in the small-angle scattering. Thus, the net scattering intensity ( $I_{net}(q)$ ) due to the morphology and structure of polymers can be obtained by background subtraction:

$$I_{net}(q) = I_{obs}(q) - I_B(q), \quad (2-32)$$

where  $I_{obs}(q)$  is the observed scattering intensity.

Among the several expressions for the background pattern, the following empirical equations proposed by Ruland and Vonk have been commonly employed [10,17,18]:

$$I_B(q) = Fl e^{aq^2} \quad (2-33)$$

$$I_B(q) = Fl + bq^n, \quad (2-34)$$

where  $Fl$ ,  $a$ ,  $b$ , and  $n$  (an even integer between 0 and 10) are arbitrary constants. Moreover,  $Fl$  is independent of  $q$  and is the so-called electron density fluctuation and accounts for the thermal scattering. The electron density fluctuation (short term: density fluctuation) originates from the statistical variations of the electron density within the polymer material owing to thermal motion and/or lattice imperfections such as disorder, distortion, and point defects [15-20]. In particular,  $Fl$  was found to be proportional to the SAXS intensities extrapolated toward a zero angle, as shown in the following equation:

$$Fl = \lim_{q \rightarrow 0} I_{obs}(q) = \frac{\langle N^2 \rangle - \langle N \rangle^2}{\langle N \rangle}, \quad (2-35)$$

where  $N$  is the number of electrons in an object volume. However, the background intensity in the observed scattering data is expressed with  $q$ -dependent terms, such as  $e^{aq^2}$  in equation (2-23) and  $bq^n$  in equation (2-34), because polymer samples generally exhibit an additional amorphous halo scattering pattern in the high- $q$  range [17]. The background scattering intensity, evaluated as a deviation from Porod's law, depends on the crystallinity of the polymers for a given temperature and thermal history [20,21]. Thus, careful background

correction in the high- $q$  range from the observed scattering intensity is expected to reveal some hidden information about polymer structures.

The following procedures were employed to determine  $I_B(q)$  for the original ETFE film, grafted ETFE film, and ETFE PEM.

- (1) To roughly determine the parameters  $Fl$ ,  $b$ , and  $n$ , the observed scattering intensity  $I_{obs}(q)$  was first fitted to empirical Vonk's equation (2-34) such that the slope of the plots of  $I_{obs}(q)$  vs.  $q^n$  seemed to be straight in the region where the observed scattering intensities were negligible.
- (2) Using the roughly estimated  $I_B(q)$ , the ratio of the background scattering intensity  $I_B(q)$  to the observed scattering intensities  $I_{obs}(q)$  ( $I_B(q)/I_{obs}(q) \times 100$ ), which is defined as the "contribution factor," was plotted over the entire  $q$  range.
- (3) The roughly estimated parameters  $Fl$ ,  $b$ , and  $n$  were again optimized such that the contribution factors plotted over the entire  $q$  range were as large as possible but did not exceed 100% (in this case, <105%) in the high- $q$  range in order to avoid overestimation of the background that would make the values of  $I_B(q)$  larger than those of the observed scattering intensities.

### **Scattering features at low $q$ -range**

The power law of SAXS profiles in low  $q$ -range can provide information related to the shape of the object, provided that one far enough away from any influence of coherent scattering due to the crystalline component [2,3]. In order works, the positions of individual particles, far apart from each other, are assumed to be uncorrelated. Under this case, the waves scattered from different particles are incoherent among them, and the observed SAXS intensity simply becomes a sum of the individual scattering. A power law decays in intensity at low  $q$ -range,  $I(q) \sim q^{-\alpha}$ , with  $\alpha = 4$  for spheres (three dimensional), 2 for thin disks (two dimensional), and 1 for long cylinders (one dimensional).

## References

- 1) K. Kato, E. Uchida, E-T. Kang, Y. Uyama, Y. Ikada, *Prog. Polym. Sci.* 28 (2003) 209-259.
- 2) N. Stribeck, *X-ray scattering of soft matter*, Springer, 2007.
- 3) R.J. Roe, *Method of X-ray and neutron scattering in polymer science*, Oxford University Press, pp. 147-154, 2000.
- 4) H.B. youcef1, S. AlkanGürsel1, A. Buisson, L. Gubler, A. Wokaun, G.G. Scherer, *Fuel cell* 10 (2010) 401-410.
- 5) S. Hasegawa, S. Takahashi, H. Iwase, S. Koizumi, N. Morishita, K. Sato, T. Narita, M. Ohnuma, Y. Maekawa, *Polymer* 52 (2011) 98-106.
- 6) S.A. Gürsel, J. Schneider, H.B. youcef, A. Wokaun, G.G. Scherer, *J. Appl. Polym. Sci.* 108 (2008) 3577-3585.
- 7) M.M. Nasef, H. Saidi, K.Z.M. Dahlan, *Radiat. Phys. Chem.* 68 (2003) 875-883.
- 8) F. Zhang, J. Ilavsky, G.G. Long, J.P.G. Quintana, A.J. Allen, P.R. Jemian, *Metal. Mater. Trans. A.* 41A (2010) 1151-1158.
- 9) G. Porod, *Kolloid-Z.* 124 (1951) 83-114.
- 10) J.T. Koberstein, B. Morra, R.S. Stein, *J. Appl. Cryst.* 13 (1980) 34-45.
- 11) M.H.J. Kim, *J. Appl. Cryst.* 37 (2004) 643-651.
- 12) W. Ruland, *J. Appl. Cryst.* 4 (1971) 70-73.
- 13) R.J. Matyi, B. Crist, *J. Polym. Sci. Polym. Phys. Ed.* 16 (1978) 1329-1354.
- 14) F. Cser, *J. Appl. Polym. Sci.* 80 (2001) 2300-2308.
- 15) C.G. Vonk, *J. Appl. Cryst.* 6 (1973) 81-86.
- 16) J. Rathje, W. Ruland, *Colloid & Polymer Sci.* 254 (1976) 358-370.
- 17) W. Wigand, W. Ruland, *Colloid & Polymer Sci.* 257 (1979) 449-456.
- 18) J.H. Wendorff, E.W. Fischer, *Colloid & Polymer Sci.* 251 (1973) 876-883.
- 19) W. Ruland, *Pure & Appl. Chem.* 49 (1977) 905-913.
- 20) C.J. Chen, G.S.Y. Yeh, *Colloid & Polymer Sci.* 269 (1991) 353-363.
- 21) W. Ruland, *Colloid & Polymer Sci.* 255 (1977) 417-427.

## Chapter 3. Properties of graft-type PEM

### 3.1. Introduction

As mentioned in Chapter 1, higher proton conductivity at low relative humidity (< 50% RH) and superior mechanical property under humidified condition (100% RH) at high temperature (> 80 °C) are main concern for PEM fuel cell because they govern the power generation efficiency and durability at severe operating conditions in fuel cell systems. It is well-known that the proton conductivity of PFSA membranes such as Nafion drops significantly under above conditions, leading to the decrease in fuel cell performance. This has triggered an extensive research and development of alternative membrane materials. The graft-type PEM is one of the promising candidates to overcome the above problems because such material comprises the substrate films having mechanically tough crystalline phase and various functional grafted polymer phases directly bond to the polymer main chain. In addition, introduction of sulfonated graft side chains in polymer main chain is an excellent way to prepare PEM materials because of the easy control of *IEC* values by a grafting degree and pronounced hydrophilic/hydrophobic phase-separated structures by sulfonation. Thus, in this chapter, the effects of RH on the conductance under 30%RH and mechanical properties (tensile strength, elongation at break) under 100%RH at 80 °C of graft-type ETFE-PEMs as a function of *IEC* (0–3.3 mmol/g) are discussed in comparison to Nafion-212. In addition, thermal stability and crystallinity evaluated using thermo gravimetric analysis (TGA) and differential scanning calorimetry (DSC), respectively were also addressed.

### 3.2. Preparation and electrochemical properties of ETFE-PEM

**Scheme 3-1** shows the preparation procedures for the ETFE-PEMs consisting of the hydrophilic polystyrene sulfonic acid grafts. Toluene has been found to be an effective solvent for styrene graft polymerization onto the ETFE films [1]. Under a constant dose rate of 15 kGy/h at 60 °C, we controlled the *GDs* ranging from 4.2% to 128% by changing the styrene concentration (10%–100%) and grafting time (1–54 h), as listed in **Table 3-1**. The grafted films with 8.8%–128% *GDs* converted the poly(styrene sulfonic acid)-grafted ETFE (ETFE-PEM) with *IECs* ranging from 0.52 to 3.3 mmol/g using sulfonation reactions in 0.2 M chlorosulfonic acid and 1,2-dichloroethane at 50 °C for 6 h. A large number of styrene sulfonic acid groups (high *IEC* values) make it possible to significantly enhance the conductivity. As expected, the proton conductivity (0.002–0.233 S/cm) and water uptake (2.7%–168%) increased with increasing *IEC* of the ETFE-PEMs. In addition, the ETFE-PEM, even with low *IEC* (2.0 mmol/g), exhibited a proton conductivity of 0.104 S/cm, which was higher than that of Nafion–212 (0.087 S/cm). Furthermore, the ETFE-PEM with a 2.7 mmol/g *IEC* showed a slightly higher water uptake than 100%. The results indicate that the ETFE-PEMs with *IECs* lower than 2.7 mmol/g (*GDs* <80%) possess high conductivities with moderate water uptakes under an equilibrated aqueous condition at room temperature. The electrochemical properties with low *IEC* (<2.4 mmol/g) are in good agreement with previously reported results [2,3].

### Scheme 3-1

Radiation induced-graft polymerization of styrene onto ETFE substrate and subsequent sulfonation for ETFE-PEM preparation.

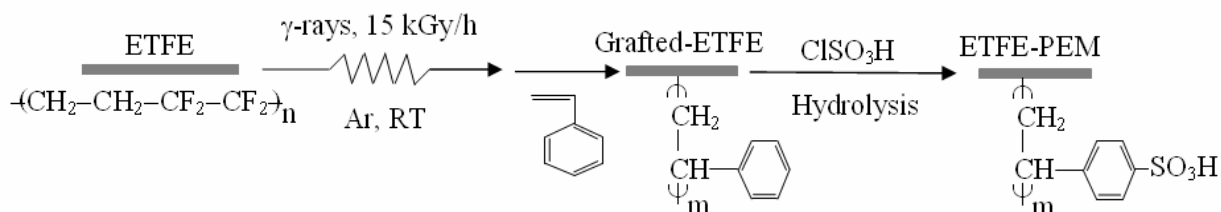


**Table 3-1**

Radiation induced-graft polymerization and sulfonation results and electrolyte properties of ETFE-PEM.

Sample	GD%	SD%	IEC (mmol/g)	$\sigma$ (S/cm)	Water uptake (%)
ETFE-PEM	4.2	-	-	0.002	2.7
ETFE-PEM	6.6	-	-	0.005	10
ETFE-PEM	8.8	71	0.52	0.007	11
ETFE-PEM	10	88	0.7	0.011	13
ETFE-PEM	19	90	1.3	0.060	21
ETFE-PEM	34	97	2.0	0.104	41
ETFE-PEM	59	87	2.4	0.120	74
ETFE-PEM	79	85	2.7	0.147	105
ETFE-PEM	102	83	2.9	0.173	127
ETFE-PEM	117	84	3.1	0.229	145
ETFE-PEM	128	87	3.3	0.233	168
Nafion-212	-	-	0.8	0.087	39

### 3.3. Grafting degree dependence of thermal stability, mechanical properties, and crystallinity

The *GD* dependence of thermal stability for grafted-ETFE films and ETFE-PEMs with *GDs* between 0%–128% was evaluated using the TGA profiles even though the decomposition behavior of grafted-ETFE films and ETFE-PEMs with relatively low *GD* (<55%) have been previously reported in References [4,5]. As reported, the grafted-ETFE films showed that the TGA profiles had two decomposition steps. One was located between 397–415 °C (Step 1) and the other step was located between 480–488 °C (Step 2). These steps attributed to the decompositions of polystyrene grafts and the pristine ETFE backbone, respectively (**Fig. 3-1**). The TGA profiles of all the ETFE-PEMs consisted of three decomposition steps (**Fig. 3-2**) between 251–267 °C (Step 1), 371–404 °C (Step 2), and 485–493 °C (Step 3), which corresponded to the decompositions of sulfo groups polystyrene grafts, and the ETFE backbone, respectively [4,5].

**Fig. 3-3** shows the grafted-ETFE decomposition temperatures of Steps 1 and 2 as a function of the *GD*. Both decomposition temperatures slightly decreased with increasing *GD*. Owing to the clear separation of the polystyrene grafts decomposition (397–415 °C), the degradation temperatures of the ETFE backbone was determined to be between 480 and 488 °C in the grafted ETFE films, which was almost the same as that of the pristine ETFE film (478 °C). From the results, it should be noted that the introduction of polystyrene grafts did not cause any significant damage to the ETFE polymers of pristine ETFE film. **Fig. 3-4** shows the effects of *GD* (*IECs* of 0–3.3 mmol/g) on the ETFE-PEMs decomposition temperatures with the *GDs* up to 128%. Step 1 decomposition temperature of 251–267 °C was lower than the grafted-ETFE because the poly(styrene sulfonic acid) is thermally less stable compared to the corresponding polystyrenes. However, the degradation temperatures (Step 1) slightly increased with increasing *GD* (251–267 °C). Furthermore, the ETFE backbone decomposition temperatures (Step 3) were not affected by increasing *GD*, thus indicating that the sulfonation reaction did not cause any significant change to the ETFE polymers in the ETFE-PEMs even with high *GD* regions.

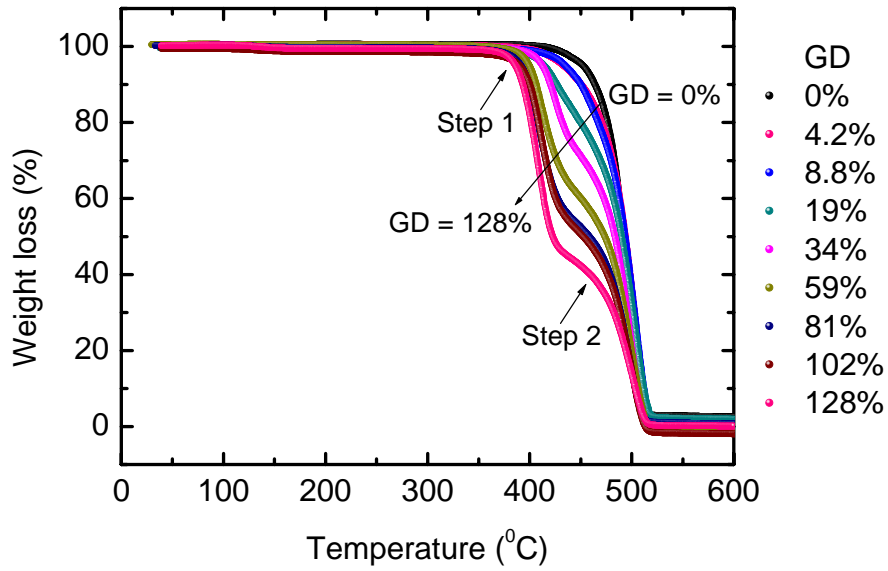


**Fig. 3-1.** TGA profiles of grafted-ETFE films with *GDs* of 0%–128%.

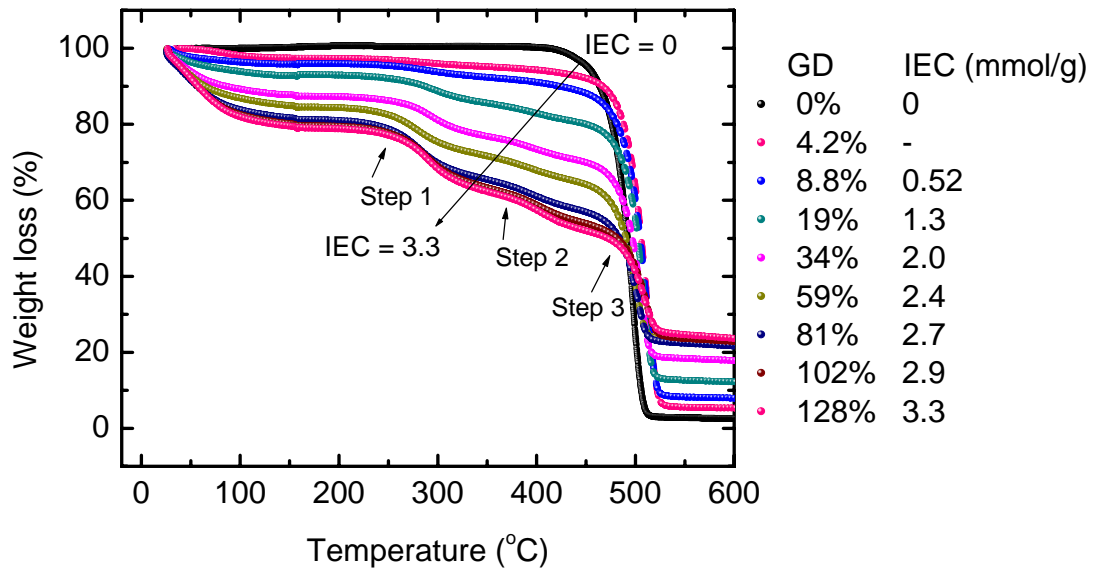


**Fig. 3-2.** TGA profiles of ETFE-PEM with *IECs* of 0–3.3 mmol/g.

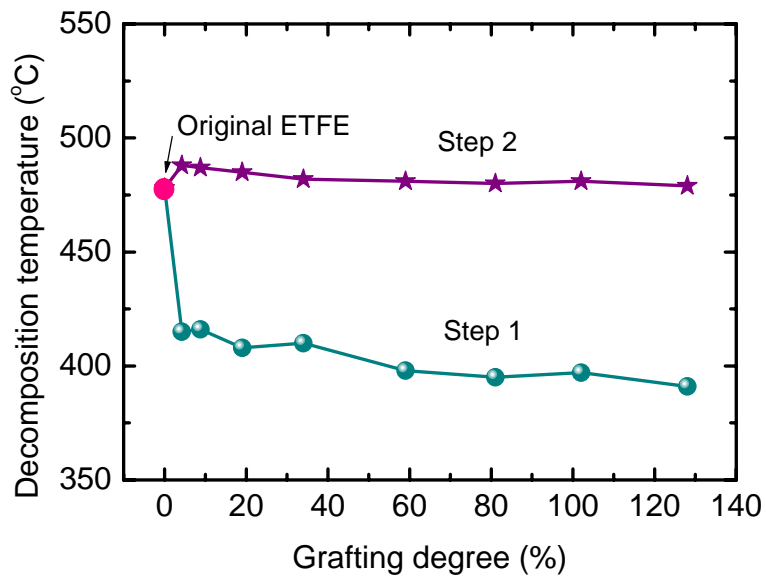


**Fig. 3-3.** Grafted-ETFE film decomposition temperatures of Steps 1 and 2 as a function of the *GD*.

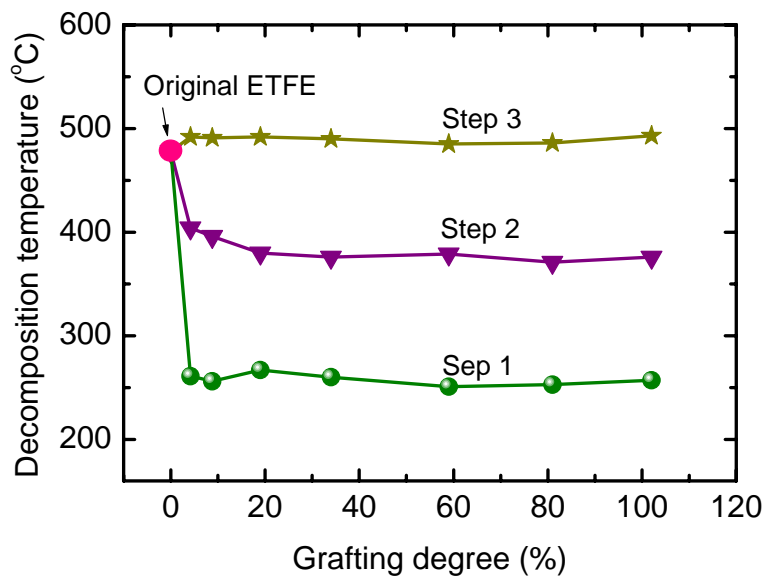


**Fig. 3-4.** The effects of *GD* on ETFE-PEM decomposition temperatures.

The *GD* dependence of mechanical properties of grafted-ETFE films with *GDs* up to 128% and ETFE-PEMs with *IECs* up to 3.3 mmol/g, such as tensile strengths (TS) and elongation at break, at room temperature is shown in **Fig. 3-5**. The ETFE-PEM mechanical properties with relatively low *GD* (<45%) have been reported in Reference [6]. All the grafted-ETFE films with various *GDs* exhibited similar TS, ranging from 36 to 44 MPa, compared to that the pristine ETFE film (46 MPa). As the *GDs* increased, the ETFE-PEM TS gradually decreased to 31 MPa. The grafted-ETFE and ETFE-PEM TSs, even *GDs* up to 128%, were much higher than that of Nafion-212 (25 MPa). The grafted-ETFE films and ETFE-PEMs exhibited nearly the same trend for the change of elongation at break with increasing *GD*; namely, the elongation at break of both films gradually decreased from 362% of the pristine ETFE film down to approximately 100% at 128% *GD*, as shown in **Fig. 3-5(b)**. Both the grafted-ETFE and ETFE-PEMs with *GDs* (>20%) possess higher TS, but lower elongation at break compared to Nafion-212. The *GD* dependence on TS and elongation at break can be reasonably explained by taking into account the mechanical properties of polystyrene and poly(styrene sulfonic acid) graft polymers for the grafted-ETFE and ETFE-PEMs, because both graft polymers have high TS and low elongation at break (very brittle). In other words, the both membranes exhibit the combined properties of ETFE and graft polymers.

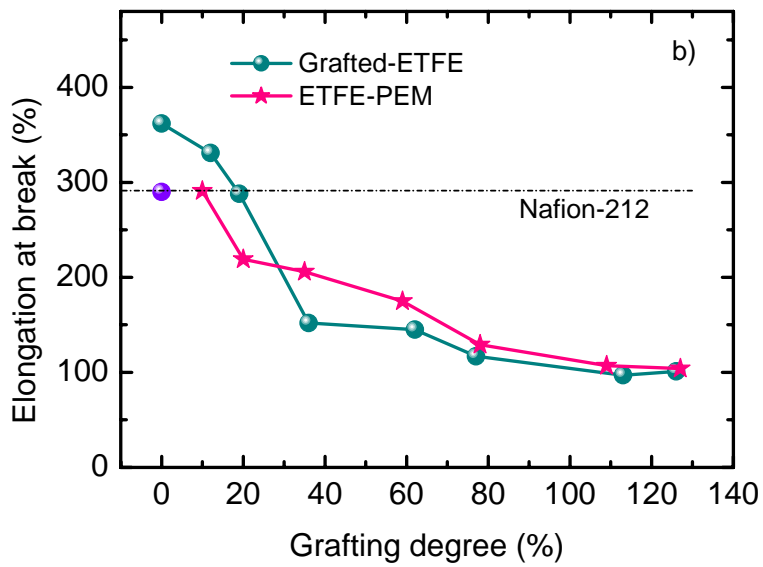
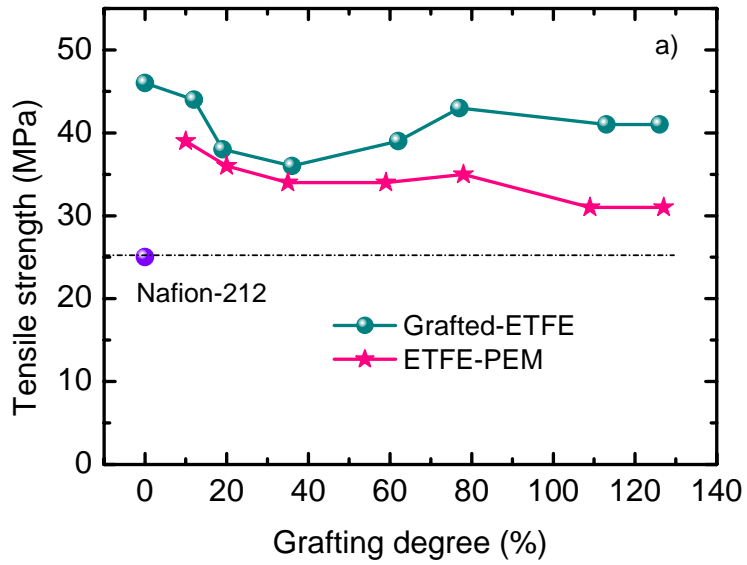


**Fig. 3-5.** The mechanical properties of grafted-ETFE films, ETFE-PEMs, and Nafion-212 as a function of *GD*: (a) tensile strength and (b) elongation at break at room temperature in the atmosphere.

The change in crystallinity of the pristine ETFE film by grafting and sulfonation processes were estimated using the comparison of DSC profiles between the pristine ETFE film, grafted-ETFE films, and ETFE-PEMs with various *GD*s (The DSC profiles are shown in **Fig. 3-6**). All the grafted-ETFE films with *GD* higher than 100% exhibited similar endothermic peaks at the same temperature range (247.5–246.4 °C), as the melting temperature ( $T_m$ ) of the pristine ETFE film (247.6 °C) (**Fig. 3-7**) [5,7,8]. The results show that the grafting process did not affect the crystalline structures of the ETFE film in the entire *GD* range. The ETFE-PEMs, even with high *GD*, showed similar  $T_m$  values (243.6–246.6 °C) compared to that of the pristine ETFE film. As the results indicate, the crystallinity of the grafted-ETFE and ETFE-PEMs can be estimated from the  $T_m$  endothermic peaks of ETFE polymers.

As shown in **Fig. 3-8**, the crystallinity of the grafted-ETFE films and ETFE-PEMs is evaluated by taking into account the dilution effect of the crystalline part of the pristine ETFE film using the introduction of amorphous polystyrene and poly(styrene sulfonic acid) in the grafted-ETFE films and ETFE-PEMs using Eq. 2-8 [5]. The crystallinity of the grafted-ETFE films decreased slightly from 35% (pristine ETFE) to approximately 32% as the *GD* increased up to 10%. However, the crystallinity appears to be independent of *GD*s higher than 10%; even the grafted-ETFE with 128% *GD* shows a crystallinity of 28.1%. In contrast, the crystallinity of the ETFE-PEMs decreased significantly (from 35.4% to 16.1%) in the *IEC* range lower than 2.4 mmol/g (*GD* <59%). In the *IEC* range higher than 2.7 mmol/g (*GD* > 81%), the crystallinity decreased gradually and then leveled off at approximately 7.6% for the PEM with an *IEC* of 3.3 mmol/g (*GD* = 128%). These results clearly suggest that only sulfonation, not the grafting process, induced severe damage to the lamellar crystals in the ETFE-PEM membranes. The crystallinity decrease in ETFE-PEMs is likely due to the attack of sulfonation reagents to the lamellar crystals and/or the subsequent hydrolytic process, which led to the clear phase separation between hydrophilic graft polymer and hydrophobic ETFE domains, thus resulting in the distortion of the lamellar crystals.

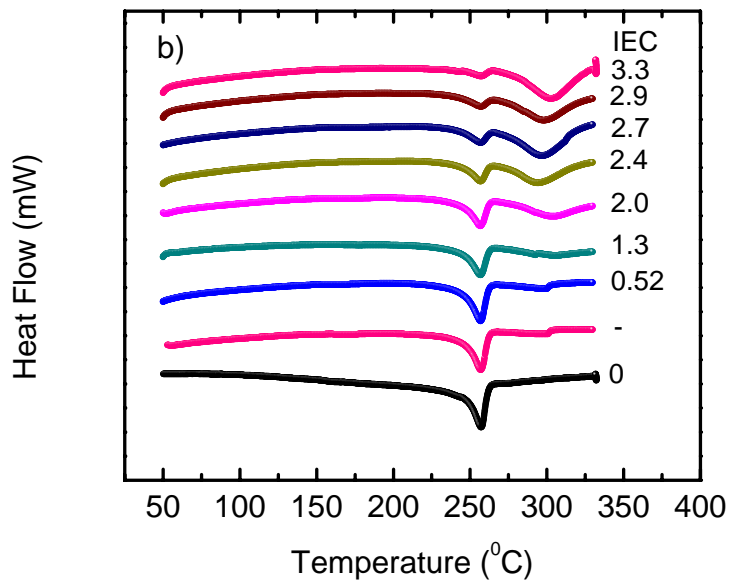
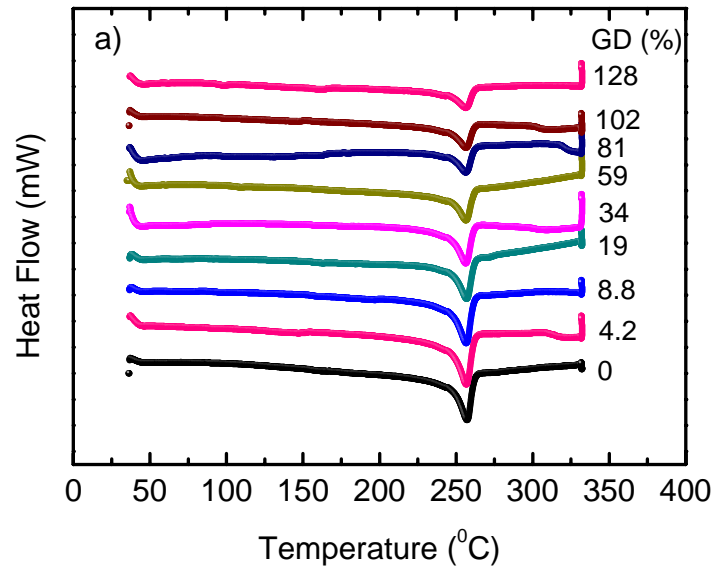


**Fig. 3-6.** DSC profiles of (a) grafted-ETFE films with *GDs* of 0%–128% and (b) ETFE-PEMs with *IECs* of 0–3.3 mmol/g.

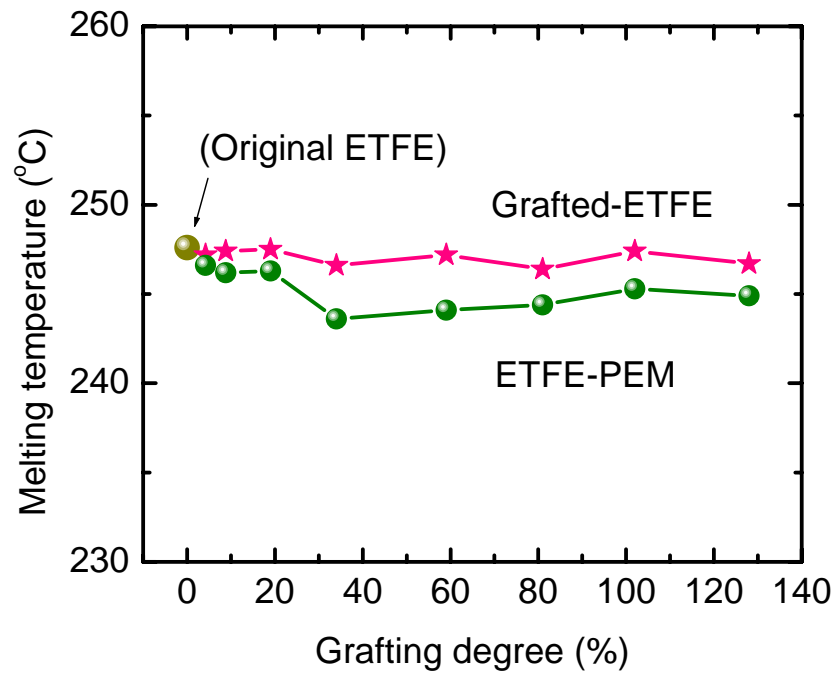


**Fig. 3-7.** Melting temperatures of original ETFE film, grafted-ETFE films, and ETFE-PEMs as a function of *GD*.

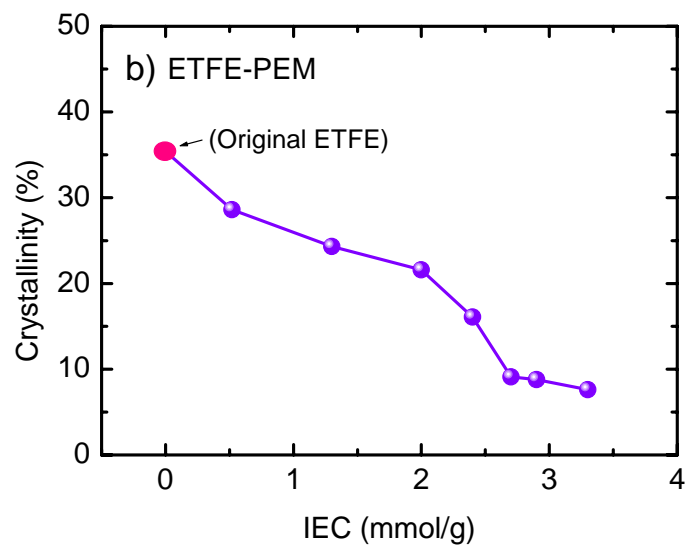
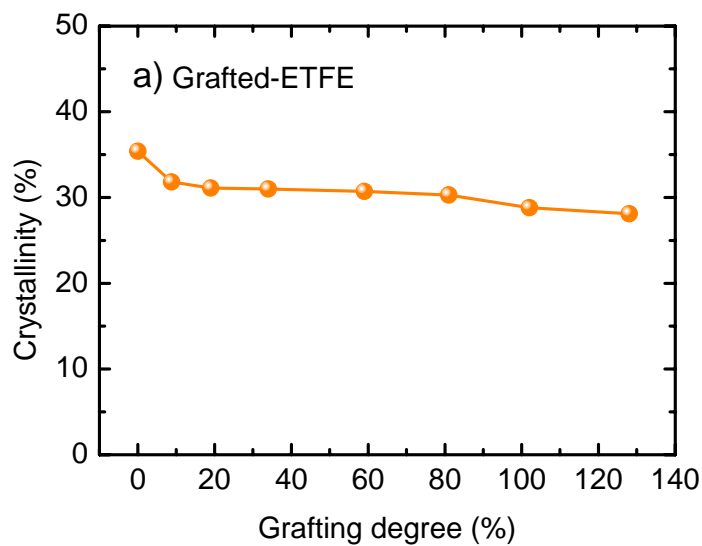


**Fig. 3-8.** Crystallinity of (a) grafted-ETFE films with *GDs* of 0%–128% and (b) ETFE-PEMs with *IECs* of 0–3.3 mmol/g.

### 3.4. Proton conductivity of ETFE-PEMs under various RH

As mentioned in the Introduction section, the RH dependence of proton conductivity and mechanical strengths are currently the main concerns due to these properties being directly related to the power generation efficiency and durability of the fuel cells. Thus, we examined the relative humidity (30%–98% RH) dependence of proton conductivity at 80 °C for the ETFE-PEMs with *IECs* of 1.3–2.9 mmol/g (*GD*: 19%–102%), together with those of Nafion–212 as a reference (**Fig. 3-9**).

The ETFE-PEMs with the various *IECs* covered a wide range of conductance with more than 3 orders of magnitude, ranging from  $1 \times 10^{-3}$  to  $5 \times 10^{-1}$  S/cm. At 30 and 98% RH, the proton conductivity ranges of the ETFE-PEMs were 0.001–0.013 S/cm and 0.16–0.52 S/cm, respectively. This result indicates that the conductance of ETFE-PEM increased with increasing *IEC* even at low RH (30% RH). ETFE-PEM with *IECs* higher than 2.7 mmol/g exhibited a higher proton conductivity compared to Nafion–212 ( $9 \times 10^{-3}$  S/cm) and much higher than sulfonated poly (arylene ether)s ( $1 \times 10^{-3}$  S/cm) [9] and sulfonated star-hyperbranched polyimides ( $\sim 1\text{--}5.5 \times 10^{-4}$  S/cm) [10] at the similar *IEC* values. In addition, RHs higher than 80%, the proton conductivity of ETFE-PEMs with *IECs* higher than 2.0 mmol/g were found to be comparable to or higher than the Nafion–212.

For the entire 30%–98% RH, the proton conductivity increased exponentially with RH; however, the increase rates start to slightly flatten out at higher RH. In order to further examine the conductivity RH dependence for each PEM, the slope values of  $\log(\text{conductivity})$  vs. RH were calculated because the slope values have been used as feasible parameters for evaluating conductance behavior of PEMs, which were designed for high conductivity under lower RH conditions [11, 12-14]. The slope value for an *IEC* of 1.3 mmol/g (*GD* = 19%) is 0.03. The slope values of the ETFE-PEMs decreased slightly with increasing *IEC*. An *IEC* of 2.9 mmol/g (*GD* = 102%) has a slope of 0.023. However, the *IEC* effect, ranging from 2.0 to 2.9 mmol/g (*GD* range of 34%–102%), on the slope value is not significant for the 30% to 98% RH range.

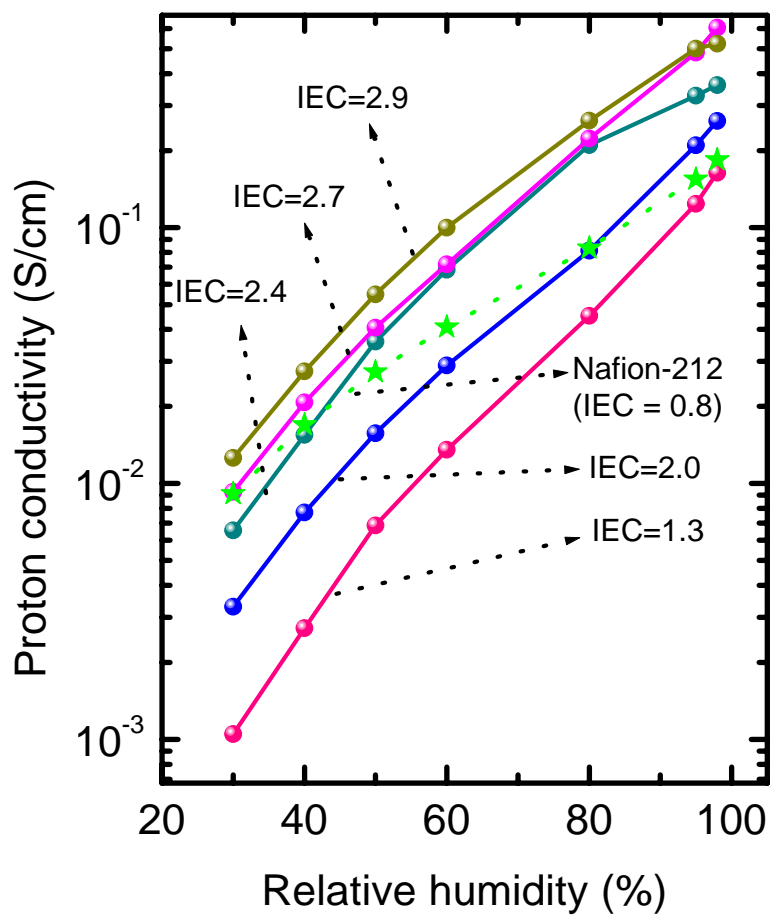


**Fig. 3-9.** Relative humidity dependence of proton conductivity at 80 °C for ETFE-PEMs with *IECs* of 1.3–2.9 mmol/g (*GD*: 19%–102%), together with those of Nafion–212 as a reference.

It is well known that Nafion-212 exhibits the least conductivity RH dependence (a slope value of 0.018) [14]. The following structural reasons are widely accepted: the Nafion contains well-separated ion-channels of several nanometers thus resulting in a superior channel connection under low RH conditions. In contrast, the aromatic hydrocarbon type PEMs, such as aliphatic/aromatic polyimide and ethynyl-terminated sulfonated-fluorinated poly(arylene ether)s, are generally subjected to significant change in conductance by 4 to 5 orders of magnitude. This corresponds to slope values of 0.027–0.048 when the RH increases from 20% to 90% [11]. Thus, the ETFE-PEM proton conductivity was less dependent on RH compared to the aromatic hydrocarbon-type PEMs. The ETFE-PEM slope with high *IECs* are similar to Nafion-212 rather than the aromatic hydrocarbon-type PEMs. This is likely because the hydrophilic grafted polymers show clearer phase separation from the hydrophobic ETFE substrate so that it retains conducting channels even under dry conditions (30% RH, 80 °C).

### 3.5. Mechanical properties at dry and humidified conditions

The PEM mechanical properties under humid conditions (100% RH), such as flooding, govern the durability under severe operating conditions of fuel cell systems because the PEMs absorb large amounts of water, which induces a large stress in the membranes resulting in the degradation. Thus, we examined the influence of the water uptakes to the change in PEM mechanical properties by observing the TS and elongation at break of the ETFE-PEMs with *IECs* of 0–3.3 mmol/g at 80 °C under dry and humidified conditions (0% and 100% RH). This was compared to Nafion-212 as a reference, as shown in **Fig. 3-10**. The ETFE-PEM TS at 0% RH increased slightly from 28 MPa (the pristine ETFE film) to 32 MPa (*IEC* = 2.9 mmol/g), whereas at 100% RH, the TS decreased significantly to 12 MPa and gradually to 7.3 MPa in the *IECs* of 0–2.0 and 2.0–3.3 mmol/g, respectively. The ETFE-PEM TS are mainly affected by water absorption in the hydrophilic graft polymer regions but not the introduction of graft polymers. The ETFE-PEM TS with the entire *IEC* range was much higher compared to the Nafion-212 (20 MPa) under dry conditions. Furthermore, the ETFE-PEMs with the *IECs* lower than 2.4 mmol/g showed higher TS than the Nafion-212 (10 MPa). It should be noted that when *IECs* increased beyond 2.4 mmol/g the TSs only decreased slightly to 7.3 MPa in

spite of the high water absorption condition. This result indicates that the increase of polystyrene sulfonic acid clusters and thus, water content at higher  $IECs$ , had less effect on the ETFE PEM TS under humid conditions (100% RH).

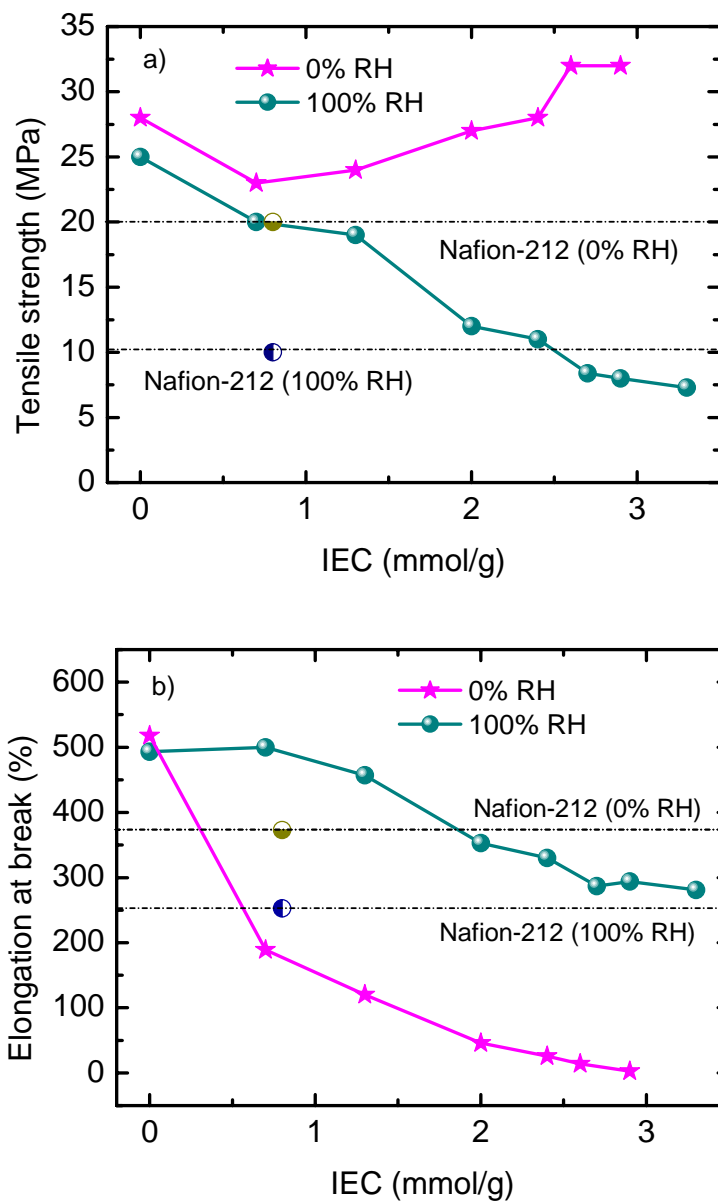


**Fig. 3-10.** Mechanical properties of original ETFE film, grafted-ETFE films, and ETFE-PEMs at 80 °C under dry conditions (0% RH) and 100% RH, together with those of Nafion-212 as a reference: (a) tensile strength and (b) elongation at break.

Under dry conditions, the *IEC* dependence of elongation at break for ETFE-PEMs decreased from 518% to 2.7%, this is opposite to the TS. These significant decreases in the elongation at break should result from addition of poly(styrene sulfonic acid) groups, which makes ETFE-PEMs possible to undergo the brittle degradation due to thermal effects with less water content. Contrary to the dry condition, the elongation at break decreased drastically from 500% to 353% for low *IECs* between 0–2.0 mmol/g and then gradually down to 281% in the *IECs* between 2.0–3.3 mmol/g under humid condition. It should be noted that all the elongation at break for all ETFE-PEMs was much higher than the Nafion-212 (252%) at 100% RH. The excellent elongation properties of the ETFE-PEMs under a humid conditions can be explained as follows: water absorption in the hydrophilic poly(styrene sulfonic acid) grafts depletes the ionic interaction in the sulfonic acid clusters to make whole the soft membranes. In order words, the absorbed water molecules in the ETFE-PEMs act as a good plasticizer, and thus, the hydrophilic poly(styrene sulfonic acid) graft domains become flexible, leading to the increases of the elongation at break but decreases of TS.

### 3.6. Conclusions

ETFE-PEM proton conductivity ranges for *IECs* of 1.3–2.9 mmol/g at 30% and 98% RH were 0.001–0.013 and 0.16–0.52 S/cm, respectively. Unlike aromatic hydrocarbon type PEMs, ETFE-PEMs have proton conductivities that are less dependent on RH because hydrophilic grafted polymers show clearer phase separation from the hydrophobic ETFE substrate, thereby maintaining conducting channels even under dry conditions. ETFE-PEM tensile strengths increased in the range of *IEC* > 2.0 mmol/g at 0% RH, but gradually decreased with increasing *IEC* at 100% RH and 80 °C. Moreover, ETFE-PEMs with *IEC* < 2.4 mmol/g showed higher tensile strengths compared to Nafion-212 at 100% RH. DSC measurements revealed that graft polymerization did not affect the crystallinity of ETFE-PEM, although sulfonation induced some damage in the crystalline domains. Further, the ETFE-PEM mechanical strength and proton conductivity were clearly related to PEM crystallinities. ETFE-PEMs with *IEC* > 2.7 mmol/g exhibited higher conductivity (>0.009 S/cm) at 30% RH and showed compatible tensile strengths of approximately 10 MPa at 100% RH and 80 °C.

## References

- 1) M.M. Nasef, E.A. Hegazy, Prog. Polym. Sci. 29 (2004) 499-561.
- 2) J. Chen, U. Septiani, M. Asano, Y. Maekawa, H. Kubota, M. Yoshida, J. Appl. Polym. Sci. 103 (2006) 1966-1972.
- 3) M. Shen, S. Roy, J.M. Kuhlmann, K. Scott, K. Lovell, J.A. Horsfall, J. Membr. Sci. 251 (2005) 121-130.
- 4) A.N. Geraldes, H.A. Zen, G. Ribeiro, H.P. Ferreira, C.P. Souza, D.F. Parra, E.I. Santiago, A.B. Lugão, Radia. Phys. Chem. 79 (2010) 246-249.
- 5) S.A. Gürsel, J. Schneider, H.B. youcef, A. Wokaun, G.G. Scherer, J. Appl. Polym. Sci. 108 (2008) 3577-3585.
- 6) H.B. youcef, S.A. Gürsel, A. Buisson, L. Gubler, A. Wokaun, G.G. Scherer, Fuel Cell 10 (2010) 401-410.
- 7) M.M. Nasef, H. Saidi, K.Z.M. Dahlan, Radiat. Phys. Chem. 68 (2003) 875-883.
- 8) M.M. Nasef, K.Z.M. Dahlan, Nucl. Instru. and Meth. B 201 (2003) 604-614.
- 9) K. Miyatake, B. Bae, M. Watanabe, Polym. Chem. 2 (2011) 1919-1929.
- 10) T. Suda, K. Yamazaki, H. Kawakami, J. Power Sour. 195 (2010) 4641-4646.
- 11) M.L. Einsla, Y.S. Kim, M. Hawley, H. Lee, J.E. McGrath, B. Liu, M.D. Guiver, B.S. Pivovar, Chem. Mater. 20 (2008) 5636-5642.
- 12) S. De, C. Cramer, M. Schönhoff, Macromolecules 44 (2011) 8936-8943.
- 13) Y. Akgöl, C. Cramer, C. Hofmann, Y. Karatas, H.D. Wiemhöfer, M. Schönhoff, Macromolecules 43 (2010) 7282-7287.
- 14) Y. Chang, G.F. Brunello, J. Fuller, M. Hawley, Y.S. Kim, M.D. Miller, M.A. Hickner, S.S. Jang, C. Bae, Macromolecules 44 (2011) 8458-8469.

## Chapter 4. Structure analysis of graft-type PEM

### 4.1. Introduction

As presented in Chapter 3, relative humidity (RH) dependence of the electrochemical and mechanical properties of ETFE-PEMs were investigated in a wide range of  $GD$  from 0 to 117%, corresponding to the  $IEC$  of 0–3.1 mmol/g. With  $IEC > 2.7$  mmol/g, ETFE-PEMs exhibited higher conductivity ( $> 0.009$  S/cm) at low RH (RH = 30%) and showed compatible tensile strengths of approximately 10 MPa at humidified condition (RH = 100% RH) and 80 °C. Such properties of ETFE-PEMs can be compared with those of current commercial membrane of Nafion-212 at the similar conditions. In order to elucidate above excellent properties, it is important to analyze the hierarchical structures of membranes such as crystalline morphology, conducting layers, consisting of graft polymers, internal structures of conducting layers such as aggregation of ionic groups and water as well as the hydrophobic/hydrophilic phase separation structures at the same range of  $GD$  and  $IEC$ . Thus, in this chapter, the higher-order structures of ETFE-PEM under dry and hydrated states were investigated using wide  $q$ -observation ( $4 \times 10^{-3} \text{ nm}^{-1} \leq q \leq 3 \text{ nm}^{-1}$ ) in SAXS/USAXS by comparison with the profiles of precursor original ETFE and polystyrene-grafted ETFE films because the grafted PEMs are well-known to keep somewhat crystalline structures and graft polymer phases of precursor original and grafted films. In addition, the structure variation with a wide range of  $GD$  ( $0 \leq GD \leq 117\%$ ) were observed to optimize the membrane's structures for high fuel cell performance. The hierarchical structures of ETFE-PEM characterized by SAXS measurement was compared with the direct images obtained from FE-SEM observation. Direct observations (FE-SEM) act as a check of indirect measurements (SAXS/USAXS).

## 4.2. The variation of hierarchical structure by preparation procedures

**Fig. 4-1(a)** shows overall SAXS profiles of the original ETFE, grafted-ETFE with a *GD* of 59%, and ETFE-PEM (sulfonated form of the grafted-ETFE) with *IEC* of 2.4 mmol/g in the  $q$ -ranges from  $4 \times 10^{-3}$  to  $3 \text{ nm}^{-1}$ . A combined small-angle scattering method using USAXS and SAXS measurements allow observation over a wide range in real  $d$  spacing (2–1600 nm). According to the scattering features (slopes, shoulders, peaks, and Porod's tail) of precursor original ETFE, grafted-ETFE and ETFE-PEM films, the scattering profiles were classified into two  $q$  regions:  $q$ -region I:  $1.5 \times 10^{-1} \text{ nm}^{-1} \leq q \leq 3 \text{ nm}^{-1}$  ( $2 \text{ nm} \leq d \leq 40 \text{ nm}$ ) and  $q$ -region II:  $4 \times 10^{-3} \text{ nm}^{-1} \leq q \leq 1.5 \times 10^{-1} \text{ nm}^{-1}$  ( $40 \text{ nm} \leq d \leq 1600 \text{ nm}$ ).

Over the entire  $q$ -range, the pristine ETFE film possessed only a pronounced peak at approximately  $q = 0.27 \text{ nm}^{-1}$  with  $d$ -spacing of 23 nm. The maximum peak of the original ETFE was assigned as the scattering from lamellar stacks, as previously reported [1,2]. Since lamellar stacks in these samples are expected to be partially or randomly oriented, the precise  $q$ -position of the scattering features relating to lamellar stacks can be obtained by Lorentz correction [3,4]. A plot of Lorentz correction of the pristine ETFE, grafted-ETFE, and ETFE-PEM are presented in **Fig. 4-1(b)**. The Lorentz plots of the original ETFE film showed the scattering peak at  $q = 0.336 \text{ nm}^{-1}$ , corresponding to the lamellar spacing of the pristine ETFE film with a  $d$ -spacing of 18.8 nm. The peak of lamellar structure followed by a dramatically decrease of the intensity with  $q^{-4}$  scaling in  $0.3 \text{ nm}^{-1} \leq q \leq 1.1 \text{ nm}^{-1}$  indicating the sharp interface between two phases, i.e., the pronounced area between crystalline and amorphous phases of inner lamellar stacks in the pristine ETFE. In  $q$ -region II, a SAXS profile was characterized by a large increase of intensity and no other features appeared.

For grafted-ETFE, in a  $q$ -region I, a shoulder-like peak appeared at  $0.192 \text{ nm}^{-1}$  ( $d$ -spacing = 32.7 nm) is similar  $q$ -position to that in the pristine ETFE film indicating that new phases consisting of PS grafts generated under the influences of the lamellar structure of the pristine ETFE film. In order words, this shoulder-like peak originated from the correlation distance between the primary lamellar units controlling the internal morphology of the lamellar stacks. It should be noted that the  $d$ -spacing of grafted-ETFE is 9.9 nm larger than that of the pristine ETFE. This expansion indicates that some portions of PS graft-polymers were introduced in

the amorphous regions in the lamellar stacks. Furthermore, the scattering intensity of the grafted-ETFE film is higher than that of pristine ETFE film in entire  $q$ -range, indicating the PS grafts, which have lower electron density, were introduced in the lamellar amorphous domains, resulting in the increases of the scattering contrast between lamellar crystals and amorphous domains consisting of lamellar amorphous and PS grafts. A shoulder-like peak appeared at  $0.192 \text{ nm}^{-1}$  was followed by a significant decrease in intensity with  $q^{-4}$  scaling in  $q$ -region I similar with the pristine ETFE film.

In  $q$ -region II, a discernible shoulder-like peak at approximately  $q_2 = 0.021 \text{ nm}^{-1}$  ( $d$ -spacing:  $d_2 = 300 \text{ nm}$ ) was observed while there was no appreciable scattering feature in the pristine ETFE film. The shoulder-like peak of  $q_2$  should be originated from the crystallites (lamellar grains) generated by graft polymerization. In addition, the SAXS profiles of grafted-ETFE exhibited another shoulder-like peak in the  $q$ -range that is lower than the peak position ( $q_2$ ) at  $q_3 = 0.0047 \text{ nm}^{-1}$  ( $d$ -spacing:  $d_3 = 1340 \text{ nm}$ ). Thus, the  $q_2$  and  $q_3$  should be a set of shoulder-like peaks of locally oriented crystallites, corresponding to two correlation distances of  $d_2$  and  $d_3$ , respectively.

As shown in **Fig. 4-1(a)** and **(b)**, the SAXS profile of ETFE-PEM exhibited three similar shoulder-like peaks to those of the grafted-ETFE in the entire  $q$ -range. This result indicates that the introduction of sulfonic acid groups by sulfonation reaction of the PS grafts did not deteriorate the lamellar stacks and crystallites; thus, the structures of the obtained PSSA grafts, which act as an ion-channel, are determined by the radiation-induce graft polymerization step. The positions of shoulder-like peaks of ETFE-PEM are slightly shifted into lower  $q$ -range indicating the larger dimension of structures resulting in the scattering features.

Contrary to the expansion of  $d$ -spacing by graft-polymerization, the expansion of the  $d$ -spacing by the sulfonation of grafted ETFE i.e., the difference of the  $d$ -spacing in grafted-ETFE and ETFE-PEM is very small (only  $0.4 \text{ nm}$ ), indicating that the introduction of sulfonic acid groups in the graft domains did not enlarge the total lamellar spacing. The scattering intensity is higher than that of pristine ETFE but lower grafted-ETFE film in entire  $q$ -range indicating that the scattering contrast was reduced by introduction of addition sulfonic acid groups. However, it is very reasonable because the PSSA has a similar electron density to ETFE, resulting in the contrast between lamellar crystals and amorphous domains containing lamellar amorphous and PSSA grafts are similar to each other.

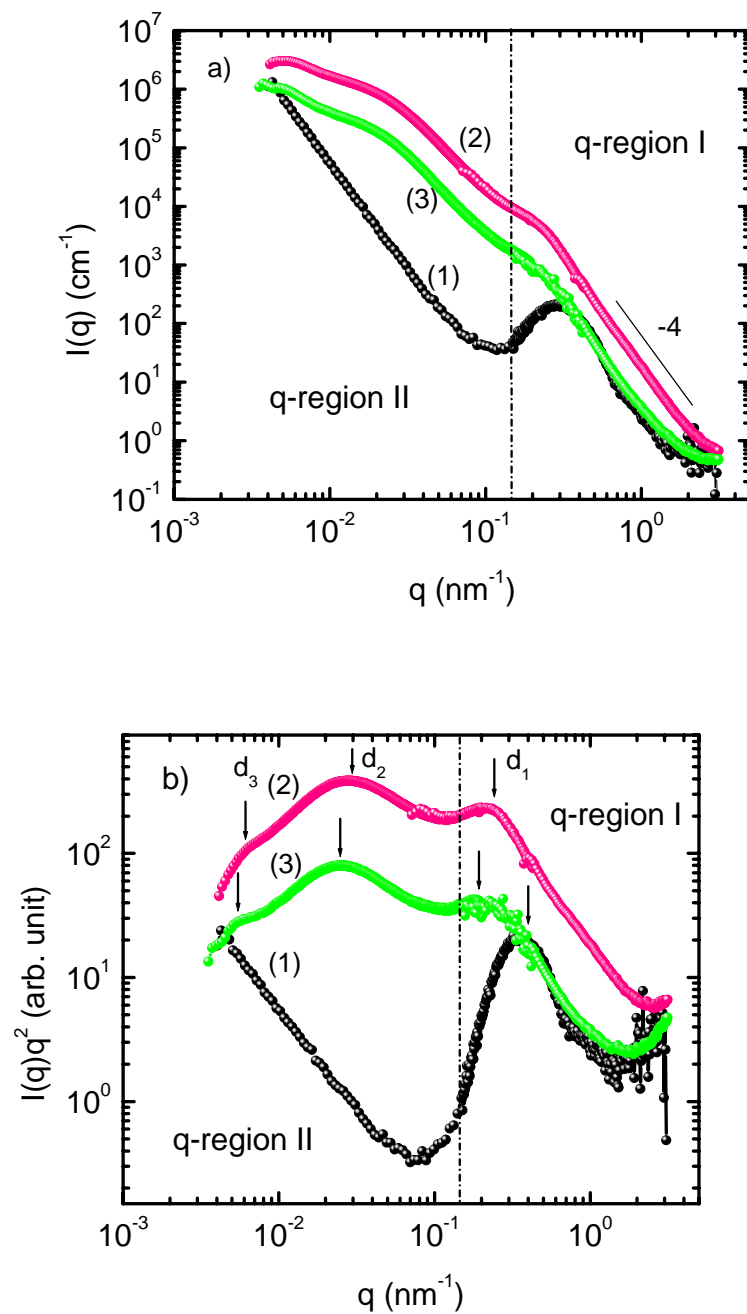


**Fig. 4-1.** (a) SAXS profiles of (1) original ETFE, (2) grafted-ETFE, and (3) ETFE-PEM with *GD* of 59%. (b) Lorentz plot from original SAXS profiles in **Fig. 4-1(a)**.

### 4.3. The variation of hierarchical structure with grafting degree

**Figs. 4-2** and **4-3** show the SAXS profiles of grafted-ETFE films with *GDs* in a range from 0 to 117% and the corresponding ETFE-PEMs with *IECs* in a range from 0 to 3.1 mmol/g. The enlarged scattering profiles in a low *q*-region ( $4 \times 10^{-3} \text{ nm}^{-1} \leq q \leq 10^{-1} \text{ nm}^{-1}$ ) were shown in **Insets of Figs. 4-2** and **4-3**. With increasing the *GD* and *IEC*, the scattering profiles and intensities of the grafted-ETFE and ETFE-PEM films changed in a different manner in *q*-region I and *q*-region II.

#### ***q*-region I ( $1.5 \times 10^{-1} \text{ nm}^{-1} \leq q \leq 3 \text{ nm}^{-1}$ , $2 \text{ nm} \leq d \leq 40 \text{ nm}$ )**

The SAXS profiles of both grafted-ETFE and ETFE-PEM exhibited clear peaks in a *GD* range of 4.2–19% and became broader shoulder-like peaks with higher *GD* range (34–117%) in *q*-region I. Thus, the lamellar periods ( $d_l = 2\pi/q_l$ ) determined by the peaks in the Lorentz plots of the SAXS profiles and scattering intensities at  $q_l$  of grafted-ETFE films and ETFE-PEMs were plotted as a function of *GDs* in **Fig. 4-4**.

The lamellar periods of the grafted-ETFE increases from 18.8 to 29.1 nm with increasing *GD* up to 59% and then keeps constant with higher *GDs* than 59%. The increase of the lamellar periods results from the introduction of PS grafts between the ETFE lamellar crystals. From the results of **Fig. 4-4**, the PS grafts were introduced only at the early stage of radiation-induced graft polymerization (*GDs* < 59%) and generated outside the lamellar stacks with *GDs* beyond 59%. Note that the lamellar period is dramatically increased from 18.8 nm (pristine ETFE film) to 21.8 nm even at very low *GD* of 4.2% and then increased to 28.7 nm for a *GD* of 59%. This result suggests that a big expansion of lamellar period occurred at very early stage of graft polymerization. The SAXS intensities  $I(q_l)$  of grafted-ETFE increased dramatically with *GDs* of 0–34% and then decreased gradually when the *GD* increased beyond 34% (**Fig. 4-4**). As mentioned in 4.2, the introduction of graft polymers into the lamellar amorphous layers results in an increase of the scattering contrast. On the other hand, the slight decrease of  $I(q_l)$  in the *GDs* of 34–117% should be due to the partial destruction of lamellar stacks by the introduction of PS grafts [5,6].

Since in the entire range of  $GD$ , the lamellar periods of ETFE-PEMs was slightly higher than those of grafted-ETFE (less than 1 nm), the introduced sulfonic acid groups has less influence to the structures of the lamellar stacks [7]. The SAXS intensities of ETFE-PEMs also increased with the increases of  $GD$  in a range of 4.2–19% and then gradually decreased with the increases of  $GDs$  beyond 19%, as were the case of the grafted-ETFE. However, it should be noted that even introducing the higher amounts of graft polymers to the original ETFE by weight (up to 117%), the lamellar stacks are maintained with slight decrease of the crystallinity. As previously reported, the decreases of the crystallinity (deterioration of lamellar stacks) are due to sulfonation reaction but not the radiation and successive graft polymerization processes [5].

As shown in **Figs. 4-2** and **4-3**, the SAXS profiles of the grafted-ETFE and ETFE-PEMs exhibit  $q^{-4}$  behavior in the  $q$ -range that was higher than the peak position ( $q_1$ ) with increasing  $GDs$  up to 59% but not in the  $GD$  range higher than 59% (power law of -3.5 to -3.7). This result indicates the miscibility between the PSSA grafts and polymer ETFE substrate resulting in the less clear boundary of the hydrophilic PSSA graft / hydrophobic ETFE crystallite domains in  $GD \geq 59\%$ .

#### **In $q$ -region II ( $q \leq 1.5 \times 10^{-1} \text{ nm}^{-1}$ , $d \geq 40 \text{ nm}$ )**

The change in the scattering profile of grafted-ETFE is clearly observed with increasing  $GD$ . Even with low  $GDs$  (4.2 to 10.2%), the scattering intensities in  $10^{-2} < q < 10^{-1} \text{ nm}^{-1}$  increased by one to two order of magnitude from the pristine ETFE film. With the increases of  $GD$  from 19 to 59%, the scattering intensity increased continuously and a new set of two discernible shoulder-like peaks appeared in  $4 \times 10^{-3} \text{ nm}^{-1} \leq q \leq 1.5 \times 10^{-1} \text{ nm}^{-1}$ .

The shoulder-like peaks in the SAXS profiles of the grafted-ETFE in  $q$ -region II are related to the structures or correlation distances of the crystallites, which are defined as lamellar grains. Thus, the shoulder-like peaks were converted into the well-defined peaks after Lorentz correction to obtain real spacing  $d_2$ . The  $d_2$  and the scattering intensities at  $q = q_2$  were plotted as a function of  $GD$  of grafted-ETFE films and ETFE-PEMs in **Fig. 4-5**. The  $d_2$  of the grafted-ETFE increased from 141 to 266 nm with increasing  $GD$  from 10% to 59%.

The continuous increases of  $I(q)$  indicated that the crystallite structure should exist even in the original ETFE film, in which the contrast between inside and outside of the crystallites should be very low. However, the contrasts between the inside and outside of the crystallites increased with the increases of a  $GD$  and became enough high for the grafted-ETFE films with higher  $GDs$  than 19% because the introduction of PS grafts into the lamellar amorphous regions in the crystallites in the grafted-ETFE enhances the contrast between the inside and outside crystallite regions.

The  $d_2$  of the grafted-ETFE suddenly decreased from 266 nm to 200 nm at the  $GD$  of 81%. When the  $GD$  increased from 81% to 117%,  $d_2$  just slightly increased from 200 to 216 nm. The increase of  $d_2$  in the  $GD$  of 10–59% is due to the increase of volume of amorphous domains consisting of addition PS grafts within lamellar stacks (**Fig. 4-4(a)**) and between the crystallites (lamellar grains). The pronounced discontinuous change in  $I(q_2)$  was observed between  $GD$  of 59 and 81%; the  $I(q_2)$  of the grafted-ETFE decreased by 66%. These discontinuous changes in  $q_2$  and  $I(q_2)$  strongly indicate the phase transition of crystallite structures. Unlike the behavior of  $I(q_2)$  with  $GDs$  of 19–59%, that only increased slightly with  $GD$  ranging from 81 to 117%. The possible reason for this behavior is that the addition PS grafts were mainly introduced somewhere between the crystallites due to the spatial limitation in and around lamellar stacks (**Fig. 4-6**).

As already mentioned, the shoulder-like peak of  $q_2$  should be originated from the crystallites (lamellar grains) generated by graft polymerization. In addition, the SAXS profiles of grafted-ETFE exhibited another shoulder-like peak at lower peak position at  $q_3 = 0.0047 \text{ nm}^{-1}$  ( $d$ -spacing:  $d_3 = 1340 \text{ nm}$ ). One possible explanation of the set of peaks,  $q_2$  and  $q_3$ , should be a set of correlation distances for the short and long periods  $d_2$  and  $d_3$ , originating from oriented crystallite structures, as shown in Fig. 4-6 ( $GDs$  of 19 and 59%). In contrast, the scattering profiles for  $GDs$  of 81-117%, which were totally changed from those for  $GDs$  of 19-59%, showed only shoulder-like peaks at  $q_2 = 2.91 \times 10^{-2} - 3.14 \times 10^{-2} \text{ nm}^{-1}$  ( $d_2 = 200\text{-}216 \text{ nm}$ ). Thus, the grafted-ETFE with  $GD \geq 81\%$  have a new phase with non-oriented crystallite structure with a correlation distances ( $d_2$ ) of 200-216 nm, as illustrated in **Fig. 4-6** ( $GDs$  of 81 and 117%).

All the ETFE-PEMs with *IEC* up to 3.1 mmol/g (*GDs* = 4.2-117%) exhibited similar scattering profiles to those of the corresponding precursor grafted-ETFE films in the *q*-region II (**Fig. 4-3**). Thus, the sulfonation process did not affect the structures of the grafted-ETFE with any *GDs* in the higher scale range than 40 nm, as is the same as those in *q*-region I. Furthermore, because the behavior of  $I(q_2)$  for ETFE-PEM is similar with that of grafted-ETFE, the same explanation could be used for addition PSSA grafts into membranes. In the entire *GD* range ( $10.2 \leq GD \leq 117\%$ ),  $d_2$  of ETFE-PEMs is higher than that of grafted-ETFE films from 8 to 18% but they have similar profiles to those of the grafted-ETFE films.

The calculated values of  $d_2/d_1$  of the grafted-ETFE films and ETFE-PEMs are showed in **Table 4-1**. The ratio values of  $d_2/d_1$  of the grafted-ETFE increased from 6.0 to 9.3 with *GD* from 10 to 59%, suddenly decreased from 9.3 to 7.0 in *GD* of 59 – 81%, and then slight increased again from 7.0 to 7.4 with *GD* from 81 to 117%. The similar behavior of the ratio values of  $d_2/d_1$  was obverted in ETFE-PEM. This result indicates that the large amounts of PS (or PSSA) grafts were introduced mainly into the amorphous phase around the lamellar crystals in the oriented crystallites for the membranes with lower *GDs* than 59% and into the outside region of the non-oriented crystallites for the membranes with higher *GDs* than 81%, respectively. In other words, when the large amounts of PS (or PSSA) grafts introduced into the ETFE films with larger *GDs* than 59%, the oriented crystallite became unstable and the phase transition of the crystallite structure occurred to take more stable forms with more randomly oriented structures than oriented crystallite structures for the membranes with *GDs* ranging from 81% to 117% (**Fig. 4-6**).

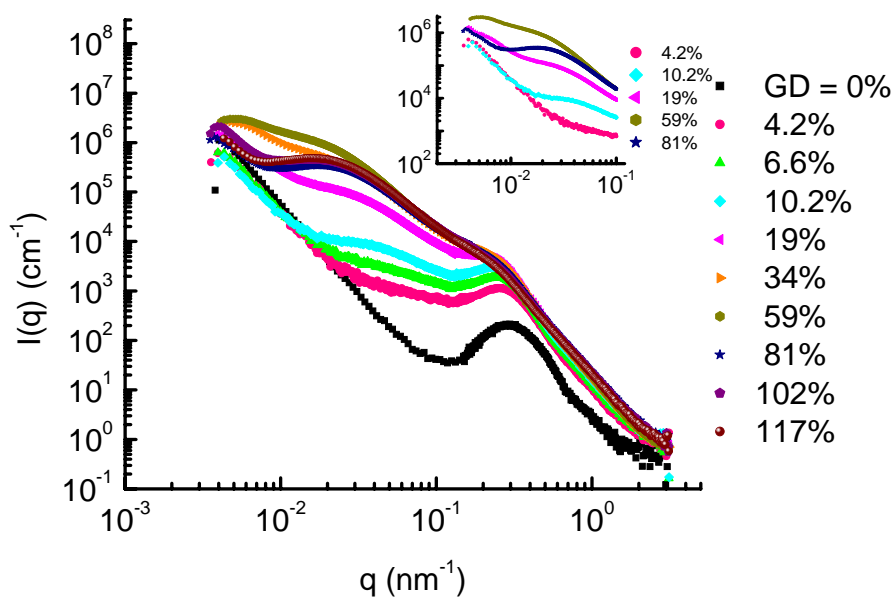


**Fig. 4-2.** *GD* dependences of SAXS profiles of grafted-ETFE. The enlarged scattering profiles in a low  $q$ -region ( $4 \times 10^{-3} \text{ nm}^{-1} \leq q \leq 10^{-1} \text{ nm}^{-1}$ ) were shown in **Inset of Fig. 4-2**.

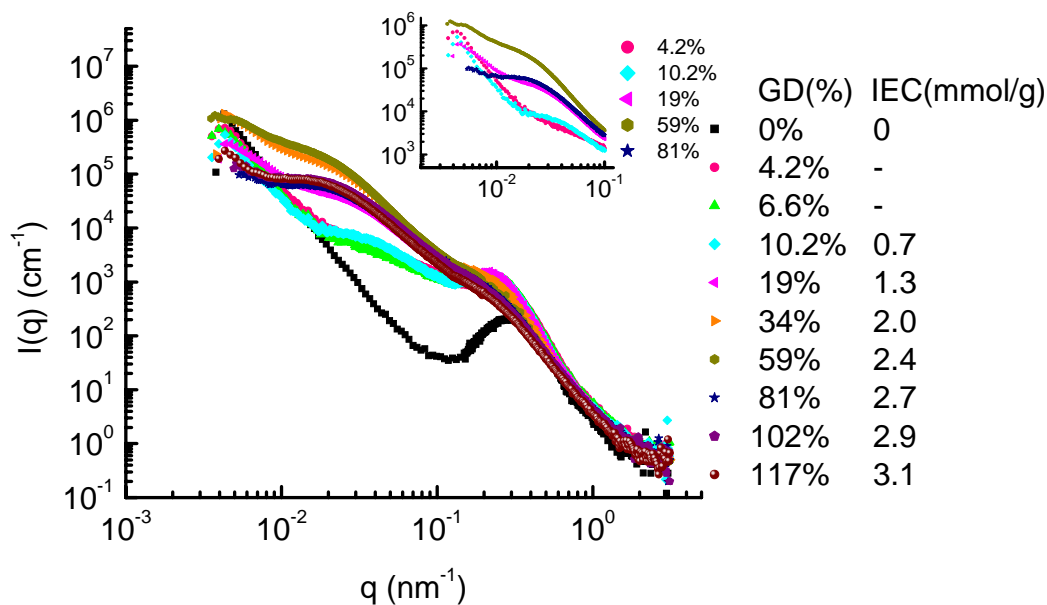


**Fig. 4-3.** *GD* dependences of SAXS profiles of dry ETFE-PEMs. The enlarged scattering profiles in a low  $q$ -region ( $4 \times 10^{-3} \text{ nm}^{-1} \leq q \leq 10^{-1} \text{ nm}^{-1}$ ) were shown in **Inset of Fig. 4-3**.

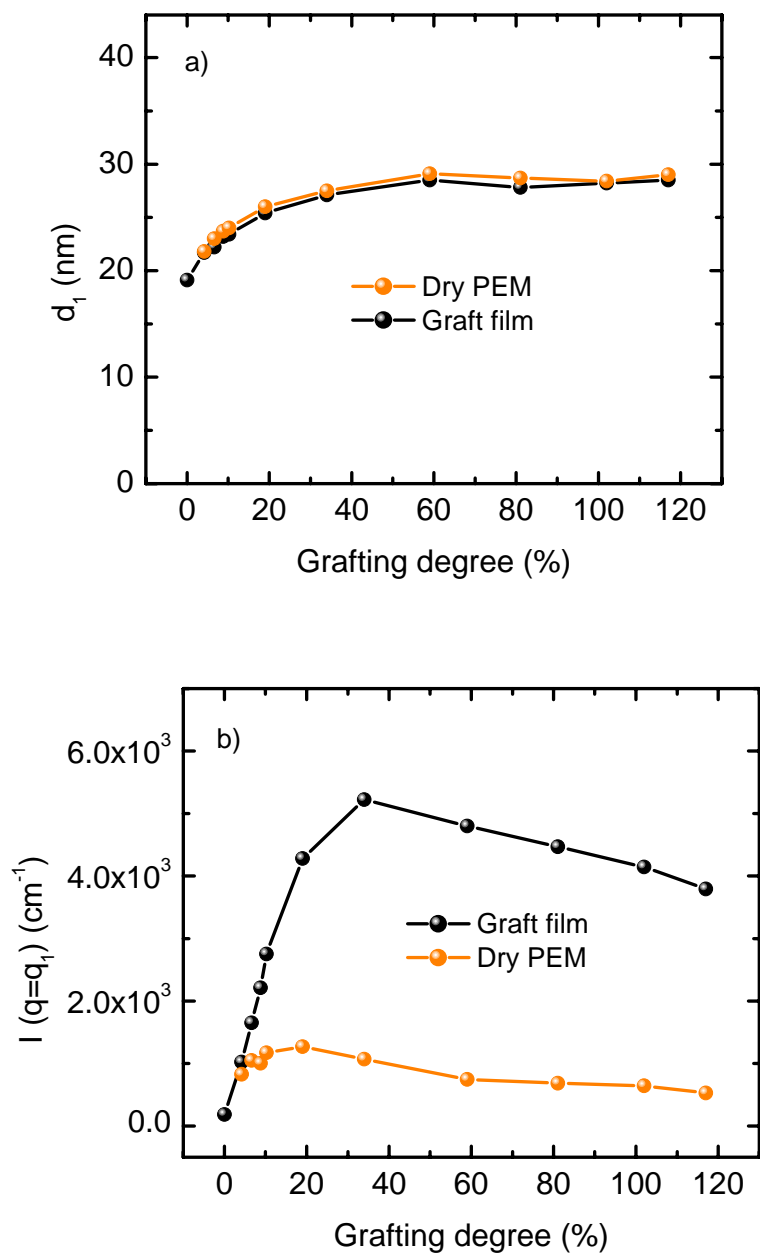


**Fig. 4-4.** GD dependences of (a)  $d_1$ -spacing and (b) peak-intensity of grafted ETFE and ETFE PEM.

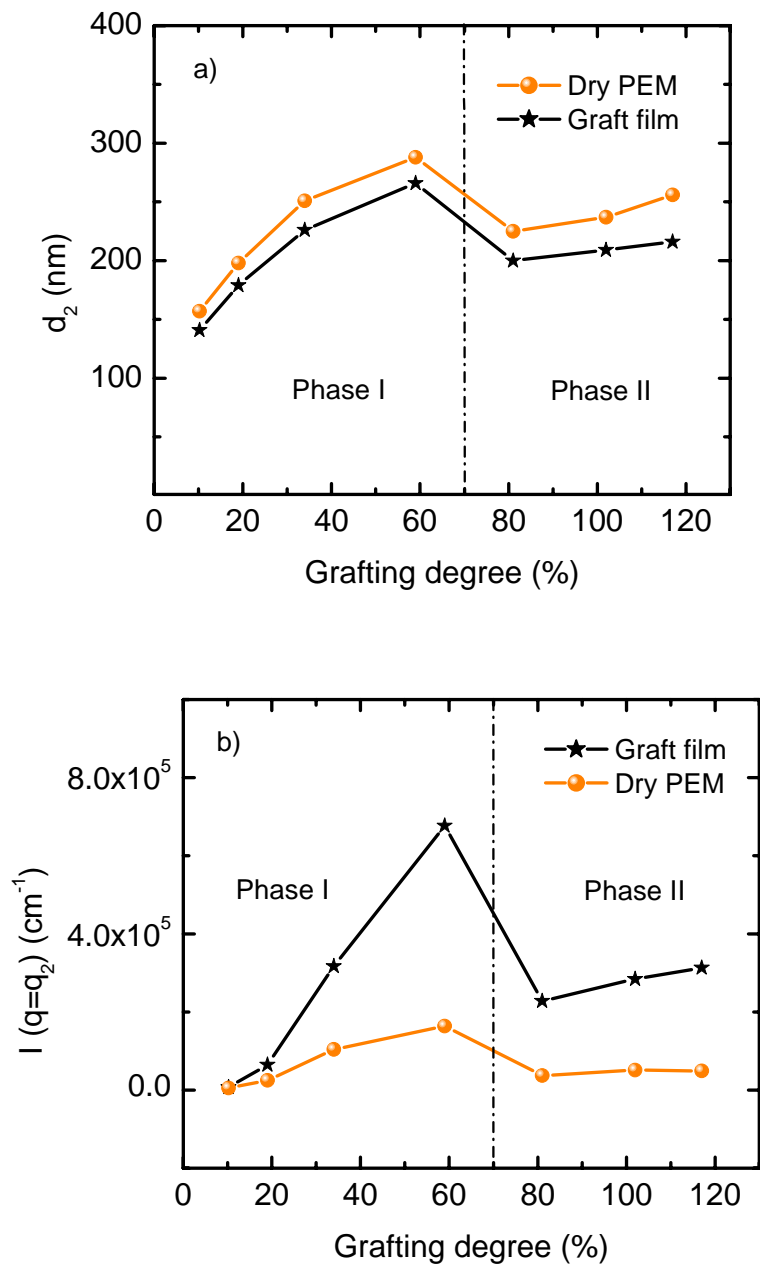


**Fig. 4-5.** GD dependences of (a)  $d_2$ -spacing and (b) peak-intensity of grafted ETFE and ETFE PEM.

**Table 4-1**

The values of  $GD$ ,  $IEC$ ,  $d_1$ ,  $d_2$ ,  $d_3$ , and  $d_2/d_1$  of grafted-ETFE and ETFE-PEM with  $GD$ s of 0-117% are presented.  $d_1$  is the lamellar period.  $d_2$  and  $d_3$  are correlation distance of the crystallites (lamellar grains).

$GD$ (%)	$IEC$ (mmol/g)	Grafted-ETFE				ETFE-PEM			
		$d_1$ (nm)	$d_2$ (nm)	$d_3$ (nm)	$d_2/d_1$	$d_1$ (nm)	$d_2$ (nm)	$d_3$ (nm)	$d_2/d_1$
0	-	18.8	-	-	-	-	-	-	-
4.2	-	21.7	-	-	-	21.8	-	-	-
6.6	-	22.2	-	-	-	23.0	-	-	-
10.2	0.7	23.4	141	-	6.0	24.0	157	-	6.5
19	1.3	25.4	179	952	7.1	26.0	198	903	7.6
34	2.0	27.1	226	1026	8.3	27.5	251	1044	9.1
59	2.4	28.7	266	1054	9.3	29.1	288	1124	9.8
81	2.7	28.6	200	-	7.0	28.7	225	-	7.8
102	2.9	28.2	209	-	7.4	28.4	237	-	8.3
117	3.1	29.3	216	-	7.4	29.0	256	-	8.8

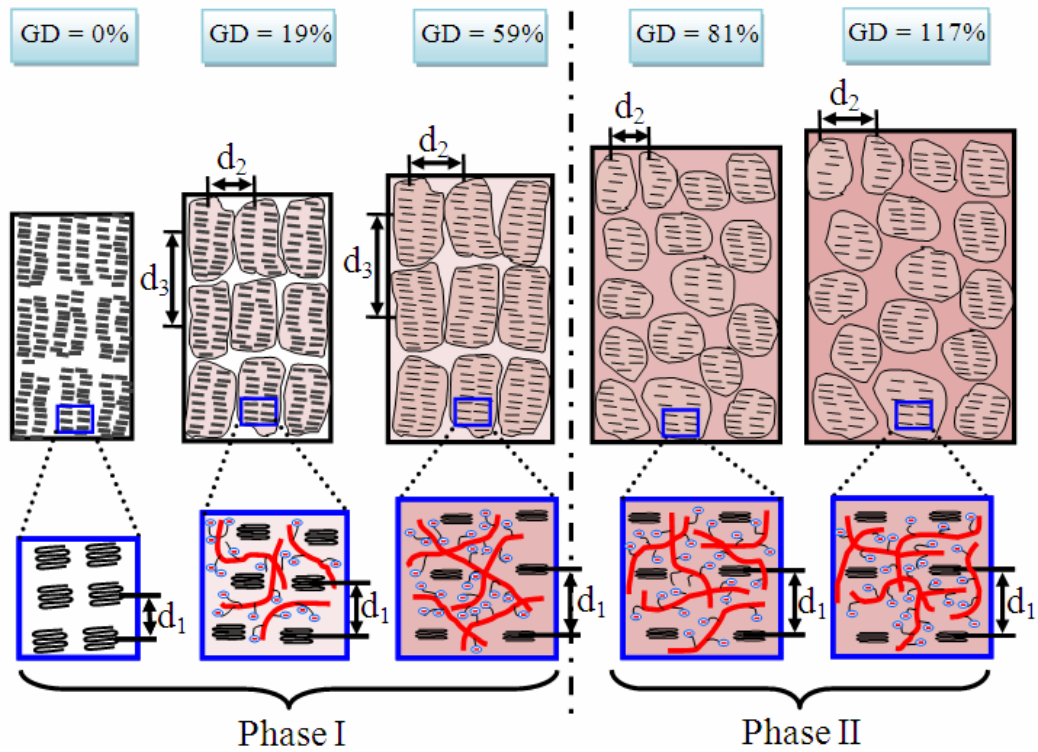


**Fig. 4-6.** Schematic illustrations of the morphology change in the higher-order structures of ETFE-PEM at *GD* of 0, 19, 59, 81%, and 117%.

#### 4.4. The variation of hierarchical structure at dry and hydrated states

The SAXS profiles of hydrated ETFE-PEMs with  $GD$ s of 0–117% ( $IEC$ s of 0–3.1 mmol/g) were measured and compared with those of dry ETFE-PEMs (**Fig. 4-7**). The enlarged scattering profiles in a low  $q$ -region ( $4 \times 10^{-3} \text{ nm}^{-1} \leq q \leq 10^{-1} \text{ nm}^{-1}$ ) were shown in **Inset of Fig. 4-7**. The SAXS profiles of hydrated ETFE-PEMs were similar to those of dry ETFE-PEMs with the entire range of  $GD$ ; however, most of the  $q$ -positions of the typical features, such as the shoulder-like peaks and the distinct peaks of Lorentz plots, were shifted to lower values with the increases of the scattering intensities  $I(q)$  (**Table 4-2**). The ETFE-PEM with the entire  $GD$  range can keep the morphology even after water absorption even though the characteristic dimensions such as the lamellar period and crystallite sizes are enlarged by the absorption of water. Thus, the lamellar periods and the dimensions of the crystallites of the ETFE-PEMs under dry and hydrated states were plotted as a function of  $GD$  in **Figs. 4-8** and **4-9**, respectively.

As shown in **Fig. 4-8**, the expansions of the lamellar spacing of the ETFE-PEMs by water absorption gradually increases with the increases of  $IEC$  ( $IEC < 2.4 \text{ mmol/g}$  or  $GD < 59\%$ ) and kept constant with the  $IEC$  range of  $2.4 \text{ mmol/g} < IEC < 3.1 \text{ mmol/g}$  ( $59\% < GD < 117\%$ ). Thus, water absorption behavior in the lamellar stacks of the ETFE-PEMs did not change between phase I ( $0 < IEC < 2.4 \text{ mmol/g}$ ) and Phase II ( $2.4 < IEC < 3.1 \text{ mmol/g}$ ). In contrast, the dimensional changes in the crystallites ( $d_2$ ) increases with increasing  $GD$  in the range of 19–59% ( $1.3 < IEC < 2.4 \text{ mmol/g}$ ) in Phase I, whereas after the phase transition (Phase II), the dimensional change in the crystallite ( $d_2$ ) were constant with the  $IEC$  range of 2.4–3.1 mmol/g (**Fig. 4-9**).

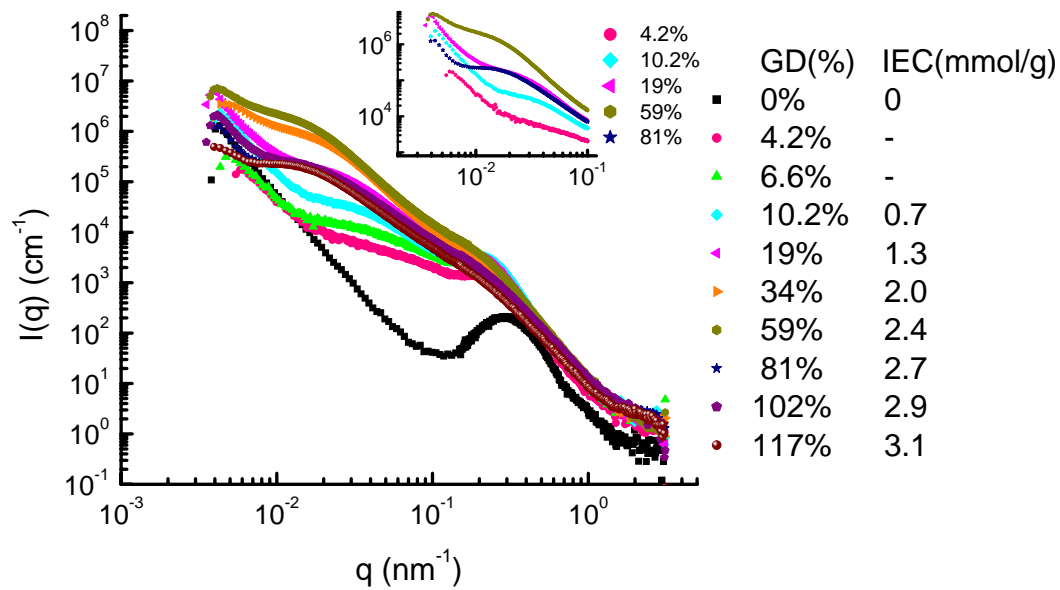


**Fig. 4-7.** GD dependences of SAXS profiles of hydrated ETFE-PEMs. The enlarged scattering profiles in a low  $q$ -region ( $4 \times 10^{-3} \text{ nm}^{-1} \leq q \leq 10^{-1} \text{ nm}^{-1}$ ) were shown in **Inset of Fig. 4-7.**

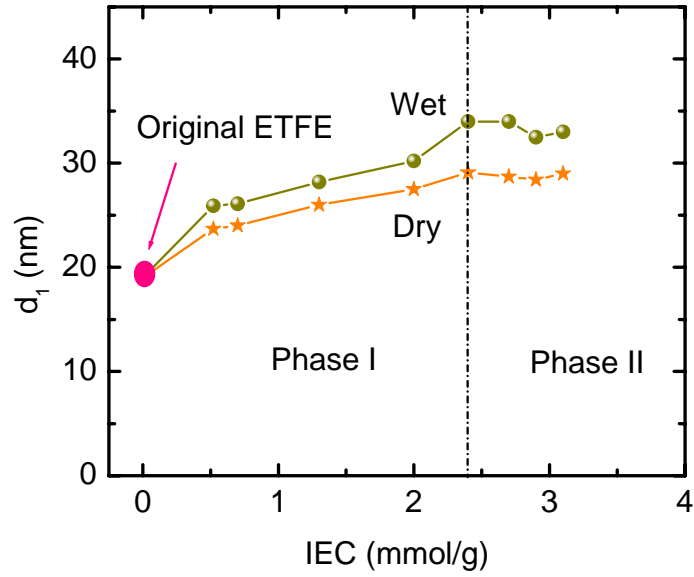


**Fig. 4-8.** IEC dependences of lamellar periods of dry and hydrated ETFE-PEMs.

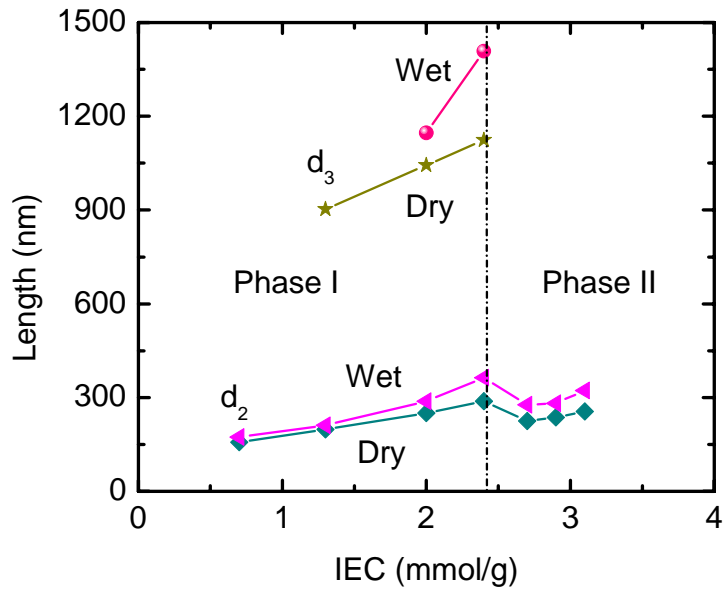


**Fig. 4-9.** IEC dependences of  $d_2$ - and  $d_3$ - spacing of dry and hydrated ETFE-PEM.

Since the effect of water absorption on the dimensional changes of ETFE-PEMs are different in different hierarchical structures as mentioned in 4.4, the quantitative analysis of the dimensional changes of each hierarchical structure of the membranes, such as lamella period, oriented crystallites and random shape of the crystallites were conducted by using swelling ratio between the volume of the hydrated and that of dried membranes,  $\phi$ , defined as the following equation.

$$\phi = \frac{\frac{m_{PSSA}}{\rho_{PSSA}} + \frac{m_{ETFE}}{\rho_{ETFE}} + \frac{m_{water}}{\rho_{water}}}{\frac{m_{PSSA}}{\rho_{PSSA}} + \frac{m_{ETFE}}{\rho_{ETFE}}} \quad (4-1)$$

where  $m_{PSSA}$  and  $\rho_{PSSA}$  are the weight and density of the PSSA grafts,  $m_{ETFE}$  and  $\rho_{ETFE}$  are the weight and density of pristine ETFE, and  $m_{water}$  and  $\rho_{water}$  are the weight and density of the absorbed water [8]. The value of  $m_{PSSA}$  in equation (4-1) was determined from the *GD* using

$$m_{PSSA} = \frac{m_{SSA} \times DOG \times m_o}{100 \times M_{St}} \quad (4-2)$$

where  $m_{SSA}$  and  $\rho_{St}$  are the molecular weights of a styrene sulfonic acid unit and styrene unit, respectively.

Earlier reported results showed that the graft-type ETFE-PEMs upon hydrated states expanded more in thickness direction than in the lateral direction, indicating deviations from the isotropic swelling [2]. In addition, the obtained small angle neutron scattering (SANS) results showed an excellent linear correlation with the macroscopic results of lateral and thickness dimensions of the hydrated and dry membranes, indicating isotropic swelling on the nanometer length scale [9]. Thus, the one-dimensional swelling ratio,  $L$ , can be assumed from  $\phi$  using the following equation as a parameter to compare the real dimensional changes calculated from SAXS profiles

$$L = \sqrt[3]{\phi} \quad (4-3)$$

The values of  $L$  are listed with the expansion ratio of lamellar spacing ( $d_1$ ) and correlation distance of the crystallites  $d_2$  of ETFE-PEMs in dry and hydrated states in **Table 4-3**. As the  $IEC$  increased from 0.7 to 3.1 mmol/g,  $L$  increased from 1.07 to 1.48. The expansion ratios of lamellar period ( $d_1$ ) were almost constant (approximately 1.1) in the entire  $IEC$  range and thus, no relation with  $L$ . This relationship implies that water molecules absorbed in the PSSA grafts around the lamellar stacks with less than 10% of the original PEM weights even when the water uptakes of the ETFE-PEMs increase from 0 to 145% with increasing the  $IEC$  from 0 to 3.1 mmol/g. In contrast, the expansion ratios of  $d_2$  increased from 1.11 to 1.26 with increasing the  $IEC$  from 1.3 to 2.4 mmol/g (phase I), being a good agreement with the increases of  $L$ . On the other hand, the correlation distances of the non-oriented crystallites ( $d_2$ ) in Phase II showed almost constant values in the ETFE-PEMs with  $IECs$  higher than 2.7 mmol/g ( $GD > 81\%$ ). The above relations between  $L$  and the expansion ratios of lamellar and crystallite structures of the ETFE-PEMs indicate that for  $GD < 59\%$ , water molecules are mainly located in the PSSA grafts around the lamellar crystals in the oriented crystallites and increase with the increases of  $IEC$ . Thus, the very early stage of ion conductance of the PEMs with a low  $GD$  ( $<10\%$ ) and low water uptakes ( $<13\%$ ) depends on the PSSA ion channels around lamellar stacks. The ETFE-PEMs with  $GDs$  of 19-59% showed the conductivity mainly depends on amounts of ion-channels consisting of PSSA grafts located in the crystallites. In addition, for the ETFE-PEM with higher  $GD$  ( $GD \geq 81\%$ ) the increases of the membrane size by the absorption of water did not affect the size of lamellar ( $d_1$ ) nor crystallites ( $d_2$ ), strongly indicates more PSSA grafts were mainly introduced outside the non-oriented crystallites, which results in the higher conductivity of the ETFE-PEM with high  $IEC$ .

**Table 4-2**

The values of  $GD$ ,  $IEC$ ,  $d_1$ ,  $d_2$ , and  $d_3$  of hydrated ETFE-PEM with  $GD$ s of 0-117% are presented.  $d_1$  is the lamellar period.  $d_2$  and  $d_3$  are dimensions of the crystallites (lamellar grains).

$GD$ (%)	$IEC$ (mmol/g)	Hydrated ETFE-PEM		
		$d_1$ (nm)	$d_2$ (nm)	$d_3$ (nm)
0	-	-	-	-
4.2	-	23.5	-	-
6.6	-	24.9	-	-
10.2	0.7	26.3	174	-
19	1.3	28.2	211	-
34	2.0	30.9	288	1147
59	2.4	31.1	364	1408
81	2.7	32.9	277	-
102	2.9	32.1	282	-
117	3.1	32.2	323	-

**Table 4-3**

The values of  $GD$ ,  $IEC$ ,  $L$ , and swelling ratio of  $d_1$  and  $d_2$  are presented.  $L$  is one-dimensional swelling ratio.  $d_1$  is the lamellar period.  $d_2$  is dimension of the crystallites (lamellar grains).

$GD(\%)$	$IEC(\text{mmol/g})$	$L$	$d_1(\text{wet})/d_1(\text{dry})$	$d_2(\text{wet})/d_2(\text{dry})$
10.2	0.7	1.07	1.10	1.11
19	1.3	1.11	1.08	1.07
34	2.0	1.19	1.12	1.15
59	2.4	1.29	1.07	1.26
81	2.7	1.38	1.15	1.23
102	2.9	1.44	1.13	1.19
117	3.1	1.48	1.11	1.26

#### 4.5. The variation of hierarchical structure by direct observation

**Fig. 4-10** shows the surface images of (a) pristine ETFE, (b) grafted-ETFE, and (c) ETFE-PEM with *GD* of 59% (*IEC* = 2.4 mmol/g) by FE-SEM observation. A clear repeating unit like structure features with random ordering appeared only in ETFE-PEM (which was immersed in AgNO<sub>3</sub> 0.5 M) while did not in pristine ETFE and grafted-ETFE. For ETFE-PEM, the bright regions of image represent the partially sulfonated PS matrix while the black regions present the hydrophobic domains. A repeating unit like structure features should be attributed to the lamellar structures, which were existed in the pristine ETFE film. The repeating units like lamellar structures with average size around 23 nm could be compared with those of SAXS measurement. In addition, the random ordering of lamellar structures having sulfonated PS grafts were interconnected network which is favorable for high ionic conductivity.

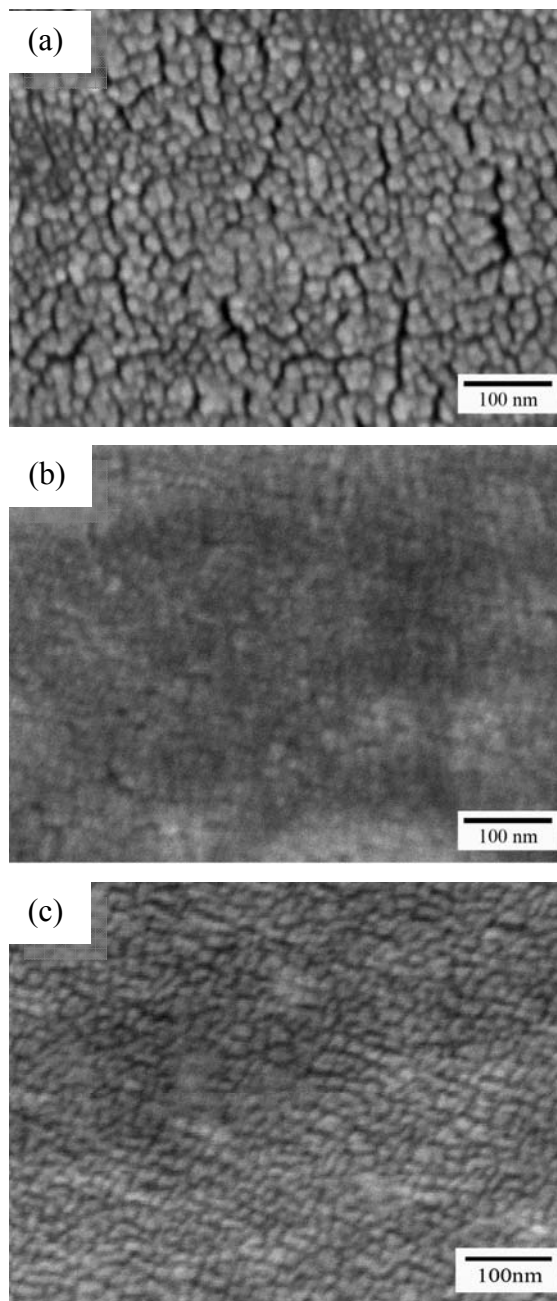


**Fig. 4-10.** Surface image of (a) pristine ETFE, (b) grafted-ETFE, and (c) ETFE-PEM with *GD* of 59% by FE-SEM observation.

## 4.6. Conclusion

The hierarchical structures of ETFE-PEMs under dry and hydrated states in wide  $GD$ s of 0-117% ( $IECs$  of 0-3.1 mmol/g) were investigated using a wide  $q$  observation ( $4 \times 10^{-3} \text{ nm}^{-1} \leq q \leq 3 \text{ nm}^{-1}$ ) in SAXS/USAXS. Two distinct scattering features can be observed in  $q$ -region I ( $1.5 \times 10^{-1} \text{ nm}^{-1} \leq q \leq 3 \text{ nm}^{-1}$ ) and  $q$ -region II ( $4 \times 10^{-3} \text{ nm}^{-1} \leq q \leq 1.5 \times 10^{-1} \text{ nm}^{-1}$ ). In a  $q$ -region I, the pristine ETFE possesses the maximum peak (at  $q$ -position of  $0.328 \text{ nm}^{-1}$ ) with  $d$ -spacing of 19.0 nm, originated from lamellar period. The grafted-ETFE with a  $GD$  of 59 % and the corresponding ETFE-PEM ( $IEC = 2.4 \text{ mmol/g}$ ) showed shoulder-like peaks (at  $q$ -positions of  $0.219$  and  $0.216 \text{ nm}^{-1}$ ) with  $d$ -spacing of 28.7, and 29.1 nm, respectively. The lamellar periods increased with increasing  $GD$  ( $< 59\%$ ) and then kept constant in a  $GD$  range of 59–117%, indicating that new phases consisting of polystyrene grafts (PS) and poly (styrene sulfonic acid) (PSSA) grafts generated around lamellar crystals with increasing the  $GD$  ( $IEC$ ) up to 59% (2.4 mmol/g). In a  $q$ -region II, the pristine ETFE film exhibited no appreciable scattering, while the grafted-ETFE films and ETFE-PEMs with  $GD$  of 19–59% showed discernible shoulder-like features, which assigned to the oriented crystallites (lamellar grains) with  $d_2 = 198\text{--}288 \text{ nm}$  and  $d_3 = 903\text{--}1124 \text{ nm}$ , determined by Lorentz correction. These membranes with  $DG \geq 81 \%$  showed shoulder-like peaks with less than half of scattering intensity than those of the membranes with  $DG \leq 59\%$  and totally different scattering features, assigned to a new phase of structure with the length of a crystallite above the observed  $q$  region ( $> 1.6 \mu\text{m}$ ). These discontinuous changes in a  $q$ -region II strongly indicate the phase transition probably from the oriented to non-oriented crystallite structures between  $GD$ s of 59–81%. The SAXS observation in the entire  $q$ -regions indicate that the ion-channels consisting of PSSA grafts located locally around the lamellar crystals in the membranes with  $GD \leq 59\%$  and expands to out of the crystallites (lamellar grains) to have higher interconnection for  $GD \geq 81\%$ . In addition, the hydrophilic/hydrophobic boundary was less clear and the ordering of lamellar stacks and lamellar crystals still remained under hydrated state even at very high  $GD$  ( $GD > 59\%$ ).

## References

- 1) K. Jokela, R., Serimaa, M. Torkkeli, F. Sundholm, T. Kallio, G. Sundholm, J. Polym. Sci. Polym. Phys. Ed., 40 (2002) 1539-1555.
- 2) S. Balog, U. Gasser, K. Mortensen, L. Gubler, G.G. Scherer, H.B. youcef, Macromol. Chem. Phys. 211 (2010) 635-643.
- 3) R.J. Matyi, J.R.B. Crist, , J. Polym. Sci. Polym. Phys. Ed., 16 (1978) 1329-1354.
- 4) F. Cser, J. Appl. Polym. Sci. 80 (2001) 2300-2308.
- 5) T.D. Tran, S. Sawada, S. Hasegawa, Y. Katsumura, Y. Maekawa, J. Membr. Sci., Submitted.
- 6) H. Iwase, S. Sawada, T. Yamaki, S. Koizumi, M. Ohnuma, Y. Maekawa, Macromolecules 45 (2012) 9121-9127.
- 7) D.M. Tigelaar, A.E. Palker, R. He, D.A. Scheiman, T. Petek, R. Savinell, M. Yoonessi, J. Membr. Sci., 369 (2011) 455-465.
- 8) L. Rubatat, C. Li, H. Dietsch, A. Nykänen, J. Ruokolainen, R. Mezzenga, Macromolecules 41 (2008) 8130-8137.
- 9) H.B. youcef, S.A. Gürsel, A. Wokaun, G.G. Scherer, J. Membr. Sci. 311 (2008) 208-215.

# Chapter 5. Background correction of SAXS profiles in high $q$ -range

## 5.1. Introduction

There have been many reports in the last two decades for graft-type polymer electrolyte membranes (PEM) based on fully or partially fluorinated polymer substrates prepared by radiation induced graft polymerization for fuel cell applications as mentioned in Chapter 1 and Chapter 3. There have been some researches for structural analysis for the graft-type PEMs using SAXS and SANS as mentioned in Chapter 4. However, most of the paper does not concern the background effects due to thermal scattering (also known as liquid scattering) and amorphous phase scattering on the PEM structures especially in high- $q$  region (short correlation distances) even though ionomer peaks, which is one of the most important structures, are located in the this region.

The background scattering intensity, evaluated as a deviation from Porod's law, depends on the crystallinity of the polymers for a given temperature and thermal history [1,2]. Careful background correction in the high- $q$  range from the observed scattering intensity is expected to reveal some hidden information about polymer structures. Accordingly, in this chapter, the background scattering intensity ( $I_B(q)$ ) in the high- $q$  range ( $q > 2 \text{ nm}^{-1}$ ) of SAXS is evaluated for ETFE-PEMs. In addition, the effects of the background scattering intensity on the typical structures of ETFE-PEMs with different scale ranges, lamellar spacings ( $0.1 \text{ nm}^{-1} \leq q \leq 0.7 \text{ nm}^{-1}$ ), interfacial thicknesses ( $5.9 \text{ nm}^{-1} \leq q \leq 8.9 \text{ nm}^{-1}$ ), and internal structures of the ion-conducting layers ( $3.0 \text{ nm}^{-1} \leq q \leq 10.5 \text{ nm}^{-1}$ ) were evaluated using the estimated  $I_B(q)$ .

## 5.2. Hierarchical structures in high $q$ range

**Fig. 5-1** shows the SAXS profiles of grafted-ETFE and ETFE-PEMs with  $GD$  from 19 to 59% in the high  $q$ -range ( $1 \text{ nm}^{-1} < q < 11 \text{ nm}^{-1}$ ). The grafted-ETFE with  $GD$  of 34 and 59% exhibited the presence of the identical shoulder-like peaks at the similar  $q$ -position of  $6.8 \text{ nm}^{-1}$  corresponding to a  $d$ -spacing of 0.9 nm while grafted-ETFE with  $GD$  of 19% and pristine ETFE did not. Thus, the peak with a  $d$ -spacing of 0.9 nm should correspond to the correlation distance of the monomer units in the polystyrene-grafted polymers. Note that the peaks at  $q$ -position of  $6.8 \text{ nm}^{-1}$  existed in the  $q$ -range with the presence of remarkable amorphous phase scattering because the SAXS profiles were characterized by a large SAXS upturn in the range of  $q$  range from  $4 \text{ nm}^{-1}$  to  $10 \text{ nm}^{-1}$ . ETFE-PEM with  $GD$  of 34 and 59% exhibited broad peaks at the similar  $q$ -position of  $3.9 \text{ nm}^{-1}$  corresponding to a  $d$ -spacing of 1.6 nm. Because the pristine ETFE film had no peak in this  $q$ -range, the peak with a  $d$ -spacing of 1.6 nm should correspond to the correlation distance of the monomer units in the PSSA-grafted polymers. The scattering peak at  $d$ -spacing of 1.6 nm may rise from an electron density difference between electron-rich sulfonic acid groups and electron-poor polystyrene parts in the graft domains. It reflects the positional correlation of the electron-rich PSSA groups resulting from the significant ionic aggregation of poly(styrene sulfonic acid) in graft domains at high grafting degree of 34-59%. Similar with grafted-ETFE, ETFE-PEM with  $GD$  of 19% did not show any feature-like peak in the high  $q$  range. The  $d$ -spacing of ETFE-PEM is 0.7 nm higher than that of grafted-ETFE probably because of the repulsion of the sulfonic acid groups (strong acid) in addition to the increases of sulfonic acid content in the graft domains. Above results indicate that the Bragg-spacing relating to internal structures of graft domains did not change with  $GD$  of 34-59%.

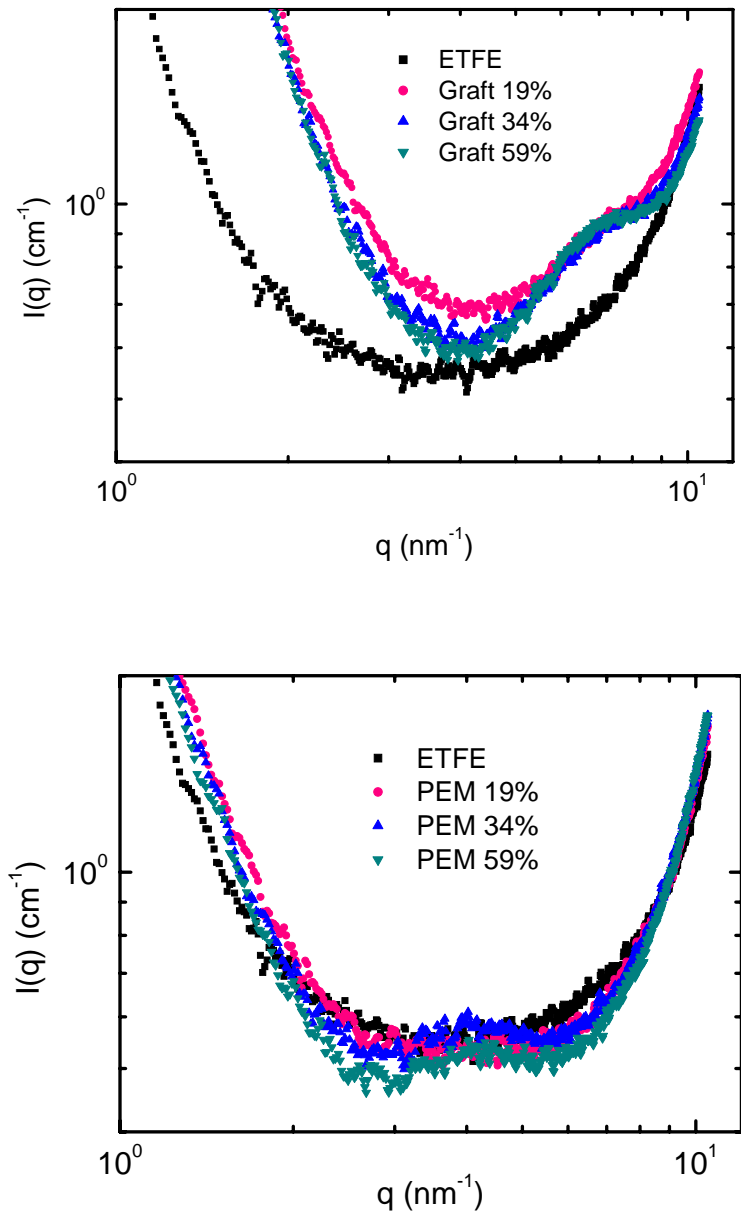


**Figure 5-1.** SAXS profiles of grafted-ETFE and ETFE-PEMs with *GD* of 19-59%.

### 5.3. Background corrections

**Fig. 5-2** presents the Porod plots for the observed scattering intensities of the original ETFE film, grafted-ETFE film, and ETFE-PEM with *GD* of 19% [1]. In the high- $q$  range ( $4.0 \text{ nm}^{-1} \leq q \leq 10.5 \text{ nm}^{-1}$ ), where the observed scattering intensities are negligible, the positive deviation from Porod's law is evident, indicating the background scattering in the Porod plots of these ETFE films. In the higher- $q$  range ( $9.5 \text{ nm}^{-1} \leq q$ ), the positive curvatures of the grafted-ETFE film and ETFE-PEM are slightly higher than that of the original ETFE film. Accordingly, the background intensities in the three films are not identical. The background scattering intensities of the grafted-ETFE film and ETFE-PEM in the high- $q$  range should increase owing to the additional amorphous volumes introduced by the grafting and sulfonation reactions, because the electron density fluctuation in the crystalline phase is less than that in the amorphous phase.

To estimate the background scattering intensities  $I_B(q)$  of the films according to Vonk's method (equation (2-34)) in Chapter 1, the observed scattering intensities  $I_{obs}(q)$  of the grafted-ETFE film were first plotted as a function of  $q^n$  using various even numbers  $n$  for rough determination of the parameters  $Fl$ ,  $b$ , and  $n$  in the empirical equation (2-34). As shown in **Fig. 5-3(a)**, a plot of  $I_{obs}(q)$  vs.  $q^n$  with  $n = 4$  leads to a straight line in the high- $q$  region, where the observed scattering intensities were negligible. Thus, the scattering intensities in the  $q$  region  $8.9\text{--}10.5 \text{ nm}^{-1}$  were fitted to Vonk's equation (2-34) in order to obtain the approximate values of  $Fl$  and  $b$  as  $0.552$  and  $9.0 \times 10^{-5}$ , respectively. When only using Vonk's equation to estimate  $Fl$ ,  $b$ , and  $n$  for  $I_B(q)$ , it is difficult to avoid overestimation of the background that makes the values of  $I_B(q)$  larger than those of the observed scattering intensities. Thus, we introduced a contribution factor defined as the ratio of the background scattering intensity  $I_B(q)$  to the observed scattering intensities  $I_{obs}(q)$  ( $I_B(q)/I_{obs}(q) \times 100$ ).

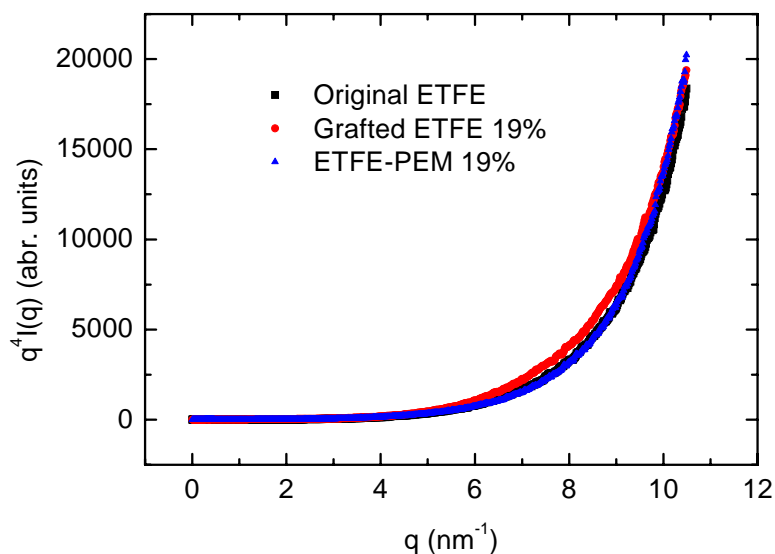


**Figure 5-2.** Porod plots of the original ETFE film (closed squares), grafted ETFE film (closed circles), and ETFE PEM (closed triangles) with a grafting degree of 19% for the observed scattering intensity.

**Fig. 5-3(b)** presents the introduction of the  $I_B(q)$  contribution factor into the observed scattering intensities over the entire  $q$  range and shows that the  $I_B(q)$  contribution factor is negligible in the low- $q$  range ( $q < 1 \text{ nm}^{-1}$ ) and dramatically increases in the high- $q$  range ( $1 \text{ nm}^{-1} < q < 4 \text{ nm}^{-1}$ ) from approximately 5% to 85%. The  $I_B(q)$  contribution factor reaches a plateau region of 85% in the  $q$  range  $4\text{--}7 \text{ nm}^{-1}$  and then further increases up to 100% in the  $q$  range  $7\text{--}9 \text{ nm}^{-1}$ . In the  $q$  range  $9.0\text{--}10.5 \text{ nm}^{-1}$ , the  $I_B(q)$  contribution factor is approximately 105%. Accordingly, it is clearly shown that the background intensity is not negligible in the high- $q$  range ( $1 \text{ nm}^{-1} < q$ ) because the presence of the background is very high ( $85\% < I_B(q)$  contribution factor  $< 105\%$ ) in the  $q$  range  $7.0 \text{ nm}^{-1} < q < 10.5 \text{ nm}^{-1}$ . These values are in good agreement with those in previous reports, in which the  $I_B(q)$  contribution factor was approximately 90% in the SAXS of polymeric materials [3]. The roughly estimated parameters  $Fl$ ,  $b$ , and  $n$  were thus optimized again using Vonk's method with  $n = 4$  such that the contribution factors plotted over the entire  $q$  range were as large as possible but did not exceed 100% much in the high- $q$  range. The same procedures were utilized for the original

ETFE film and ETFE-PEM to achieve the corresponding  $I_B(q)$ . Thus, the  $I_B(q)$  results could be subtracted from the observed intensities  $I(q)$ .

The applicability of equation (2-34) with  $n = 4$  has also been presented in numerous previous studies [2,4]. The value  $n = 6$  is also used in equation (2-34) because the plot of  $I_B(q)$  vs.  $q^n$  exhibits a straight line at large  $q$  ranges compared with that obtained with  $n = 4$  [5,6]. Accordingly,  $I_B(q)$  obtained using Vonk's equation (2-34) with  $n = 6$  must overestimate the actual  $I_B(q)$ , which must be lower than  $I_{obs}(q)$  in the entire  $q$  range. For instance, the  $I_B(q)$  contribution factor of the grafted ETFE film is 100%–130% in the  $q$  range 3.0-10.5 nm<sup>-1</sup> for equation (2-34) with  $n = 6$ .

To further investigate the validity of various methods for appropriate background correction, the modification of Ruland's method in equation (2-33) can be written as follows:

$$I_B(q) = Fl e^{aq^n}, \quad (5-1)$$

where  $n$  is an even integer. Using equation (5-1) with  $n = 2$  leads to a weak straight line in the high- $q$  region in the plot of  $\ln(I_{obs}(q))$  vs.  $q^2$ , whereas with  $n = 4$ , it overestimates the  $I_B(q)$  contribution factor for the observed scattering intensities of the grafted-ETFE film up to 110% in the  $q$  range 3.5 nm<sup>-1</sup> <  $q$  < 10.5 nm<sup>-1</sup>. Therefore, only Vonk's equation (2-34) with  $n = 4$  exhibits the appropriate background correction for the current ETFE films.

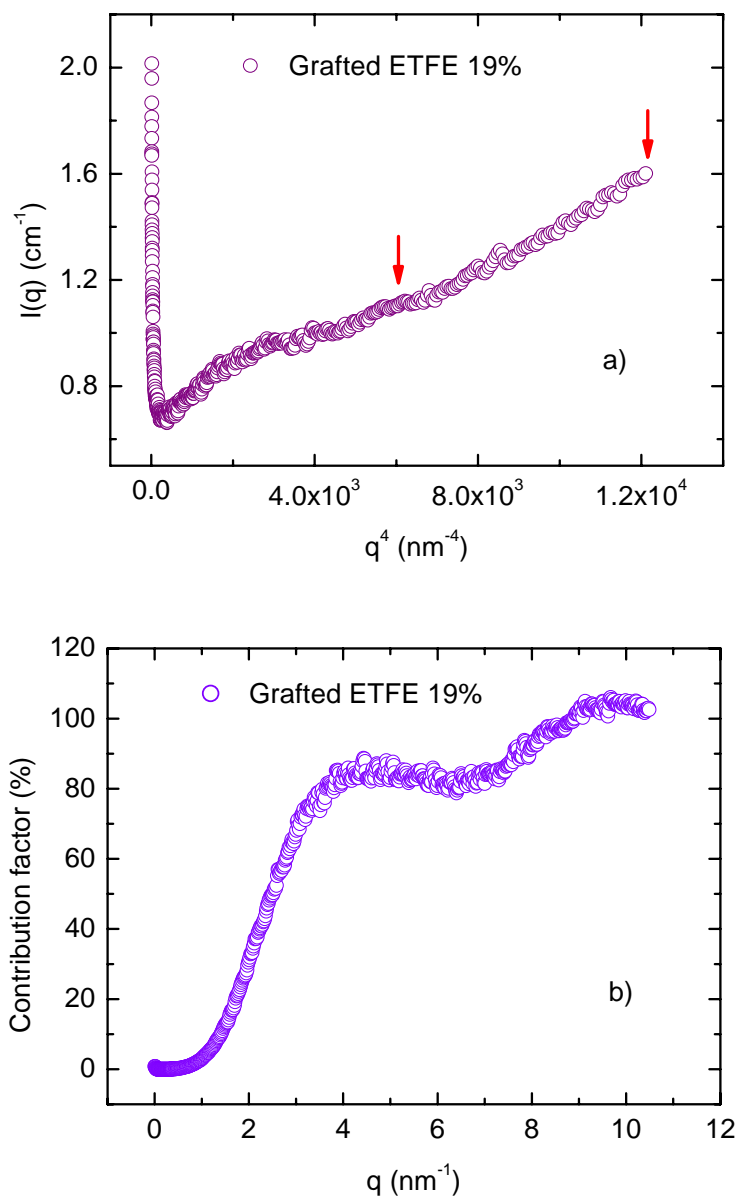


**Figure 5-3.** (a) Background determination for the grafted-ETFE film with a grafting degree of 19% using Vonk's method and  $I_B = a+bq^4$ . (b) Contribution factor for the background scattering intensity into the observed scattering intensity.

## 5.4. Hierarchical structure analysis with background corrections

**Fig. 5-4** shows the effects of the Lorentz correction using equation (2-14) with  $n = 2$  for the lamellar structures of the grafted-ETFE film with  $GD$  of 19% in the low- $q$  range ( $0.1 \text{ nm}^{-1} \leq q \leq 0.7 \text{ nm}^{-1}$ ). The scattering profiles obtained using the Lorentz correction with the background correction (open triangles) is similar to that of the original profiles (open circles). The fact that the lamellar periods were not altered by the background correction seems to be reasonable because the scattering background was negligible in the  $q$  range lower than approximately  $1 \text{ nm}^{-1}$ , judging from the  $I_B(q)$  contribution factor (**Fig. 5-3(b)**).

The lamellar period (lamellar spacing) comprises the average summation of the crystalline phase, amorphous phase, and boundary layer thicknesses. The existence of boundary layers was found to deplete the high-angle scattering and result in the negative derivation from Porod's law. Thus, the determination of the boundary layer thickness is highly desirable for the observation of Porod's law behavior from a nonideal two-phase system and is essential for the accurate evaluation of the linear crystallinity of lamellar stacks, which is defined as the ratio of the crystallite phase thickness to the lamellar period.

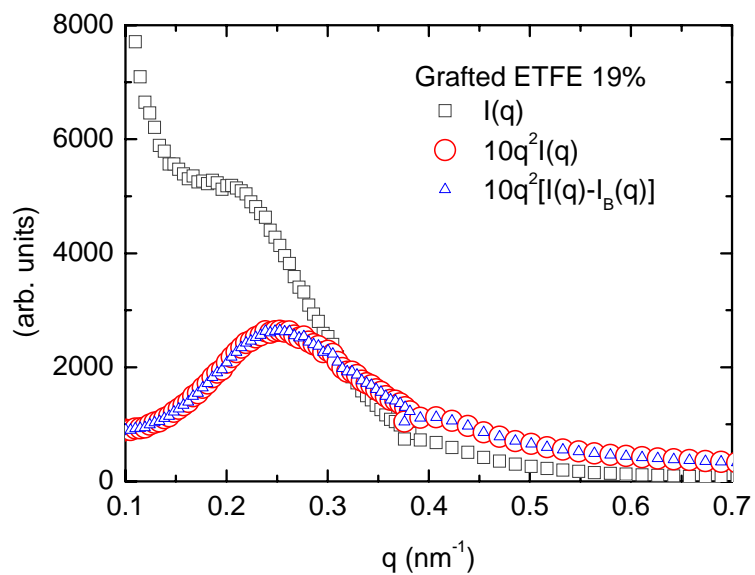


**Figure 5-4.** The original SAXS profile of the grafted ETFE film (open squares) and the scattering profiles obtained using the Lorentz correction without (open circles) and with the background correction (open triangles).

The boundary layers between the crystalline and amorphous phases within the lamellar stacks of semicrystalline polymers have been defined by the electron density distribution, in which the electron density of the boundary layers linearly decreases from the crystalline to the amorphous phases [7,8]. The interfacial thickness was evaluated using the model for the deviation from Porod's law first proposed by Ruland [9]:

$$\ln \{q^4 [I_{obs}(q) - I_B(q)]\} = \ln(K_p) - \sigma^2 q^2, \quad (5-2)$$

where  $I_{obs}(q)$  is the observed scattering intensity,  $K_p$  is Porod's constant, and  $\sigma$  is the standard deviation of the Gaussian smoothing function, which describes the electron density profile across the interface due to the boundary layers. The standard deviation  $\sigma$  can be experimentally obtained as the slope of the straight line in the plot of  $\ln \{q^4 [I_{obs}(q) - I_B(q)]\}$  vs.  $q^2$  ( $-\sigma^2$ ). The average thickness  $E$  of an interfacial layer is calculated from the obtained  $\sigma$  given that the smoothing function describing the electron density profile across the boundary layers is a box function [8]. In particular,  $E$  can be used as the interfacial thickness and calculated from  $\sigma$  using the following equation:

$$E \approx \sqrt{12}\sigma. \quad (5-3)$$

Because equation (5-2) is expressed as an exact form (no Taylor expansion), no truncation error is included for the determination of the interfacial thickness.

**Fig. 5-5** shows the plots of  $\ln \{q^4 [I_{obs}(q) - I_B(q)]\}$  and  $\ln \{q^4 I_{obs}(q)\}$  for the grafted-ETFE film as a function of  $q^2$  with/without the background correction in a  $q$  region ( $1 \text{ nm}^{-1} < q$ ) for the determination of the interfacial thickness within the lamellar stacks. The negative slope only appeared after the subtraction of the background scattering intensity  $I_B(q)$ . Because a line with a negative slope is evident in  $q^2 > 62 \text{ nm}^{-2}$ , the value of  $\sigma$  and then  $E$  could be calculated using a least squares fitting of the intensity data to the straight line over the range  $62 \text{ nm}^{-2} \leq q^2 \leq 79 \text{ nm}^{-2}$ . The same procedure was utilized for the determination of  $\sigma$  and  $E$  for the original ETFE film and ETFE-PEM. The interfacial thicknesses  $E$  of the original ETFE film, grafted-ETFE film, and ETFE-PEM are 0.97, 1.08, and 1.11 nm, respectively. The above results clearly revealed that the grafted-ETFE film and ETFE-PEM possess relatively sharp boundary zones between the crystallite and amorphous layers even after the grafting and sulfonation procedures, as is the case for the original ETFE film.

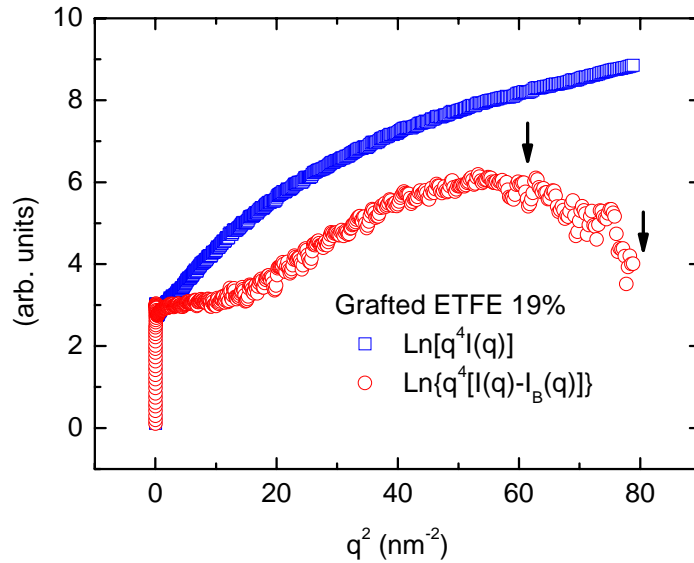


**Figure 5-5.** Determination of the interfacial thickness of the 19%-grafted-ETFE film using the deviation from Porod's law without (open squares) and with the background correction (open circles).

Note that the negative slope in **Fig. 5-5** only appeared in a high- $q$  range ( $62 \text{ nm}^{-2} \leq q^2 \leq 79 \text{ nm}^{-2}$ ) after the background subtraction. Because the value of the negative slope is very sensitive to the background correction, the determination of the background value is dependent on the empirical methods [equations (2-33) and (2-34)], even with the arbitrary values of  $n$  in equation (2-34). For instance, using Vonk's method with  $n = 6$ , the profile in **Fig. 5-5** showed a straight line with a negative slope at a much lower  $q$  position ( $q^2 = 2.8 \text{ nm}^{-2}$ ), resulting in a better least squares fitting in the  $q$  range  $2.8\text{-}7.6 \text{ nm}^{-2}$ . In particular, the values for the interfacial thickness of the original ETFE film, grafted-ETFE film, and ETFE-PEM in this case were larger (1.46, 1.58, and 1.83 nm, respectively) than that obtained using the contribution factors because Vonk's method with  $n = 6$  overestimates the value of  $I_B(q)$  in the high- $q$  range for the ETFE films [4,8,9]. This result is reasonable because the background overestimation makes the slope of the straight line in the plot of  $\ln\{q^4 [I_{obs}(q) - I_B(q)]\}$  vs.  $q^2$  in equation (5-2) decrease faster, and consequently, result in the overestimation of the interfacial thickness compared to the true values.

**Fig. 5-6** shows the SAXS profiles of the original ETFE film, 19%-grafted ETFE film, and ETFE-PEM (obtained by the sulfonation of the grafted ETFE film) (a) without and (b) with the background correction. For the grafted-ETFE film, the scattering maximum at a  $q$  value of  $6.8 \text{ nm}^{-1}$  corresponding to a  $d$ -spacing of 0.9 nm appeared only after the background correction (**Fig. 5-6(b)**). This result indicates that the background scattering is not negligible in the high- $q$  range ( $4.0 \text{ nm}^{-1} \leq q \leq 10.5 \text{ nm}^{-1}$ ) compared with the scattering intensities of the grafted-ETFE film and ETFE-PEM (**Fig. 5-2**). Because the original ETFE film had no peak in this  $q$ -range, the peak with a  $d$ -spacing of 0.9 nm should correspond to the correlation distance of the monomer units in the polystyrene-grafted polymers. The scattering peak at a  $d$ -spacing of 0.9 nm may arise from the electron density difference between the polystyrene graft domains and ETFE polymer substrate. It reflects the fact that a grafted-ETFE film with even a grafting degree of 19% can exhibit a sufficiently high electron density difference to induce discernible scattering. In addition, the very broad and weak peak at a  $d$ -spacing of 0.9 nm indicates the weak ordering of the polystyrene graft chains in the graft domains.

In contrast, no scattering peak was observed in the ETFE-PEM, even after background correction (**Fig. 5-6(b)**). No appreciable scattering in the ETFE-PEM seems to result from the less-ordered poly(styrene sulfonic acid) chains after sulfonation and weak scattering intensity due to a higher absorption factor. Moreover, the internal structures of the ion-conducting layers of the ETFE-PEM might have appeared in the high- $q$  range, which must be dramatically affected by the larger amorphous halo background, as shown in **Fig. 5-6(a)**. The above results indicate that the crystalline morphology of these films is modified during the film preparation procedures, and thus, the comparison of the structures at each preparation step (original ETFE film, grafted-ETFE film, and ETFE-PEM) provides very essential information for gaining a systematic understanding of the hierarchical structures of PEMs. Note that the peak position at  $6.8 \text{ nm}^{-1}$  did not change in the SAXS profile of the grafted-ETFE film when Vonk's method with  $n = 6$  in equation (2-34) and the modification of Ruland's method,  $I_B(q) = Fle^{aq^4}$ , were utilized, although these equations overestimate the background in the high- $q$  range. This result is in significant contrast to the determination of the interfacial thickness that is largely influenced by the overestimation of  $I_B(q)$  in the high- $q$  range  $4.0\text{-}10.5 \text{ nm}^{-1}$ .

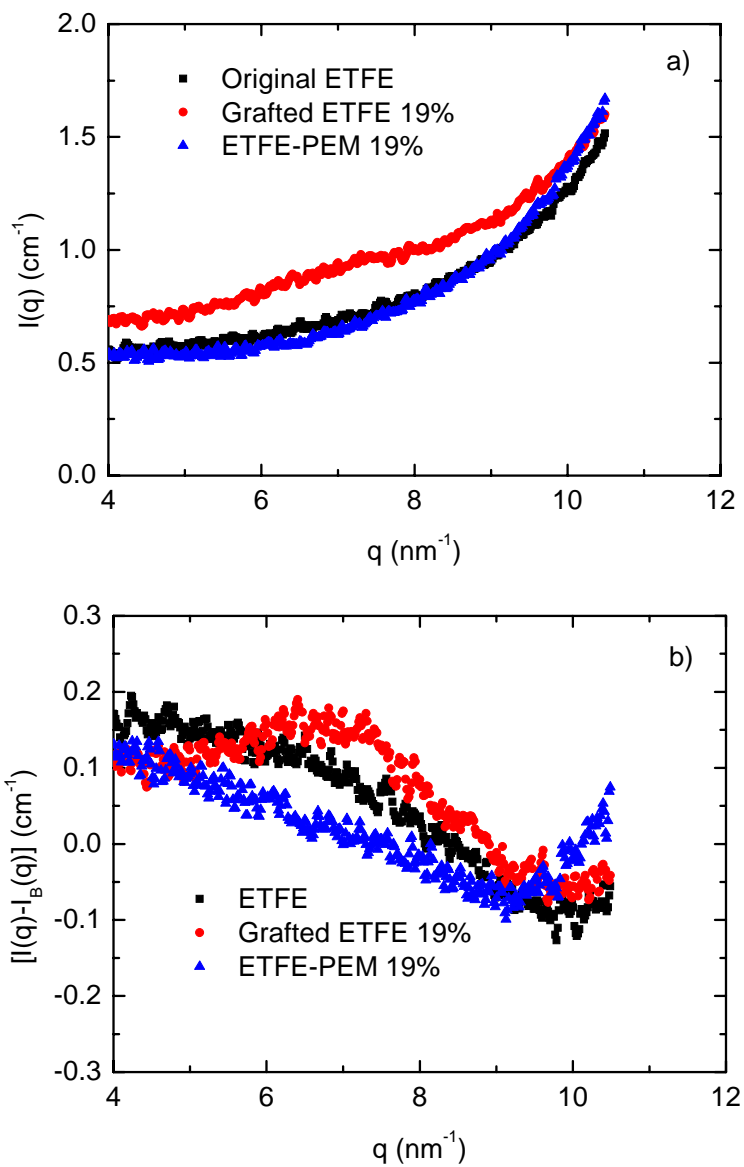


**Figure 5-6.** SAXS profiles of the original ETFE film, grafted-ETFE film, and ETFE-PEM over the large  $q$  range from 4 to  $10 \text{ nm}^{-1}$  (a) without and (b) with the background-corrected scattering intensity

## 5.5. Conclusions

The hierarchical structures of original ETFE film, grafted ETFE film, and ETFE PEMs were investigated by SAXS in terms of background scattering correction in the high- $q$  range. A simple procedure using a newly defined contribution factor for reliable background correction has been proposed for avoiding the overestimation of  $I_B(q)$  in order to show the effects of background behavior over the entire  $q$  range. The precisely estimated  $I_B(q)$  indicates that the structures of interfacial thicknesses and intra-structures of the polystyrene graft domains, appearing in the high- $q$  range, were dramatically affected by background correction. Moreover, the new method for background correction dramatically affects the value of the interfacial thickness but not the correlation distance of the grafted polymers in the graft domain. In particular, the lamellar periods ( $19.1 \text{ nm} \leq d_L \leq 26.0 \text{ nm}$ ) in the low- $q$  range were not altered by  $I_B(q)$ , whereas the interfacial thickness ( $0.97 \text{ nm} \leq E \leq 1.11 \text{ nm}$ ) or ( $1.46 \text{ nm} \leq E \leq 1.83 \text{ nm}$ ) using Vonk's method with  $n = 4$  or  $6$  in the high- $q$  range was only obtained (from the negative deviation of Porod's law) after determining the background-corrected scattering intensity. The scattering peak of the grafted ETFE film ( $d = 0.9 \text{ nm}$ ) only appeared after background correction (and was independent of the background correction methods), whereas the ETFE PEM still did not appear. After background correction, the negative deviation from Porod's law increases from the original ETFE film to the grafted ETFE film and ETFE PEM, and this increase indicates a relatively sharp boundary zone between the crystallite and amorphous layers within the lamellar structures of the grafted ETFE film and ETFE PEM. The above results indicate that the hierarchical structures of graft-type PEMs in the high- $q$  range were strongly affected by background correction.

## References

- 1) R.A. Register, S.L. Cooper, *Macromolecules* 23 (1990) 318-323.
- 2) J.A. Miller, S.L. Cooper, *J. Polym. Sci. Polym. Phys. Ed.* 23 (1985) 1065-1077.
- 3) N. Stribeck, *X-ray Scattering of Soft Matter*, (Springer, 2007).
- 4) R.J. Roe, *J. Appl. Cryst.* 15, (1982) 182-189.
- 5) P. Perrin, R.E. Prud'homme, *Macromolecules* 27 (1994) 1852-1860.
- 6) T.P. Russell, *J. Polym. Sci. Polym. Phys. Ed.* 22 (1984) 1105-1117.
- 7) J.T. Koberstein, B. Morra, R.S. Stein, *J. Appl. Cryst.* 13 (1980) 34-45.
- 8) M.H.J. Kim, *J. Appl. Cryst.* 37 (2004) 643-651.
- 9) W. Ruland, *J. Appl. Cryst.* 4 (1971) 70-77.

## **Chapter 6. Structure-property relationship of graft-type PEM**

### **6.1. Introduction**

In order to prepare high performance PEM for fuel cell applications, understanding of structure-property relationship is utmost importance. This is due to the fact that PEMs exhibit differences in their structures resulting in the differences in their corresponding properties. Recently, the main concern of structure-property relationships of PEM is to develop the PEM materials which exhibit higher levels of proton conductivity under low RH (< 50% RH) and high temperature (> 80 °C), at the same time, good mechanical properties under humidified condition (100% RH) via higher ionic content and/or improvement of proton transport pathway, with moderate water uptake [1]. The increase of ionic content leads to the increase order of the hydrophilic domains which are favorable for higher levels of proton conductivity but result in the loss of mechanical integrity. Thus, controlling the orientation and alignment of ionic domains as well as the crystalline morphology to improve proton transport pathway through membrane is higher desirable [1]. As showed in Chapter 3, ETFE-PEM exhibited high level of conductivity under low RH (30% RH) and excellent mechanical property under high RH (100%RH) at 80 °C. This well-balanced conductivity-mechanical property seems to meet above requirements. Thus, in this chapter, the structure-property relationship of graft-type ETFE-PEMs will be investigated to elucidate the origin of the electrochemical and mechanical properties of these membranes for fuel cell applications.

### **6.2. Structure–property relationship of ETFE-PEM**

SAXS measurement of hierarchical structures of hydrated ETFE-PEMs revealed that the lamellar unit has been considered to be the smallest structural unit with periods of 23.5 – 32.1 nm in the pristine ETFE film which is composed of higher order structure of oriented crystallites ( $d_2 = 198 - 288$  nm) and non-oriented crystallites (length > 1600 nm) dependence on  $GD$  ( $IEC$ ) in membranes. The lamellar period were also observed by a FE-SEM

measurement. The addition PSSA grafts are located locally in the amorphous domains within and around lamellar stacks and in and out of the crystallites, depending on the *GD* (*IEC*) of the membranes. Thus, on the basis of SAXS results, the structure-property relationship of graft-type ETFE-PEMs was elucidated on the basis of *GD* and *IEC*.

It is well known in fuel cell applications that PEMs require efficient proton conduction under low RH (< 50% RH) and, at the same time, high inherent mechanical properties under humidified condition (100% RH) at high temperature (> 80 °C). Therefore, we showed (a) proton conductivities under 30% RH and (b) tensile strengths (TSs) under 100% RH at 80 °C as a function of *IEC* of ETFE-PEMs together with those of Nafion-212 as a reference in **Fig. 6-1**. The proton conductivity of ETFE-PEMs with the *IECs* of 1.3 – 2.9 mmol/g was 0.001 – 0.013 S/cm (**Fig. 6-1(a)**). The conductance of membranes increased with the increase of *IEC* even at low RH (30% RH). ETFE-PEM with *IECs* higher than 2.7 mmol/g exhibited higher proton conductivity of  $9.3 \times 10^{-3}$  S/cm than Nafion-212 ( $9 \times 10^{-3}$  S/cm) and much higher than other aromatic-hydrocarbon-polymer based PEMs ( $1 \times 10^{-4}$  -  $1 \times 10^{-3}$  S/cm) [2,3] at the similar *IEC* values. As mentioned in 4.3, the ETFE-PEMs with higher *IEC* than 2.7 mmol/g possessed the ion-channels consisting of PSSA grafts located outside of crystallites. Thus, the high conductivity under low RH condition (less water molecules) should result from the well interconnected ion-channels around the crystallites. It should be noted that this structural model for high conductivity with less water molecules are totally different from the Nafion and aromatic hydrocarbon-type PEMs, in which well phase separated nano-scale ion channels are the origin of ion conducting paths with less amounts of water molecules under a low RH condition. In other words, this kind of hierarchical structure is expected to provide the effective route for higher proton transportation through the ETFE-PEMs.

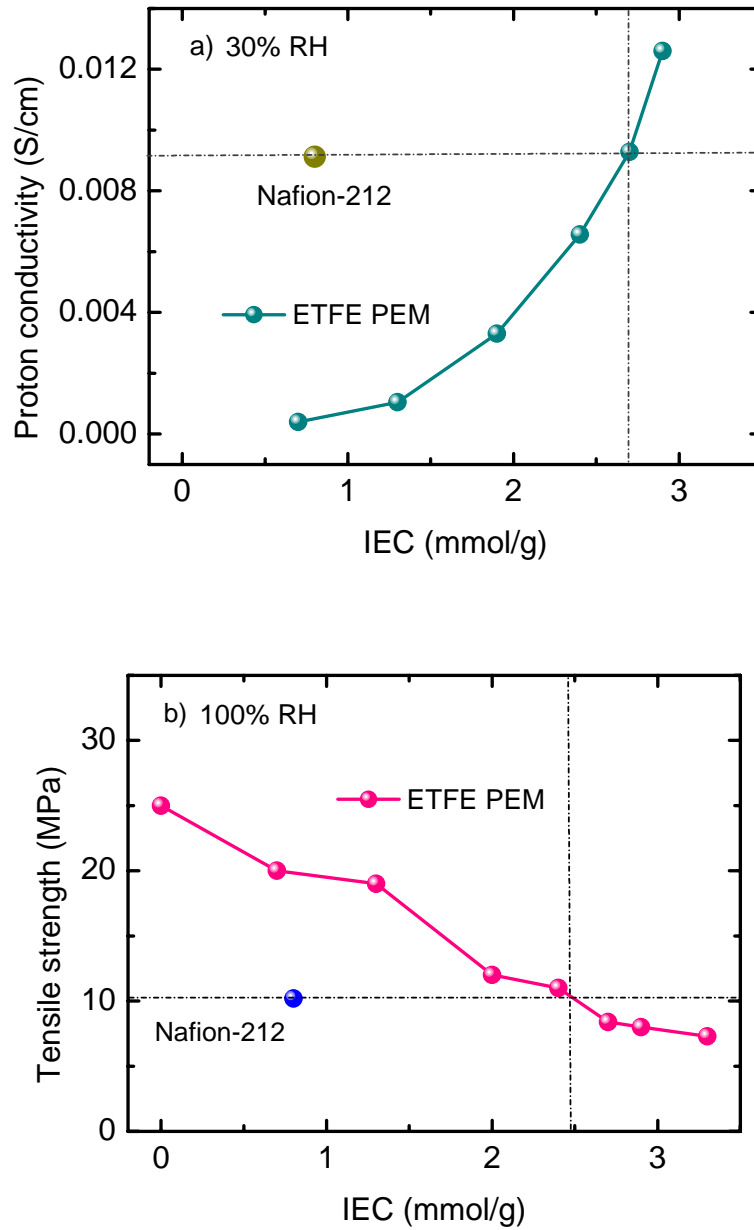


**Figure 6-1.** (a) Stress at maximum at 80 °C and 100% RH and (b) proton conductivity at 80 °C and 30% RH of ETFE-PEMs and Nafion-212.

In **Fig. 6-1(b)**, the ETFE-PEMs with *IECs* of 0 – 2.4 mmol/g showed higher TS of 11-25 MPa than Nafion-212 (10 MPa). In addition, TS just slightly decreased to 7.3 MPa at *IEC* of 3.3 mmol/g in spite of the high water absorption (**Table 3-1**). The excellent tensile strength of the ETFE-PEMs at high *IEC* must originate from the remaining the lamellar stacks and crystallites (lamellar grains) under hydrated state at high temperature in the ETFE-PEM with even high *IEC* (3.1 mmol/g) as showed in **Figs. 4-8, 4-9, and 4-10**. Furthermore, as the results of **Fig. 4-5**, the ETFE-PEMs with higher *GDs* than 59% (*IEC* = 2.4 mmol/g) possessed the ion conducting PSSA grafts mainly outside of the crystallites; thus, these additional ion channels, compared with low *IEC* PEMs, are effective to enhance the conductivity but not affect to the deterioration of the lamellar stacks and the crystallites. As the results, the crystallinity of membranes did not decrease in the range of *IECs* of 2.4 – 3.3 mmol/g as mentioned in 3.3. This is in good agreement with the behavior of mechanical property showed in **Fig. 6-1(b)**. In addition, it should be noted that the lamellar stacks play an important role to keep high inherent mechanical strength at higher swelling levels especially for the PEMs with higher *GDs* than 59% (lamellar period did not changed with *GDs* > 59%).

Another possible reason to elucidate the excellent mechanical strength of ETFE-PEMs is the swelling behavior under humidified condition. The swelling of graft domains should result in the local stress at the interfacial area between hydrophobic polymer substrates and hydrophilic PSSA grafts [4]. However, with higher *GD* than 59% (*IEC* > 2.4 mmol/g), the hydrophilic/hydrophobic boundary was less clear due to the partial miscibility of PSSA grafts with polymer substrates found by Porod's law as mentioned in 4.3. This behavior prevented the stress degradation at the boundary induced by the swelling. As the results, when *IEC* increased from 2.4 to 3.3 mmol/g, the TSs just slightly decreased from 11 to 7.3 MPa while that of Nafion-212 was 10.2 MPa. Such TSs values of ETFE-PEMs are high enough for fuel cell application even at high level of absorbed water.

The hierarchical structures of ETFE-PEMs exhibited totally different with those of Nafion (**Fig. 6-2**). The maximum peak at very high  $q$  of  $4 \text{ nm}^{-1}$  ( $d$ -spacing = 1.6 nm) was attributed to the correlation distance between PS sulfonic acid groups. Contrary to Nafion, this peak appeared at  $q$ -range higher than Porod's tail [5,6]. The matrix peak related to lamellar structures appeared at mid  $q$  range with  $d$ -spacing of 24 – 32 nm. This matrix peak followed by a dramatically decrease of the intensity (Porod region) similar with ionomer peak of Nafion

[7,8]. The ETFE-PEMs have the crystallites (lamellar grains) which are higher order structures of the lamellar structures with length scale ( $> 900$  nm) which is much higher than crystallite length of Nafion ( $> 100$  nm). For higher  $GD$  ( $GD > 59\%$ ), only amorphous domains consisting of PSSA grafts and amorphous ETFE existed outside of the crystallites but not those in lamellar stacks and the crystallites acted as the main conducting ion channels under low RH conditions. This behavior is favorable for high conductivity but keep high mechanical strength of membranes at high swelling levels. Thus, the ETFE-PEM with  $IECs$  higher than  $2.7$  mmol/g exhibited higher conductivity ( $> 0.009$  S/cm) at 30% RH and the compatible tensile strengths of approximately 10 MPa at 100% RH at  $80$  °C, compared with those of Nafion-212.

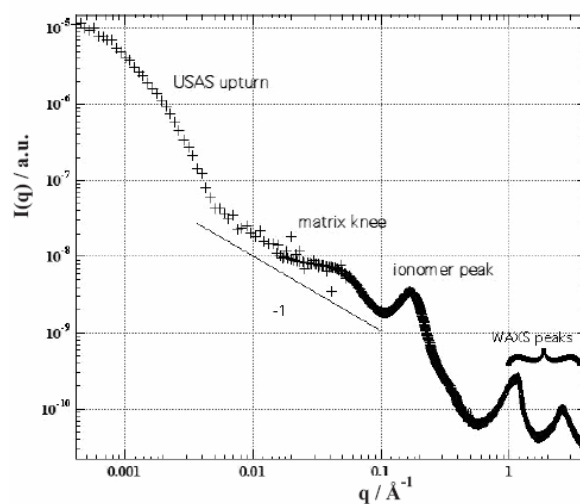


**Figure 6-2.** SAXS profile of hydrated Nafion membrane [9].

### 6.3. Conclusions

Study on structure-property relationship of ETFE-PEM revealed that the ETFE-PEM with high *IECs* ( $>2.7$  mmol/g) exhibited high conductivity ( $> 0.009$  S/cm) at 30% RH and compatible tensile strengths (approximately 10 MPa) at 100% RH at 80 °C should result from the well interconnected ion-channels around the crystallites and the remaining of the lamellar stacks and crystallites in the PEMs, respectively. When *GD* increased beyond 59% (*IEC*  $> 2.4$  mmol/g), the hydrophilic/hydrophobic boundary was less clear due to the miscible of PSSA grafts with polymer substrates. In addition, in this range of *GD*, only amorphous domains consisting of PSSA grafts and amorphous ETFE existed outside of the crystallites but not those in lamellar stacks and the crystallites acted as the main conducting ion channels under low RH conditions. This behavior is favorable for high conductivity at low RH but keep high mechanical strength at high swelling levels.

## References

- 1) U. Lappan, U. Geißler, U. Gohs, S. Uhlmann, *Radia. Phys. Chem.* 79 (2010) 1067-1072.
- 2) K. Miyatake, B. Bae, M. Watanabe, *Polym. Chem.* 2 (2011) 1919-1929.
- 3) T. Suda, K. Yamazaki, H. Kawakami, *J. Power Sour.* 195 (2010) 4641-4646.
- 4) K. Enomoto, S. Takahashi, T. Iwase, T. Yamashita, Y. Maekawa, *J. Mater. Chem.* 21 (2011) 9343-9349.
- 5) S. Balog, U. Gasser, K. Mortensen, H.B. youcef, L. Gubler, G.G. Scherer, *J. Membr. Sci.*, 383 (2011) 50-59.
- 6) S. Balog, U. Gasser, K. Mortensen, H.B. youcef, L. Gubler, Günther G. Scherer, *Polymer* 53 (2012) 175-182.
- 7) K. Jokela, R., Serimaa, M. Torkkeli, F. Sundholm, T. Kallio, G. Sundholm, *J. Polym. Sci. Polym. Phys. Ed.*, 40 (2002) 1539-1555.
- 8) S. Balog, U. Gasser, K. Mortensen, L. Gubler, G.G. Scherer, H.B. youcef, *Macromol. Chem. Phys.* 211 (2010) 635-643.
- 9) G. Gebel, O. Diat, *Fuel cells* 5 (2005) 261-276.

## Chapter 7. General Conclusion

The main current concern of structure-property relationships of PEM is to develop the PEM materials which exhibit higher levels of proton conductivity at low relative humidity (<50% RH) and superior mechanical properties under humid conditions (100%RH) at high temperatures (>80 °C) via higher ionic content and/or improvement of proton transport pathway, with moderate absorbed water. Among the graft-type PEM materials, ETFE-PEM has been considered as a promising candidate to solve above problems. Thus, the structure-property relationship of ETFE-PEM was investigated systematically with a wide *GD* of 0-117% (*IEC* = 0 – 3.1 mmol/g).

At 30%RH and 80 °C, ETFE-PEM with *IECs* higher than 2.7 mmol/g exhibited a higher proton conductivity ( $9.3 \times 10^{-3}$  S/cm) compared to Nafion-212 ( $9 \times 10^{-3}$  S/cm) and much higher than aromatic hydrocarbon types such as sulfonated poly (arylene ether)s ( $1 \times 10^{-3}$  S/cm) and sulfonated star-hyperbranched polyimides ( $\sim 1-5.5 \times 10^{-4}$  S/cm) at the similar *IEC* values. Unlike aromatic hydrocarbon type PEMs, ETFE-PEMs have proton conductivities that are less dependent on RH because of clearer phase separation between the hydrophilic PSSA grafted polymers and the hydrophobic ETFE substrate, thereby maintaining conducting channels even under dry conditions.

At 100%RH and 80 °C, ETFE-PEMs with *IEC* < 2.4 mmol/g showed higher tensile strengths (> 11 MPa) compared to Nafion-212 (10.2 MPa) at the same conditions. When *IECs* increased beyond 2.4 mmol/g the TSs of ETFE-PEM only decreased slightly to 7.3 MPa in spite of the high absorbed water. Thus, the increase of polystyrene sulfonic acid clusters and then, water content at higher *IECs*, had less effect on the ETFE-PEM TS under humid conditions (100% RH). Note that ETFE-PEMs with *IEC* > 2.7 mmol/g exhibited higher conductivity (>0.009 S/cm) at 30% RH and showed compatible tensile strengths of approximately 10 MPa at 100% RH and 80 °C, compared with those of Nafion-212.

The results indicate that graft-type ETFE-PEM exhibited high level of conductivity under low RH (30% RH) and excellent mechanical property under high RH (100%RH) at 80 °C. In order words, ETFE-PEM showed the good balance between the conductivity and mechanical

property which are the most important PEM properties for fuel cell applications under severe operation conditions.

A combination of SAXS and USAXS measurement for bulk analysis along with direct observation such as SEM for surface analysis allow the fully detail investigation of the structure of PEM system. The results showed that the hierarchical structures of ETFE-PEMs with  $19\% \leq GD \leq 59\%$  ( $1.3 \text{ mmol/g} \leq IEC \leq 2.4 \text{ mmol/g}$ ) were characterized as being composed of the conducting PSSA graft domains around lamellar stacks with 26-29 nm and the oriented crystallites (lamellar grains) with correlation distance  $d_2 = 198\text{--}288 \text{ nm}$  and  $d_3 = 903\text{--}1124 \text{ nm}$ . The lamellar periods increased with increasing  $GD$  ( $\leq 59\%$ ) and then kept constant in the  $GD$ s of 59-117%. These membranes with  $GD \geq 81\%$  ( $IEC \leq 2.7 \text{ mmol/g}$ ) showed totally different scattering features, assigned to a non-oriented crystallite structure with correlation distances of 225–256 nm. These discontinuous changes in a low  $q$ -region ( $4 \times 10^{-3} \text{ nm}^{-1} \leq q \leq 10^{-1} \text{ nm}^{-1}$ ) strongly indicate phase transition from oriented to non-oriented crystallite structures between  $GD$ s of 59 – 81%. The SAXS observation in whole  $q$ -regions indicate that the ion-channels consisting of PSSA grafts located locally around the lamellar crystals in the membranes with  $GD \leq 59\%$  and expands to out of the crystallites (lamellar grains) to have higher interconnection for  $GD \geq 81\%$ .

A simple procedure using a newly defined contribution factor for reliable background correction has been proposed for avoiding the overestimation of  $I_B(q)$  in order to show the effects of background behavior on the hierarchical structures in the high  $q$  range ( $q > 2 \text{ nm}^{-1}$ ). The precisely estimated  $I_B(q)$  indicated that the structures of interfacial thicknesses and intra-structures of the polystyrene graft domains, appearing in the high- $q$  range, were dramatically affected by background correction. Moreover, the new method for background correction dramatically affects the value of the interfacial thickness but not the correlation distance of the grafted polymers in the graft domain. The above results indicate that the hierarchical structures of graft-type PEMs in the high- $q$  range were strongly affected by background correction.

Study on structure-property of graft-type ETFE-PEMs revealed that the membranes with high  $IECs$  ( $\geq 2.7 \text{ mmol/g}$ ) exhibited higher conductivity at 30% RH and compatible tensile strengths at 100% RH at 80 °C, compared with those of Nafion, should result from the superior interconnected ion-channels around the crystallites and the remaining of the lamellar

stacks and crystallites (lamellar grains), respectively. In addition, the less clear boundary between the hydrophilic/hydrophobic domains with higher *IEC* ( $IEC \geq 2.4$  mmol/g) prevented the stress degradation at the boundary and thus, kept inherent crystallinity and mechanical properties of ETFE-PEM even under high absorbed water conditions.

The results show that the organization of lamellar stacks and crystallites (size, shape, connectivity) plays an important role to impact on the effective route comprising PSSA grafts for higher proton transportation through membrane as well as keep the inherent mechanical property and crystallinity of membranes.

This is the first systematic and comprehensive understanding of structure-property relationship of graft-type PEM at high *IEC* ( $IEC > 2.4$  mmol/g) under severe operation conditions. From these achievements, it is no doubt that ETFE-PEM with *IEC* around 2.4–2.7 mmol/g exhibited the promising electrochemical and mechanical properties for fuel cell applications, especially for clean electric source of vehicles. These achievements will offer optimization of higher-order structures as well as proper production processing of graft-type PEMs for high fuel cell performance. In addition, the obtained results will also provide the fundamental understand of structure-property relationship of graft-type PEMs.

In order to gain further understanding of structure-property relationship of graft-type ETFE-PEM, more detail structural analysis of SAXS measurement is necessary. In high  $q$ -range ( $2 \text{ nm}^{-1} < q < 10.5 \text{ nm}^{-1}$ ) where the ionomer peaks are located, SAXS measurement for ETFE-PEMs under dry and hydrated states with higher *GD* ( $GD > 59\%$ ) should be performed. The aggregations and distributions of the ionic groups and water in this  $q$ -range (several nanometers in correlation distance) are crucial for improvement of proton transportation. In intermediate  $q$ -range ( $1.5 \times 10^{-1} \text{ nm}^{-1} < q < 2 \text{ nm}^{-1}$ ) where the maximum peak originated from lamellar period appeared, the detail lamellar structure such as crystalline, amorphous, and interfacial thickness could be determined using one-dimensional correlation function of lamellar structure [1-3]. In addition, the detail analysis of Porod's tail following this peak allows determining several certain structural parameters of the system such as volume fractions and average sizes of each phase [4-6]. In low  $q$ -range ( $4 \times 10^{-3} \text{ nm}^{-1} \leq q \leq 1.5 \times 10^{-1} \text{ nm}^{-1}$ ) where the power law of SAXS profiles can provide information related to the shape of the

object, the further analysis of SAXS profiles should be carried out to evaluate the contribution of form factor and structure factor into the total SAXS intensities [7].

Beside SAXS, small angle neutron scattering (SANS) is also the powerful tool to investigate the hierarchical structures of graft-type PEM because of its advantages to X-ray scattering such as sensitivity to elements and their isotopes [8]. Finally, direct observation methods such as SEM, atomic force microscope (AFM), transmission electron microscope (TEM), and polarized optical microscope (POM) should be conducted further to obtain the cross-section images of membranes.

## References

- 1) M. Fatnassi, F.B.C. Larbi, J.L. Halary, International Journal of Polymer Science 2010 (2010) 1-6.
- 2) P. Zhu, J. Tung, G. Edward, Polymer 46 (2005) 10960-10969.
- 3) C.S. Cruz, N. Stribeck, H.G. Zachmann, F.J.B. Calleja, Macromolecules 24 (1991) 5980-5990.
- 4) J.T. Koberstein, B. Morra, R.S. Stein, J. Appl. Cryst. 13 (1980) 34-45.
- 5) M.H.J. Kim, J. Appl. Cryst. 37 (2004) 643-651.
- 6) W. Ruland, J. Appl. Cryst. 4 (1971) 70-73.
- 7) G. Gebel, J. Lambard, Macromolecules 30 (1997) 7914-7920.
- 8) M. Shibayama, Polymer Journal 43 (2011) 18-34.

## Publications

1. **Tap Tran Duy**, Shin-ichi Sawada, Shin Hasegawa, Yojiro Oba, Masato Ohnuma, Yosuke Katsumura, and Yasunari Maekawa, Hierarchical structure analysis of graft-type fluorinated polymer electrolyte membranes by small-angle X-ray scattering in the high-q range, Polymer Journal, Submitted.
2. **Tap Tran Duy**, Shin-ichi Sawada, Shin Hasegawa, Yosuke Katsumura, and Yasunari Maekawa, ETFE-based graft-type polymer electrolyte membranes with various IEC: Relative humidity dependence for fuel cell applications, J. Membr. Sci. Submitted.
3. **Tap Tran Duy**, Shin-ichi Sawada, Shin Hasegawa, Kimio Yoshimura, Yojiro Oba, Masato Ohnuma, Yosuke Katsumura, and Yasunari Maekawa, Hierarchical structure / property relationship in graft-type fluorinated polymer electrolyte membranes using small and ultra-small angle X-ray scattering analysis, Preparing.

## Presentations

### International conferences

1. **Tap Tran Duy**, Shin-ichi Sawada, Shin Hasegawa, Kimio Yoshimura, Yojiro Oba, Masato Ohnuma, Yosuke Katsumura, Yasunari Maekawa, Analysis of the hierarchical structure - property relationship of ETFE-based graft-type polymer electrolyte membranes, 2nd International Workshop on Radiation Effects in Nuclear Technology, 2012. 02. The University of Tokyo (**Poster**).
2. **Tap Tran Duy**, Shin-ichi Sawada, Shin Hasegawa, Kimio Yoshimura, Yojiro Oba, Masato Ohnuma, Yosuke Katsumura, Yasunari Maekawa, Small Angle X-ray Scattering Studies of Hierarchical Structure in ETFE-Based Graft-Type Polymer Electrolyte Membranes, International Union of Material Research Societies – International Conference on Electric Materials 2012, 2012. 09. Pacifico Yokohama (**Oral**).

3. **Tap Tran Duy**, Shin-ichi Sawada, Shin Hasegawa, Kimio Yoshimura, Yojiro Oba, Masato Ohnuma, Yosuke Katsumura, Yasunari Maekawa, Hierarchical Structure Analysis of Poly(ethylene-co-tetraflouroethylene)-Based Graft-Type Polymer Electrolyte Membranes by Small Angle X-ray Scattering, 15th International Small-Angle Scattering Conference 2012, 2012. 11. Sydney Convention and Exhibition Center, Australia (**Oral**).
4. **Tap Tran Duy**, Shin-ichi Sawada, Shin Hasegawa, Kimio Yoshimura, Yojiro Oba, Masato Ohnuma, Yosuke Katsumura, Yasunari Maekawa, Analysis of Small Angle X-ray Scattering Profiles of Poly(ethylene-co-tetraflouroethylene)-Based Graft-Type Polymer Electrolyte Membrane, 15th International Small-Angle Scattering Conference 2012, 2012. 11. Sydney Convention and Exhibition Center, Australia (**Poster**).

### **Domestic conferences**

1. **Tap Tran Duy**, Shin-ichi Sawada, Shin Hasegawa, Anada Putra, Daisuke Yamaguchi, Yojiro Oba, Satoshi Koizumi, Masato Ohnuma, Yasunari Maekawa, Yosuke Katsumura, Structural analysis of ETFE-based graft-type polymer electrolyte membranes by small angle X-ray/neutron scattering method, (2011), 2011. 08, Tokyo University of Agriculture and Technology (**Oral**).
2. **Tap Tran Duy**, Shin-ichi Sawada, Shin Hasegawa, Yojiro Oba, Masato Ohnuma, Yosuke Katsumura, Yasunari Maekawa, Analysis of hierarchical structure of ETFE-based graft-type polymer electrolyte membranes by small angle X-ray scattering, (Japanese Society of Radiation Chemistry), 2011. 09. Osaka University (**Oral**).
3. **Tap Tran Duy**, Shin-ichi Sawada, Shin Hasegawa, Yojiro Oba, Masato Ohnuma, Yosuke Katsumura, Yasunari Maekawa, Hierarchical structure analysis of ETFE-based graft-type polymer electrolyte membrane by small angle X-ray scattering, The 6th Takasaki Advanced Radiation Research Symposium (JAEA), 2011. 10. Takasaki City Hall (**Poster**).
4. **Tap Tran Duy**, Shin-ichi Sawada, Shin Hasegawa, Kimio Yoshimura, Yojiro Oba, Masato Ohnuma, Yosuke Katsumura, Yasunari Maekawa, Hierarchical structure / property analysis of ETFE-based graft-type polymer electrolyte membranes, Annual Meeting of the Chemical Society of Japan, 2012. 03. Keio University (**Oral**).

5. **Tap Tran Duy**, Shin-ichi Sawada, Shin Hasegawa, Kimio Yoshimura, Yojiro Oba, Masato Ohnuma, Yosuke Katsumura, Yasunari Maekawa, Analysis of the structure / property of graft-type polymer electrolyte membranes based on partially fluorinated polymers, Radiation Process Symposium, 2012. 06. The University of Tokyo (**Poster**).
6. **Tap Tran Duy**, Shin-ichi Sawada, Shin Hasegawa, Kimio Yoshimura, Yojiro Oba, Masato Ohnuma, Yosuke Katsumura, Yasunari Maekawa, Structure-property relationship of graft-type polymer electrolyte membranes based on partially fluorinated polymers, Radioisotopes and Radiation Research, 2012. 07. The University of Tokyo (**Oral**).
7. **Tap Tran Duy**, Shin-ichi Sawada, Shin Hasegawa, Yosuke Katsumura, Yasunari Maekawa, Fluorinated polymer-based graft-type polymer electrolyte membrane: Relative humidity dependence of properties for fuel cell applications, Radiation chemistry 55th, 2012. 09. Sendai (**Poster**).
8. **Tap Tran Duy**, Shin-ichi Sawada, Shin Hasegawa, Yosuke Katsumura, Yasunari Maekawa, Relative humidity independence of properties of ETFE-based graft- type polymer electrolyte membranes for fuel cell applications, The 7th Takasaki Advanced Radiation Research Symposium (JAEA), 2012. 10. Takasaki City Hall (**Poster**).
9. **Tap Tran Duy**, Shin-ichi Sawada, Shin Hasegawa, Kimio Yoshimura, Yojiro Oba, Masato Ohnuma, Yosuke Katsumura, Yasunari Maekawa, Analysis of structure-property relationship of fluorinated graft-type polymer electrolyte membranes using quantum beams, The Yayoi meeting on radiation graft-polymerization and radiation-ionking, 2013. 03. The University of Tokyo (**Oral**).
10. **Tap Tran Duy**, Shin-ichi Sawada, Shin Hasegawa, Kimio Yoshimura, Yojiro Oba, Masato Ohnuma, Yosuke Katsumura, Yasunari Maekawa, Study on the structure - property relationship of graft-type fluorinated polymer electrolyte membranes using quantum beams, Workshop on Radiation Isotope 50<sup>th</sup>, 2013. 07. The University of Tokyo (**Oral**).

## Scientific reports

1. **T. D. Tran**, S. Sawada, S. Hasegawa, K. Yoshimura, Y. Oba, M. Ohnuma, Y. Katsumura, Y. Maekawa, Wide-q observation in small angle X-ray scattering of ETFE-based graft-type polymer electrolyte membranes, JAEA-Review 2012-046, p. 32, 1, 2013.

## Awards

1. The best poster award, The 2nd International Workshop on Radiation Effects in Nuclear Technology (2012. 02, The University of Tokyo): “Analysis of the hierarchical structure - property relationship of ETFE-based graft-type polymer electrolyte membranes”, **Tap Tran Duy**, Shin-ichi Sawada, Shin Hasegawa, Kimio Yoshimura, Yojiro Oba, Masato Ohnuma, Yosuke Katsumura, Yasunari Maekawa.

## Acknowledgements

I would like to express my sincere gratitude to my supervisor, Prof. Yosuke Katsumura at Department of Nuclear Engineering and Management, Graduate School of Engineering, The University of Tokyo and my supervisor, Dr. Yasunari Maekawa at High Performance Polymer Group, Takasaki Advanced Radiation Research Institute, Japan Atomic Energy Agency for their variable suggestion, constant comments, and hearty encouragement in my research work and preparing the dissertation.

I would like to express my grateful appreciation to Prof. Hisaaki Kudo (Department of Nuclear Engineering and Management, Graduate School of Engineering, The University of Tokyo), Dr. Shin-ich Sawada, Dr. Shin Hasegawa, and Dr. Kimio Yoshimura (High Performance Polymer Group, Takasaki Advanced Radiation Research Institute, Japan Atomic Energy Agency) for their valuable suggestions and comments and eager guidance.

I gratefully acknowledge to Drs. Masaharu Asono, Tetsuya Yamaki, Jinhua Chen, Hiroshi Koshikawa (High Performance Polymer Group, Takasaki Advanced Radiation Research Institute, Japan Atomic Energy Agency), Dr. Yusa-sanken Muroya, Dr. Shinichi Yamashita, Dr. Kazuhiro Iwamatsu (Department of Nuclear Engineering and Management, Graduate School of Engineering, The University of Tokyo) for their considerable supports and useful comments.

I would like to extend my sincere thanks to Dr. Masato Ohnuma, Dr. Yojiri Oba (SAXS at NIMS, Stukuba), staffs of USAXS at beam line BL19B2, SPring-8 for considerable supports and useful comments.

I wish to thank gratefully Ms. Suda as a staff at High Performance Polymer Group, JAEA and Ms. Yukika Asahi and Ms. Sayaka Tokoro as staffs at Katsumura's Lab in the University of Tokyo, Ms. Vu Thi Lien Huong as a staff of Vietnam International Education Development (VIED). I wish to thank gratefully the other who helped me throughout my Ph.D work.

Finally, I would like to express heartily my appreciation to my family for their encouragement and supports during this study.

June 03, 2013

Tran Duy Tap